01 Feb 1980

Ultimate strength of cold-formed steel z-purlins

M. A. A. Razak

Teoman Peköz

Department of Structural Engineering
School of Civil and Environmental Engineering
Cornell University

Report No. 80-3

— PROGRESS REPORT —

ULTIMATE STRENGTH OF COLD-FORMED STEEL Z-PURLINS

by

M.A.A. Razak

Teoman Peköz, Project Director

A Research Project Sponsored by the
American Iron and Steel Institute
and the
Metal Building Manufacturers Association

Ithaca, New York February 1980

PREFACE

This progress report is based on a thesis presented to the faculty of the Graduate School of Cornell University for the degree of Master of Science.

The sponsorship of the American Iron and Steel Institute and of the Metal Building Manufacturers Association as well as the cooperation of the committees of the sponsors are gratefully acknowledged.

TABLE OF CONTENTS

CHAPTER Page

LIST OF TABLES

LIST OF FIGURES

CHAPTER 1

INTRODUCTION

1.1 General

Cold-formed steel structures are being widely used in various forms of construction such as industrial plants, gymnasiums, hangars and metal buildings. One important feature of metal building construction is the use of light gage roof panels connected to purlins, particularly of the Z-section. This section is, besides the channel-section, the simplest two-flange section which can be produced by cold-forming. The purlins have span lengths of 20 to 25 feet, generally made continuous over the building rigid frames by nesting. Construction details vary from manufacturer to manufacturer. The purlins available would typically have prepunched holes for connection of various types of bracings, overlapping connections, etc.

1.2 Previous Studies

Studies involving such purlin-panel assemblies have been carried out by a limited number of investigators. Cornell University carried out a series of studies on channel and Z-section behavior as regards lateral, flexural, torsional and flexural-torsional buckling. It is not the intention of this particular study to investigate any of such buckling modes as these have been well reported in the various Cornell University reports referenced and others.

A particularly important study on laterally unbraced compression flanges is that of Douty[6] undertaken at Cornell University. Section 3, Part III of the American Iron and Steel Institute (AISI) Cold-Formed Steel Design Manual[1] was formulated based on Douty's design approach. It is noted that this approach was intended for sections which have overall lateral stability. This study is presented in Chapter 2.

Douty's approach as formulated in the AISI Design Manual is frequently used for calculating the allowable stress on a beam in which the tension flange is continuously braced while the compression flange is either free or braced at intervals along its length. This would be the case when a purlin is subjected to an uplift load, braced continuously by the diaphragm strength of the roof panel.

In a survey undertaken by Ellifritt[7] of the Metal Building Manufacturers Association, there was observed considerable variation in the computed allowable stresses. He attributed this almost exclusively to the selection of the spring constant, β, which represents the rotational restraint of the purlin-panel assembly. Hence, the accurate determination of β is critical in predicting the ultimate load capacity of the purlins.

Another important Cornell study was on diaphragm-braced channel and Z-sections by Celebi.[4] He studied the theoretical basis for the design of diaphragm-braced thin-walled channel and Z-section beams and obtained the solution to the differential equation involved. A computer program, coded based on

his investigations and conclusions, is used by the metal building industry to check their design recommendations. One significant aspect of this study is the consideration of both the shear rigidity and the rotational rigidity of the diaphragm in bracing of purlins.

A follow-up of Celebi's study was done by Peköz.[11] He developed further the computer program coded by Celebi[4] and conducted tests on three span continuous diaphragm-braced purlin assemblies. The test results were correlated with the computer program solutions.

A significant study on the strength of elastically stabilized beams was done by Haussler.[8] In many respects, this study is comparable to that of Douty.[6]

1.3 Objectives of this Study

This study will attempt to establish by full-scale testing of diaphragm-braced purlins under simulated uplift loads a reliable failure criteria of such purlins. The current AISI Design Manual, particularly that of Section 3, Part III, shall be employed as a suitable foundation for such a criteria. Further inputs shall be considered from the differential equation solution as coded in a computer program by Celebi. The study will particularly look into the problem of the rotational restraint factor, F, from which the spring constant, β, is computed.

Chapter 2 will detail the analytical studies as presented by Douty[6] on the stability analysis of laterally unbraced compression flange. Chapter 3 presents the details of the experi-

mental program with particular emphasis on what is called the vacuum test procedure for testing the purlins. Analysis of the results are done in Chapter 4, followed by conclusions, design recommendations and suggestions for future work in Chapter 5.

2.2 Stability Analysis

2.2.1 Portion of Compression Flange Acting as a Column

Considering the simple case of the U-shaped beams, when the compression flange is subjected to the critical bending forces $\sigma_{cr}A_f$, where σ_{cr} is the critical stress and A_f is the area of the flange, the component normal to the deflected flange is $A_f d^2x_a/dz^2$, where x_a is the displacement of the top flange in the x-direction (see Figure 2.2). The differential equation for the deflection of the flange as a beam is

$$EI_f \frac{d^4x_a}{dz^4} = -\sigma_{cr}A_f d^2x_a/dz^2 \qquad 2.1$$

The lateral force component on a unit length of the deflected web is $\sigma t_w d^2x/dz^2$, where σ is assumed to be a linear function of the distance from the neutral axis, i.e., directly proportional to y, and t_w is the thickness of the web. Figure 2.3 shows the distribution of the lateral force on the web. The lateral force in the tension region C_t is directed opposite to the direction of displacement while in the compression region C_c, it is directed in the direction of displacement. The lateral force in the web is transmitted to the compression flange and the magnitude of the total force per unit length of beam is obtained by taking moments about the base of the web giving the following result:

$$R_a = \sigma_{cr} \frac{A_{web}}{\left(\frac{12C_c}{3C_c - C_t}\right)} \frac{d^2x_a}{dz^2} \qquad 2.2$$

where R_a = total lateral force transmitted to the compression flange by the buckled web.

A_{web} = area of web.

C_c = distance from the neutral axis to the extreme compression fiber.

C_t = distance from the neutral axis to the extreme tension fiber.

The equation of equilibrium of the compression flange then would be:

$$EI_f \frac{d^4x_a}{dz^4} + \sigma_{cr} \left[A_f + \frac{A_{web}}{\left(\frac{12C_c}{3C_c - C_t}\right)}\right] \frac{d^2x_a}{dz^2} = 0 \qquad 2.3$$

and the corresponding nontrivial eigenvalue leads to:

$$\sigma_{cr} = \frac{\pi^2 E}{(L/r)^2} \qquad 2.4$$

where $$r = \sqrt{\frac{I_f}{A_f + A_{wtb}/[12C_c/(3C_c - C_t)]}}$$

r is the radius of gyration of the flange together with a portion of the web of depth $d(3C_c - C_t) / 12C_c$, where d is the depth of the beam. This is the portion of the web which, along with the compression flange, can be considered as the column subjected to buckling.

2.2.2 The Effect of Torsional Instability

2.2.2.1 Stability Condition

The analysis in Section 2.2.1 is for the type of column

supported on an elastic foundation where the elastic support is provided by the remaining portion of the web and the tension flange acting together as an elastic frame. The effect of torsional weakening in the combined flexural-torsional stability of the effective column is considered by using the theorem of minimum potential energy. The following analysis is based on the analysis for the stability of the upper chord of a pony truss bridge presented by Bleich.[3]

The change in the entire potential energy of the system, U is given by:

$$U = V_1 + V_2 + U_w$$

$$= \frac{1}{2}\int_0^L [EI_y(u'')^2 + EC_w(\phi'')^2 + GJ(\phi')^2]dz$$

$$+ \frac{1}{2}\int_0^L (C_1 u^2 - 2C_2 u\phi + C_3\phi^2)dz$$

$$- \frac{P}{2}\int_0^L [(u')^2 + 2y_o u'\phi' + (\frac{I_p}{A})(\phi')^2]dz \qquad 2.5$$

where P = axial load on the effective column.

U = the change in the entire potential energy of the system consisting of the effective column and its supporting elastic frame.

V_1 = strain energy accumulated in the bent and twisted column.

V_2 = strain energy of the deflected supporting frame.

U_w = the change of potential energy of the external forces acting on the system.

I_y = moment of inertia of the column about its vertical y axis.

u = horizontal displacement of the shear center.

ϕ = rotation of the column.

J = torsional rigidity of the column.

y_o = vertical distance between the shear center and the centroid of the column.

I_p = polar moment of inertia of the column about its shear center.

C_w = warping constant.

$C_1 = \delta_\phi / (\delta_u \delta_\phi - \delta_{u\phi}^2)$

$C_2 = \delta_{u\phi} / (\delta_u \delta_\phi - \delta_{u\phi}^2)$

$C_3 = \delta_u / (\delta_u \delta_\phi - \delta_{u\phi}^2)$

δ_u = horizontal displacement of the shear center due to a unit load.

$\delta_{u\phi}$ = horizontal displacement of the shear center due to a unit moment.

δ_ϕ = rotation of column due to a unit moment.

To minimize the integral U so that $\delta U = 0$, the following Euler-Lagrange differential equations must be satisfied:

$$\frac{\partial F}{\partial u} - \frac{d}{dz}\left(\frac{\partial F}{\partial u'}\right) + \frac{d^2}{dz^2}\left(\frac{\partial F}{\partial u''}\right) = 0 \qquad 2.6a$$

$$\frac{\partial F}{\partial \phi} - \frac{d}{dz}\left(\frac{\partial F}{\partial \phi'}\right) + \frac{d^2}{dz^2}\left(\frac{\partial F}{\partial \phi''}\right) = 0 \qquad 2.6b$$

where $U = \int_0^L F(z,u,u',u'',\phi,\phi',\phi'')dz$

To satisfy the boundary conditions, substitute the eigenfunctions

$$u = A_1 \text{Sin } n\pi z/L$$

$$\phi = A_2 \text{Sin } n\pi z/L \quad \text{where} \quad n = 1,2,3,...$$

A nontrivial solution can exist only if the determinant of the coefficients of A_1 and A_2 is zero (A_1 and A_2 are indeterminate):

$$\begin{vmatrix} 1 + \mu_n - \frac{P_{cr}}{P_n} & -\frac{C_u}{C_1}\mu_n - \frac{P_{cr}}{P_n} y_o \\ -\frac{C_2}{C_1}\mu n - \frac{P_{cr}}{P_n} y_o & \frac{L^2 GJ}{n^2\pi^2 EI_y} + \frac{C_w}{I_y} + \frac{C_3}{C_1}\mu_n - \frac{P_{cr}}{P_n}\frac{I_p}{A} \end{vmatrix}$$

where $\mu_n = \dfrac{C_1 L^2}{n^2\pi^2 P_n}$ 2.7

$$P_n = \frac{n^2\pi^2 EI_y}{L^2}$$

L = length of column without elastic foundation.

Expanding 2.7 gives the following quadratic equations:

$$\left(\frac{I_p}{A} - y_o^2\right)\left(\frac{P_{cr}}{P_n}\right)^2 - \left[\frac{C_3}{C_1}\mu_n + \frac{I_p}{A}(1 + \mu_n) + 2y_o\frac{C_2}{C_1}\mu_n + \frac{C_w}{I_y} + \frac{L^2 GJ}{n^2\pi^2 EI_y}\right]\frac{P_{cr}}{P_n} + \left[\frac{C_3}{C_1}(1 + \mu_n)\mu_n - \left(\frac{C_2}{C_1}\mu_n\right)^2\right.$$

$$+ \frac{C_w}{I_y}(1 + \mu_n) + \frac{L^2 GJ}{n^2 \pi^2 EI_y}(1 + \mu_n)] = 0 \qquad 2.8$$

Equation 2.8 is the general equation of torsional-flexural stability for a column on an elastic foundation if a Winkler foundation, i.e., closely spaced springs, is assumed. Although the support provided by that part of the beam considered to be the elastic foundation is continuous, the difference is significant only for very short columns when compared with that of closely spaced discrete springs. The Winkler foundation is more conservative as it is less firm than that provided by a continuous foundation.

2.2.2.2 Simplification of Stability Condition

Equation 2.8 can be expressed in a general form as:

$$A\left(\frac{P_{cr}}{P_n}\right)^2 - B\left(\frac{P_{cr}}{P_n}\right) + C = 0 \qquad 2.9$$

Numerical investigations done by Douty on various shapes as indicated in Reference 6 show that A is insignificant when compared with B and C for short column length. It becomes more insignificant as the column length increases since A remains static while B and C increases with length. Thus, the second order term of (P_{cr}/P_n) can be neglected reducing the general stability equation to:

$$\frac{P_{cr}}{P_n} = \frac{\frac{C_3}{C_1}(1 + \mu_n)\mu_n - \left(\frac{C_2}{C_1}\mu_n\right)^2 + \frac{C_w}{I_y}(1 + \mu_n) + \frac{GJ}{P_n}(1 + \mu_n)}{\frac{C_3}{C_1}\mu_n + \frac{I_p}{A}(1 + \mu_n) + 2y_o\frac{C_2}{C_1}\mu_n + \frac{C_w}{I_y} + \frac{GJ}{P_n}} \qquad 2.10$$

Winter[12] published the following equations for determining the strength of a column on an elastic foundation which buckle flexurally:

$$\frac{P_{cr}}{P_e} = \left(1 + \frac{\beta L^2}{\pi^2 P_e}\right) \quad \text{for} \quad \beta L^2/P_e \leq 30 \qquad 2.11$$

$$\frac{P_{cr}}{P_e} = \left(0.6 + \frac{2}{\pi}\sqrt{\frac{\beta L^2}{P_e}}\right) \quad \text{for} \quad \beta L^2/P_e > 30 \qquad 2.12$$

where P_{cr} = critical load of equivalent column.

P_e = Euler critical load = $\pi^2 EI/L^2$

β = spring constant = $1/D$

D = lateral deflection of the column centroid due to a unit force applied to the web at the level of the column centroid.

L = unbraced length of equivalent column

Equation 2.10 can be manipulated and rewritten as:

$$\frac{P_{cr}}{P_n} = \left[1 + \frac{\frac{C_3}{C_1}\mu_n - \left(\frac{C_2}{C_1}\right)^2 \mu_n + \frac{C_w}{I_y} + \frac{GJ}{P_n}}{\frac{C_3}{C_1}\mu_n + \frac{C_w}{I_y} + \frac{GJ}{P_n}} \left(\frac{C_1 L^2}{\pi^2 P_n}\right)\right] x$$

$$\left[\frac{1}{1 + \frac{\frac{I_p}{A}(1 + \mu_n) + 2y_o \frac{C_2}{C_1}\mu n}{\frac{C_3}{C_1}\mu_n + \frac{C_w}{I_y} + \frac{GJ}{P_n}}}\right] \qquad 2.13$$

Comparison of Equation 2.13 with Equation 2.11 shows that the former is completely analogous to the latter if β is the following expression:

$$\beta_{eq} = \left(\frac{\frac{C_3}{C_1}\mu_n - \left(\frac{C_2}{C_1}\right)^2\mu_n + \frac{C_w}{I_y} + \frac{GJ}{P_n}}{\frac{C_3}{C_1}\mu_n + \frac{C_w}{I_y} + \frac{GJ}{P_n}}\right) C_1 \qquad 2.14$$

The additional multiplier within the second bracket of Equation 2.13 can be regarded as a reduction factor due to the torsional weakness of the cross-section. The value of C_w/I_y is generally small in relation to the other terms. Hence, β_{eq} can be reduced to:

$$\beta_{eq} = \frac{(C_1C_3 - C_2^2)\frac{L^2}{\pi^2} + GJC_1}{C_3\frac{L^2}{\pi^2} + GJ} \qquad 2.15$$

For short columns, it can be shown that β_{eq} is a function of L and the torsional constant J. As L increases, the asymptotic limit of Equation 2.15 is:

$$\beta_{eq} = \frac{C_1C_3 - C_2^2}{C_3} \qquad 2.16$$

which in turn reduces to:

$$\beta_{eq} = 1/\delta_u \qquad 2.17$$

This is the modulus of the elastic foundation which restraints the deflection perpendicular to the web of the beam. Douty's study showed that $\beta_{eq} = 1/\delta_u$ is an accurate approximation for longer columns, and conservative to use for short columns. Thus, Equations 2.11 and 2.13 are identical except for the term

in the second bracket of Equation 2.13 which will be called the torsional reduction factor:

$$T = \frac{1}{1 + \dfrac{\dfrac{I_p}{A}(1 + \mu_n) + 2y_o \dfrac{C_2}{C_1}\mu_n}{\dfrac{C_3}{C_1}\mu_n + \dfrac{C_w}{I_y} + \dfrac{GJ}{P_n}}} \qquad 2.18$$

2.2.2.3 Design Approximation for Torsional Reduction Factor

It is necessary to reduce Equation 2.18 to a simple enough expression applicable to cold-formed light gage columns on an elastic foundation. The expression for T can be simplified to:

$$T = \frac{1}{1 + \dfrac{\dfrac{I_p}{A}(1 + \mu_n) + 2y_o \dfrac{C_2}{C_1}\mu_n}{\dfrac{C_3}{C_1}\mu_n}} \qquad 2.19$$

Equation 2.19 is justified from consideration of the terms C_w/I_y and GJ/P_n which are negligible when compared with $(C_3/C_1)\mu_n$, for typical light gage beams.

From Equation 2.12, the length of one half wave in the asymptotic limit is $L' = \pi\sqrt[4]{EI/\beta}$. The total length is nL'. Substituting for n^4 in $\mu_n = C_1L^4/n^4\pi^4EI$ and $\beta = (C_1C_3 - C_2^2)/C_3$, gives the asymptotic form of T:

$$T_a = \frac{1}{1 + \dfrac{2C_1C_3 - C_2^2}{C_3^2}\dfrac{I_p}{A} + 2\dfrac{C_2}{C_3}y_o} \qquad 2.20$$

From consideration of the three common types of elastic support configurations found in light gage steel construction (see Figure 2.4), C_1, C_2 and C_3 can be simplified. C_1, C_2 and C_3 are constants, each of which involves the three possible displacements caused by a unit moment and a unit force applied to the column on elastic support. The three cases considered, Case I, Case II and Case III correspond to the elastic support configuration as shown in Figure 2.4. The deflections at the top of the web produced by a unit moment and unit force at that point on a unit length of beam for each of the three cases are:

	δ_u	$\delta_{u\phi}$	δ_ϕ
Case I	$\frac{h^3}{3EI_w} + \frac{h^2 b}{2EI_f}$	$\frac{h^2}{2EI_w} + \frac{hb}{2EI_f}$	$\frac{h}{EI_w} + \frac{b}{2EI_f}$
Case II	$\frac{h^3}{3EI_w} + \frac{h^2 b}{4EI_f}$	$\frac{h^2}{2EI_w} + \frac{hb}{4EI_f}$	$\frac{h}{EI_w} + \frac{b}{4EI_f}$
Case III	$\frac{h^3}{3EI_w} + \frac{h^2 b}{12EI_f}$	$\frac{h^2}{2EI_w} + \frac{hb}{12EI_f}$	$\frac{h}{EI_w} + \frac{b}{12EI_f}$

2.21

Substituting δ_u, $\delta_{u\phi}$, δ_ϕ in the expressions for C_1, C_2 and C_3, Equation 2.20 can be simplified to:

For Case I (and for $I_w = I_f$):

$$T_a = \frac{1}{1 + \frac{RI_p}{h^2 A} + S\frac{y_o}{h}} \qquad 2.22$$

where $$R = \frac{15 + 30(\frac{b}{h}) + 9(\frac{b}{h})^2}{(2 + 3\frac{b}{h})^2}$$

$$S = \frac{b(1 + \frac{b}{h})}{2 + 3\frac{b}{h}}$$

Expressions for Cases II and III can be easily derived. The expressions obtained however are still too complex and cumbersome for design use, although sufficient for detailed structural analysis. Douty showed, however, that R and S become asymptotic to 1.0 and 2.0, respectively, as the ratio b/h increases (see Figure 2.5). He showed that it is conservative and expedient to consider the case b = h. Thus, further simplifying for the three cases with b = h:

$$\text{Case I:} \quad T_a = \frac{1}{1 + \frac{2.16}{h^2}\frac{I_p}{A} + \frac{2.4\,y_o}{h}} \qquad 2.23a$$

$$\text{Case II:} \quad T_a = \frac{1}{1 + \frac{2.63}{h^2}\frac{I_p}{A} + \frac{2.57y_o}{h}} \qquad 2.23b$$

$$\text{Case III:} \quad T_a = \frac{1}{1 + \frac{3.24}{h^2}\frac{I_p}{A} + \frac{2.8y_o}{h}} \qquad 2.23c$$

From examination of the term μ_n in Equation 2.19, T is highly dependent on L for low values of L. μ_n ($= C_1L^4/n^4\pi^4EI_y$) becomes dominant as L/n increases. At the transition point:

$$L = L_{lim} = \pi \sqrt[4]{EI/C_1} \qquad (n = 1) \qquad 2.24$$

For Case I, C_1 is computed using the applicable values of δ_u, δ_ϕ and $\delta_{u\phi}$ to give:

$$C_1 = \frac{6EI_t}{h^3}\left(\frac{2h + b}{h + 2b}\right)$$

For $b = h$ and $I_t = t^3/12$

$$L_{lim} = \pi\sqrt[4]{2I_y(h/t)^3} \qquad 2.25$$

Douty did a numerical investigation by computer of Equation 2.19 for several shapes representing Case I for varying lengths and n = 1 to 4 for each of the length. Results for one shape with the dimensions indicated is as shown in Figure 2.6. Other results showed similar asymptotic behavior of the curves indicating for Case I, the expression for L_{lim} is a good approximation. Above L_{lim}, T becomes quite independent of L and is reasonably equal to T_a.

The problem of the stability of the effective column on elastic foundation taking the torsional weakening of the flange into consideration is finally reduced to the following:

$$P_{cr} = T\left(1 + \frac{\beta L^2}{\pi^2 P_e}\right)P_e \quad \text{when } \beta L^2/P_e \leq 30 \qquad 2.26$$

$$P_{cr} = T\left(0.60 + 0.635\sqrt{\frac{\beta L^2}{P_e}}\right)P_e \quad \text{when } \beta L^2/P_e > 30 \qquad 2.27$$

T, the torsional reduction factor is determined as follows:

$$T = T_o = \frac{h}{h + 3.4y_o} \quad \text{if } L \geq L_{lim} \qquad 2.28$$

$$T = T_o\left(\frac{L}{L_{lim}}\right) = \left(\frac{h}{h + 3.4y_o}\right)\left(\frac{L}{L_{lim}}\right) \quad \text{if } L < L_{lim} \qquad 2.29$$

where $L_{lim} = \pi\sqrt[4]{2I(h/t)^3} = 3.7\sqrt[4]{I(h/t)^3}$

y_o = distance from the centroid of the equivalent column to its shear center

h = distance from the tension flange to the centroid of the equivalent column

For the case where the beams are braced at large distances, the following expression for P_{cr} may be used:

$$P_{cr} = T_o \sqrt{4\beta EI} \qquad 2.30$$

Equation 2.28 for T_o is the expression further simplified from Equation 2.23a, developed by the AISI and the one in use in its Design Manual.[1] Equation 2.29 represents the linear interpolation $T = LT_a/L_{lim}$.

CHAPTER 3

EXPERIMENTAL INVESTIGATION

3.1 General

The general theory of laterally unbraced compression flanges is quite involved as was discussed in the preceding chapter. In order to bear out the theory and simplifying assumptions, and to test the reliability and/or validity of the treatment of laterally unbraced compression flanges for diaphragm-braced beams, a series of tests was performed. The rationale behind this series of tests was to restrict variables to the minimum: hence the testing of simple spans and single bay assemblies.

3.2 General Procedure

The experimental investigations conducted were to examine the ultimate load capacity together with the relevant parameters involved, of Z-section purlins assembled as roof systems with galvanized panels. The loading is to simulate uplift load due to wind on the roof system. Several purlin sections were made available by two manufacturers who also provided galvanized panels and their required fasteners. Two sets of tests were performed for each purlin-section. These are referred to as vacuum tests and beam tests. The details are described below. The choice of the Z-section purlins is essentially due to the common usage of this type of section as roof purlins in industrial-type metal buildings.

3.3 Vacuum Tests

A series of tests referred to as vacuum tests were carried out for each purlin section. Two twenty foot sections of the same purlin were assembled with galvanized roof panels to form the roof. This length was chosen to represent the portion of the purlins in the exterior span of a continuous purlin assembly. The distance between the exterior support and the first inflection point in the common case of twenty-five foot span purlins is about twenty feet. The purlins lie horizontal and parallel at five feet apart. The panels were screwed to the purlins using self-tapping screws for purlins already provided with prepunched holes. For purlins without prepunched holes, self-drilling screws were used. The screws were at one foot spacing. An overlay of polyethylene sheeting was provided between the purlins and the panels, and was taped to the floor before testing. A vacuum suction was then applied using a workshop vacuum cleaner. Two valves were provided to control the required vacuum suction. The applied pressure load was measured using a water manometer.

Figure 3.1 shows the overall view of the purlin assembly, and Figure 3.2 gives the dimensional details. The panels used has the cross-sectional dimensions shown in Figure 3.6. It should be noted that the initial assembling of the roof assembly was done in the 'correct' position, i.e., the panels were on top of the purlins. The assembly was then inverted, the polyethylene sheeting taped to the floor, thus enabling a convenient

method of applying the uplift load. Reference to these tests are designated by the letter 'V' followed by a number signifying the sequence, e.g., test V3 means the third vacuum test done.

With the exception of the first vacuum test (test V1) which had rigid end supports, all the tests had simply supported ends. The simple supports were provided by placing rollers under the support I-beams at both ends of the purlins to which they were connected to by using only one bolt not tightly bolted. The rigid end conditions for test V1 were obtained by attaching the purlin ends by means of two bolts to the end supports which were not free to rotate.

The initial sweeps at midspan of the top web to flange junction of the purlins were measured relative to the same point at the purlin ends (see Figure 3.7). The strains and deflections under load were measured at midspan. The strains were measured using strain gages located mainly at the top flange region i.e., the compression flange. The horizontal and vertical displacements were measured by dial gages suitably located. The relative locations of the strain gages are as shown in Figure 3.9. All the tests were continued until failure occurred in one or both of the purlins.

3.4 Beam Tests

A parallel part of the experimental program was a series of tests on similar Z-section purlins as in the vacuum tests referred to as the beam tests. Two twenty feet sections of the

same purlins were connected together along their bottom flanges by sixteen channel sections at one foot apart. This arrangement provided a bracing system for the purlins. At one-fifth points along the spans, a sixteen-inch small I-section was used instead of the channel sections. These were the locations of the applied load. The ends of the beam test assembly were simply supported with rollers.

A four point loading system was applied to the bottom flanges parallel to the web. The loads were applied via the four small I-sections connected to the bottom flanges. The test was done using a universal testing machine. Figure 3.3 gives an overall view of the beam test assembly under load. Figure 3.4 shows a schematic diagram of the assembly and some dimensions.

As in the vacuum tests, the initial sweeps of the purlins at midspan were measured prior to testing (see Figure 3.8). Also, the strains and deflections were obtained at similar locations at the midspan.

3.5 Rotational Restraint Tests

A series of tests were conducted to determine the rotational restraint provided by each purlin-panel system. For each purlin section, a three feet section was obtained and connected to a section of the roof panel with the screws as used in the vacuum test assembly. The procedure followed was that proposed by Haussler.[9] A schematic diagram of the assembly is shown in Figure 3.10. An initial test was done according

to a modification by Peköz[11] of a procedure used by Celebi[4] and used for similar purposes as this study. Both procedures gave near identical results for the rotational factor, F, in the initial tests. However, the Haussler method was preferred since it is simpler and was used in subsequent tests.

The tests were continued until excessive rotation of the purlins and substantial buckling of the roof panels were observed. Care was taken to measure the gage and load direction heights at each loading as these differ substantially as the purlin rotations increase.

Some measure of the rotational restraint on the purlins in the beam test set-up was needed. The F value for these tests would evidently be different from that of the vacuum tests. A two feet section of a purlin was taken. Two channel sections used for bracing in the beam tests were bolted at one end each to the purlin. Figure 3.11 shows the set-up used, which is a modification of the Haussler procedure used for the purlin-panel rotational restraint tests described above. The channels are rigid, hence the presence of the small I-beams at one-fifth points along the actual beam test assembly should not alter the rotational restraint provided significantly.

3.6 Shear Rigidity Tests

The shear rigidity of the roof panels was determined using a method called the centilevel shear test used by Peköz,[11] among others. A schematic diagram of the assembly is shown in Figure 3.12. The specimens for the two tests done were the

two halves of the purlin-roof panel assembly of the vacuum test V3. The results of these tests are shown graphically in Figure 4.24.

3.7 Material Properties

Three tensile coupons were prepared according to ASTM standards from lightly stressed regions of the failed purlin for each purlin type used in the vacuum tests. The average of the tensile yield stresses obtained are presented in Table 3.1.

3.8 Section Dimensions

The purlin section dimensions were determined using a procedure that has been used in the metal building industry. This involves obtaining a portion from each purlin about eighteen inches long, and squaring one end reasonably flat. Next, a profile of the purlin was obtained by placing the flat end on a piece of tracing paper, and paint sprayed lightly around the perimeter of the section. The dimensions of the purlin were then conveniently measured from the image obtained. For the same purlin type, the dimensions are averaged and presented in Table 3.2.

3.9 Discussion of Test Results

3.9.1 Test Results

Under ideal circumstances, one would expect the purlin failure to be due to buckling in the compression region and in the vicinity of the midspan. The tests conducted showed

buckling in essentially three ways: (i) buckling at the compression flange-web junction at midspan or at the prepunched holes used for sag rods in an actual roof assembly, (ii) buckling at the web compression region at midspan or at the prepunched holds, and (iii) buckling at the lip-stiffener of the compression flange. These are shown in Figures 3.13 to 3.18, and a summary of the results is presented in Table 3.3.

Details of the failures observed are as follows:

Vacuum Tests:

Test V1: --Purlin type A. Failure occurred in one purlin by local buckling at 4.8 in. from the midspan where the prepunched holes were. The purlin ends were fixed, hence a high failure load obtained and the purlin maximum rotation was comparatively small (see Figure 3.13).

Test V2: --Purlin type B. Local buckling occurred in one purlin at the hole location 1.6 in. from midspan. Yielding was observed as failure load was approached resulting in large lateral deflections of both purlins. The vertical deflection of the assembly was also observed to be large (see Figure 3.15).

Test V3: --Purlin type D. Local buckling occurred in one purlin at the web and at midspan. It occurred after some observable yielding of the failed purlin. This test was one of two that showed the failure described, i.e., at the web only.

Also, from this test onwards care was taken to ensure that the purlins' holes are symmetrical about their midspan (see Figure 3.17).

Test V4: --Purlin type C. Local buckling occurred at 6 in. from midspan at the location of prepunched holes of one purlin. No noticeable yielding was observed (see Figure 3.16).

Test V5: --Purlin type A. This was essentially a duplicate test for purlin A, except that the ends of the purlins were simple i.e., free to rotate. The failure occurred in one purlin by local buckling at the compression flange-web junction. The failure load was lower, and rotations and deflections larger than in test V1.

Test V6: --Purlin type E. Self-drilling screws were used on this purlin type for panel connection. The failure occurred at midspan by flange lip-stiffener failure of one purlin followed by the other. The stiffeners were twisted outwards until buckling occurred (see Figure 3.18).

Test V7: --Purlin type B. This was a duplicate of test V2 to verify the results obtained earlier. Failure occurred at the prepunched hole location by local buckling in the web compression region of one purlin.

Beam Tests

Test B1: --Purlin type A. Failure occurred by sudden local buckling of the compression flange-web region at the location of the prepunched holes of one purlin. This was 15 in. from the midspan of the purlins (see Figure 3.14).

Test B2: --Purlin type A. One of the two purlins used in this test was the purlin that did not fail in test B1. This purlin failed in this test in the same manner as in test B1, 12 in. from the midspan. The failure load was lower.

Test B3: --Purlin type A. This is a duplicate of test B1. Failure occurred in one purlin by local buckling as in test B1, but at midspan. The failure load was nearly the same as in test B1.

Test B4: --Purlin type D: Failure occurred by buckling of the flange lip-stiffener of one purlin. The other purlin deflected considerably and was restrained by the test machine column. It is envisaged that failure would have occurred in this purlin by local buckling of the compression flange-web region had not it been for the restraint described. The failure was violent (see Figure 3.17).

Test B5: --Purlin type B. Failure occurred in one purlin at midspan after large lateral deflections

indicating yield. Failure was of the local buckling of the compression flange-web-type.

Test B6: --Purlin type C. Failure occurred in one purlin at 6 in. from midspan at the prepunched hole location. The failure was as in test B1. However, at failure, the other purlin reacted violently and showed failure in the lip-stiffener of the compression flange (see Figure 3.16).

Test B7: --Purlin type E. The failure occurred in one purlin by buckling of the compression flange lip-stiffener. Small lateral deflections were observed as was the case in test V6 for similar type purlin (see Figure 3.18).

3.9.2 Discussion of Vacuum Test Results

The failures in the tests conducted occurred mainly in the compression flange-web region of one purlin. With the exception of test V3 and V7 where the local buckling was observed to be at the webs only, it was difficult to observe whether the local buckle appeared initially in the flange or the web as it happened suddenly in most cases. For tests V2, V3 and V7, the purlins used were of low flange-width to thickness (w/t) ratios (purlin types B and D with w/t = 24.3 and 22.3, respectively).

The approaching failures were easily anticipated by the large lateral deflections observed with each load increment,

indicating yield. In general at failure, the purlins deflected laterally in a continuous manner at constant load until local buckling occurred at the location of high compression stress.

The purlins of high w/t ratios, namely purlin types A, C and E all failed by sudden local buckling in the compression flange-web region in the case of purlin types A and C, or at the lip-stiffener of the compression flange in the case of purlin type E.

It is interesting to note the failure of purlin type E. The initial sweep (see Figs. 3.7 and 3.8) of this purlin type tended to be negative as defined by Figure 4.2 Hence, the twisting outwards of the lip-stiffener of the compression flange began almost immediately upon loading. It is envisaged that a higher load could be obtained if the initial sweep had a small positive value. For the other purlin types, the tests did indicate a tendency to buckle at the prepunched holes. The absence of these holes should give higher ultimate load capacities for these purlins.

3.9.3 Discussion of Beam Test Results

The failure modes in the beam tests conducted are generally of the same type as those in the vacuum tests. For the various purlin types, the behavior at failure was the same. The beam tests thus model the behavior in the vacuum tests adequately. Considering the two types of tests as a whole it can be observed that the purlins of low w/t ratios tended to buckle locally at midspan, whereas those of higher w/t ratios tended to do so at the location of the prepunched holes.

CHAPTER 4

ANALYSIS OF RESULTS

4.1 General

The analysis of diaphragm-braced purlins is a complex problem. Among other procedures for analysis, that of the AISI Cold-Formed Steel Design Manual[1]-Part III, Section 3, was tried. The basis for this procedure is the study by Douty[6] which has been described in some detail in Chapter 2. The studies presented by Desmond[5] and Yu[13] will also be utilized to assist in understanding the analytical and design problem and arrive at suitable design recommendations. An available computer program based on analytical studies by Celebi[4] and modified by Peköz[11] was also used to obtain theoretical values to compare the test data with.

4.2 Background for Evaluation of Results

4.2.1 AISI Design Manual (Part III, Section 3) Approach (Douty Approach)

Part III, Section 3 of the American Iron and Steel Institute (AISI) Cold-Formed Steel Design Manual[1] (henceforth referred to as the Douty approach), is the basis used for analyzing the quantitative information obtained from the experimental program of this study. The Douty approach requires the following:

1. The location of the neutral axis is determined for the purlin section. The "equivalent column" is defined as the portion of the beam from the extreme compression fiber to a

level which is $(3C_c - C_t)/12C_c$ d distance from the extreme compression fiber. Here, C_c and C_t are the distances from the neutral axis to the extreme compression and tension fibers respectively, and d is the depth of the purlin section.

2. The shear center is located for the distance y_o measured parallel to the web from it to the centroid of the equivalent column (see Figure 4.1). Approximation is allowed, for example, if the flanges of the channel-shaped compression portion of the section are of unequal width, one can take w as the mean of the two flange widths. More exact methods of analysis can be used to locate the shear center.

3. The spring constant, β, is then determined. This is done by taking 1 inch long portion of the purlin, apply a force of 0.001 kip perpendicular to the web at the level of the column centroid, and compute the corresponding lateral deflection D of that centroid. The spring constant is then

$$\beta = 0.001/D$$

4. The torsional reduction factor, T_o, is computed as follows:

$$T_o = \frac{h}{h + 3.4y_o}$$

where h is the distance from the tension flange to the centroid of the equivalent column, and y_o is as defined in 2.

5. For the flange braced at less than two points, (which is the case for this study), the critical load of the equivalent column, P_{cr} is computed as follows:

$$P_{cr} = T_o\sqrt{4\beta EI}$$

where I is the moment of inertia of the equivalent column about its y axis parallel to the web, β is as defined in 3, and E is the modulus of elasticity. If the flange is laterally braced at two or more points, P_{cr} is computed as in p. 19 of Part III of Reference 1.

6. The slenderness ratio of the equivalent column is then determined as follows:

$$\left(\frac{KL}{r}\right)_{eq} = k\sqrt{\frac{\pi^2 E}{P_{cr}/A_c}}$$

where k is an experimental correction factor for the post-buckling strength of the section and equals 1/1.1, and A_c is the cross-sectional area of the equivalent column. With E = 29500 ksi, the equation reduces to:

$$\left(\frac{KL}{r}\right)_{eq} = \frac{490}{\sqrt{P_{cr}/A_c}}$$

7. The axial stress F_{al}, at the level of the centroid of the equivalent column, corresponding to $(KL/r)_{eq}$, is computed from the equations in paragraph (a) of Section 3.6.1.1 of Reference 1 (using Q = 1 and K = 1). These equations, without the factor of safety, are:

For $\frac{KL}{r} \leq \sqrt{\frac{2\pi^2 E}{F_y}}$

$$F_{al} = F_y - \left(\frac{F_y^2}{4\pi^2 E}\right)\left(\frac{KL}{r}\right)^2$$

$$\text{For } \frac{KL}{r} > \sqrt{\frac{2\pi^2 E}{F_y}}$$

$$F_{a1} = \frac{\pi^2 E}{(KL/r)^2}$$

A note about the above formulas is in order. The value of $\sqrt{2\pi^2 E/F_y}$ is the limiting KL/r ratio corresponding to a stress equal to $F_y/2$ in flexural column buckling. When the KL/r ratio is greater than this limiting ratio, the column is assumed to be governed by elastic buckling, and when the KL/r ratio is smaller than this limiting ratio, the column is to be governed by inelastic buckling. In the actual design formulas, the factor of safety of 23/12 is used.

8. The compression bending stress in the extreme compression fiber, F_{b2}, is then computed by extrapolating linearly the axial stress F_{a1}:

$$F_{b2} = \left(\frac{C_c}{Y_c}\right) F_{a1}$$

where C_c is the distance from the neutral axis of the beam to the extreme compression fiber, and Y_c is the distance from the neutral axis of the beam to the centroid of the equivalent column. In the Design Manual, F_{b2} is multiplied by a factor of 1.15 being the ratio of the factor of safety used for column buckling (23/12) to the factor of safety used for beam yielding (5/3), F_{a1} having the factor of safety of (23/12) applied to it beforehand.

4.2.2 Discussion of the Douty Approach

In the second step of the Douty Approach, the computation of y_o, the distance from the centroid of the compression area to the shear center, parallel to the web, is easily established for a channel-shaped configuration with equal flanges. A reasonable approximation can be made for a channel with unequal flanges by taking the flange width as the mean of the two unequal flanges. For a channel with one flange angled, the required shear center distance is computed more accurately by a method as presented in Appendix A. It is observed that the computed values of y_o by this method is smaller as compared to the values obtained by the approximate method suggested by the Douty Approach. For the same section, this leads to a higher computed stress being obtained.

In the third step of the procedure, a spring constant, β, is computed. This spring constant represents the rotational restraint provided by the section when subjected to an applied moment. In the procedure for computing β suggested by the Douty approach, a one inch long portion of the member is isolated, a force of 0.001 kip is applied perpendicular to the web at the level of the column centroid, the corresponding lateral deflection D of that centroid is computed, β is then equal to 0.001/D. This study involves purlins braced continuously by panels. There is a restraining action by the panel on the rotation of the purlin section, hence the value of β must reflect this action. An analytical procedure would be too

complex for ease of computation. Two experimental procedures are available for a reasonably accurate determination of the rotational restraint factor, F, from which β can be easily computed for sections such as the Z-sections used in this study.

$$\beta = F/d_r^2$$

where d_r is the distance from the centroid of the equivalent column to the axis of rotation, which for the Z-section is the web-tension flange corner.

The procedures as used by Peköz and proposed by Haussler[9] were discussed in Section 3.5. The significance of using different values of F for a particular cross-section is discussed further in Section 4.3.4.

The concept of effective width of a plate element under compressive stress is well established in cold-formed steel design. Winter's commentary on the AISI Cold-Formed Steel Design Manual (Part II of Reference 1) gives a summary of this concept as currently used by the AISI. This concept is of great significance in the procedure discussed since the ultimate load capacity of a purlin depends on the sectional modulus used. Other computations involve the determination of the centroid of the compression area (equivalent column) and its moment of inertia. These geometrical parameters depend on the amount of the compression flange considered. In general, the Douty approach is currently applied assuming the compression flange as fully effective. However, in the evaluation of the test results

in Section 4.3, the use of the effective section properties were also tried. The work of Desmond[5] was used in this regard since it uses the concept of effective width for a stiffened as well as partially stiffened and unstiffened plate elements.

4.2.3 Adequacy of Compression Elements

The material discussed in this section is drawn from the study by Desmond[5] on the behavior and strength of thin walled compression elements with longitudinal stiffeners. Desmond presented the stiffener requirements and design procedures for predicting effective widths of edge and intermediately stiffened elements. He adhered to existing design procedures of the AISI Design Manual[1] as far as possible. In his design method, the flange stiffened by an edge stiffener is examined, depending on its (w/t) ratio and the yield stress, whether it is fully effective as an unstiffened element, fully effective when adequately stiffened or it is in the post-buckling range. The last two categories require adequate stiffening for which formulas are provided.

The edge stiffeners are then examined for their adequacy. For an adequately stiffened flange, the flange and stiffener effective widths are then computed. For a partially stiffened flange, its effective width and the reduced area of the partial stiffener are determined. From the reduced area of the partial stiffener, the reduced length is obtained. The reduced length is treated like an effective width for computations of section properties. All the effective width equations are drawn from Winter's[1] equivalent width relationship or modifications of it.

Essentially, Desmond presented modified values of the buckling stress coefficient. A summary of Desmond's design method is presented in Appendix B.

4.3 Evaluation of Results

4.3.1 Test Ultimate Loads

The ultimate loads for the vacuum tests and the beam tests are presented in Table 3.3. A uniformly distributed load was applied in the vacuum tests. The maximum moment occurs at midspan and is equal to $wl^2/8$ where w is the uniformly applied load per linear foot of purlin, and l is the purlin span. For a section modulus S of a purlin, $w_v = 8\sigma S/l^2$, where σ is the stress in the extreme fibers and w_v is the distributed load corresponding to stress σ. A four point loading is applied in the beam test (see Figure 3.4). By considering the maximum moment at midspan, the load per linear foot is $w_b = (20/3)\sigma S/l^2$. For the situation where the purlins in both tests have the same failure stress, $w_v/w_b = 1.2$. From an inspection of the ratios of the actual test values, the theoretical ratio does not hold, the mean being 0.83. However, w_b/w_v has a mean value of 1.22. A possible explanation is that in the actual tests, the purlins of the same section do not reach the same failure stress in the vacuum as well as the beam tests, as assumed above. It is expected that since the rotational restraint factors, F, for the same purlin section in the two set-ups, vacuum and beam, are different, (the latter is expected to be higher), the ultimate stresses, hence ultimate loads are predictably no longer in the

ratio of 1.2. Further, the purlins were not subjected to pure flexural action.

4.3.2 Test Ultimate Stresses

The ultimate stresses (computed from the last recorded strains before failure occurred) reached in the vacuum and beam tests are presented in Table 4.1. Load-strain curves for the five purlin types tested are presented in Figures 4.3 to 4.12. The locations of the strains recorded are indicated by numbers corresponding to those in Figure 3.9. All the tests indicated the highest stresses (corresponding to the highest strains) occurred at locations 4 and 5 on one purlin, or the corresponding locations 9 and 10 on the other purlin in the pair, depending on which purlin failed. The exception was for tests on purlin type E, where the failures were due to local buckling of the lip-stiffener of the compression flange. Both purlins in test V6 showed high stresses at similar locations 2 and 7, and 5 and 10 (at top of web). In test B7, one purlin showed highest stress at location 1 (at lip-stiffener) on one purlin and at location 10 (at web) on the other purlin. It is interesting to note that the initial sweeps of the purlins in test V6 are both negative (see Figure 3.7), whereas that of B7 are both equal and opposite.

In the vacuum tests, the failures occurred at stresses varying from 45.3 to 87.3 percent of yield stress (see Table 4.1). One test of purlin type B failed at yield, another at 79.2 percent of yield stress. Generally, purlin types with high flange width to thickness ratios failed at lower stresses

(average of 62.2 percent of yield stress) than that of low ratios, i.e., thicker purlins (average of 83.2 percent of yield stress). The failures in these tests than are governed by buckling of the plate elements rather than by yielding, as can be expected.

The load-stress curves of the highest stressed location for each purlin type in the vacuum tests were compared with the curves obtained for the same location using an available computer program (due to Celebi[4] and Peköz[11]). These curves are shown in Figures 4.13 to 4.17. With the exception of curves for purlin type B, all the curves show fair correspondence, less so at higher loads. The test stresses were computed directly by multiplying the strains with the modulus of elasticity (29500 ksi). These would then be comparable directly with the computer program results where elastic behavior is assumed for any load.

4.3.3 Test Ultimate Rotations

The maximum rotations computed from deflection measurements are presented in Table 4.2. The load rotation curves for the two types of tests are presented in Figures 4.18 and 4.19. The behavior of purlin type E in the vacuum test, as have been pointed out in this report previously, is somewhat different from the other purlin types. Due to the compression area twisting outwards (i.e. in the negative direction according to Figure 4.2), which led to the failure of the lip-stiffener, it did not show the torsional behavior exhibited by the other purlin types. The load-rotation curve is linear up to failure,

with the maximum rotation only of the order of one quarter of the other purlin types.

The maximum rotations, with the exception of that for purlin type E for the vacuum tests and purlin types D and E for the beam tests, are fairly close with one another. The mean is 0.243 radians with a standard deviation of 0.029. It has been suggested that a failure criteria based on ultimate rotations could be formulated.

4.3.4 Rotational Restraint Factor, F

An important factor in considering the ultimate strength of the purlins is the rotational restraint the roof panels provide when the whole assembly is loaded. The degree of rotational restraint is dependent to a certain degree on the cross-sectional dimensions of the purlins, the rigidity of the panels to which they are connected and the nature of the connection. The last two factors were different for the vacuum and beam tests. These have been described in the assembly details for the two types of tests in Chapter 3, and is further discussed below.

Three initial tests to evaluate the rotational restraint factors F, were done according to the method used by Peköz,[11] all the remaining twelve tests were conducted using the procedure proposed by Haussler[9] (see Section 3.5). The results of the tests (1) with the purlins diaphragm-braced and (2) with the purlins braced with sixteen inch length channel sections are presented in Figures 4.20 to 4.22. The rotational deformation of the purlin web with respect to its bottom (tension)

flange was also computed from the deflections measured at a point near the mid-point of the web, parallel to the bottom flange. The ratios of these rotations to the total rotations were computed and are presented in Table 4.3.

The rotational restraint factor, F, was computed for each purlin and test type by obtaining the moment M corresponding to the maximum large-scale test rotation. M is then divided by the maximum test rotation. This was done since the moment-rotation curve is nonlinear. The value of F increases with increasing rotation. The F values are presented in Table 4.2.

It is generally observed that the F value is higher for a purlin section that has a low web depth to thickness ratio (H/t). This is indicated in a plot of H/t vs. F shown in Figure 4.23. Also from Table 4.3, it is observed that generally, purlin types of high H/t ratios suffer more cross-sectional rotational deformation than those of lower H/t ratios. Purlin type E is consistently enigmatic in its behavior, even in this case since in both the diaphragm-braced and channel-braced F tests, its web cross-sectional rotational deformations (per total rotations) are higher although its H/t ratio can be considered as intermediate between those of B and D, and A and C.

4.3.5 Shear Rigidity of Panels

The knowledge of the shear rigidity of the panels is required for use in the computer program computations. The shear rigidity, Q, computed from Figure 4.24 is 30 kips, calculated according to a method given by Apparao and Errera.[2]

This value is somewhat lower than those obtained by Peköz.[11] There are intentional differences in the framing of the panels in the tests done in the two cases (see Figure 68 of Reference 11 and Figure 3.12 of this report).

4.3.6 Initial Sweeps of Compression Flanges

The initial sweeps of the compression flange-web junction of the purlins were measured relative to a straight line joining the two ends (for the same locations) at the supports. The values obtained are presented in Figures 3.7 and 3.8 for the vacuum and beam tests respectively. The initial sweep seems significant in predicting which purlin out of the two in the test assembly would fail and what kind of failure would occur, namely local buckling in the vicinity of the compression flange-web area or local buckling at the lip-stiffener of the compression flange. The purlin that had the larger initial sweep of the two generally tended to fail first. Local buckling at the web-flange junction occurred when the initial sweep was positive (see Figure 4.2 for deflection sign convention used). This type of failure occurred in most types of purlins tested and in these purlins the initial sweep was in the negative direction. This was the case for purlin type E in both the vacuum and beam tests. It must be added that comparing with the other purlin type whose H/t ratio is fairly close, the ultimate load obtained for purlin type E was low. It is envisaged that besides the nature of the initial sweep discussed above, purlin type E has a comparatively longer flange width and shorter lip-stiffener which probably contributed to the lower ultimate strength reached.

4.4 Ultimate Loads

4.4.1 General

The tested purlin sections, with measured dimensions as in Table 3.2, were analyzed for ultimate loads using various relevant sections of the current AISI Specification for the Design of Cold-Formed Structural Members (Part I of Reference 1), henceforth referred to as the Specification, as well as the Douty approach (Part II, Section 3 of Reference 1). Specifically, the effective widths of flanges were used for computation of the section properties necessary for determining ultimate loads. The adequacy of the lip-stiffeners were checked. The procedure was repeated using the findings of Desmond regarding flange and stiffener adequacy.

4.4.2 Computations Based on Full Widths of Flanges

The procedure outlined in Section 4.2.1 (the Douty approach) was used in computing the ultimate stress at the extreme fibers under compression. From consideration of the loading system used, uniform loading for the vacuum tests and a four point loading for the beam tests, the ultimate load was computed. Using basic mechanics, the load per linear foot of purlin, q in the vacuum tests is:

$$q = 8\sigma S/L^2$$

where σ = ultimate stress

S = section modulus of purlin

L = span length

For the loading in the beam test set-up, the total load, W, is:

$$W = \frac{20}{3} \cdot \frac{\sigma S}{L}$$

The ultimate loads were computed based on the full widths of the purlin dimensions for determination of section properties. This assumes that particularly the compression flange is fully effective. The computations were done on the basis of sharp corners at the web-flange and flange-stiffener junctions. From Table 3.2, it is observed that the corner radius to thickness ratios are generally of the order of four or greater. Hence, this approximation relieves computations of the corners.

The computed ultimate loads were compared with the ultimate test loads for each purlin type. The results are tabulated in Tables 4.6 and 4.7 (Column a) for the vacuum tests and beam tests respectively. These computations used the tensile coupon test yield stress as ultimate stress. Also, the rotational restraint factor, F, has different values for each purlin type. Further, for each purlin type, the F values are different for the case when it is diaphragm braced and when it is rigidly braced as in the beam test setup.

A similar series of computations were done using F_{bw} given below, as ultimate stress:

$$F_{bw} = [1.257 - .000508\ (h/t)\ \sqrt{F_y}]\ F_y$$

The above equation is proposed by Yu[13] for the maximum compressive stress in the web for beams with unstiffened compression flanges. For the purlin sections used, F_{bw} is presented in

Table 4.4. The load ratios are presented in Tables 4.6 and 4.7 (Column b).

4.4.3 Computations Based on Effective Widths (AISI)

The relevant sections of the Specification used here are Section 2.3.1.1 for effective width determination:

Flanges are fully effective up to $(w/t)_{lim} = 221/\sqrt{f}$

For flanges with w/t larger than $(w/t)_{lim}$

$$\frac{b}{t} = \frac{326}{\sqrt{f}} \left[1 - \frac{71.3}{(w/t)\sqrt{f}}\right]$$

where w/t = flat-width ratio

b = effective design width, inches

f = actual stress in the compression element computed on the basis of the effective design width, ksi.

and Section 2.3.2.1 for edge stiffener requirements.

The minimum moment of inertia:

$I_{min} = 1.834t^4 \sqrt{(w/t)^2} - 4000/F_y$ but not less than $9.2t^4$

where w/t = minimum allowable moment of inertia of stiffener about its own centroidal axis parallel to the stiffened element, in^4.

Using the above, the effective widths were computed using the yield stress, F_y, as the ultimate stress. In computing I_{min}, the fact that the lip-stiffeners in the test purlins were angled at less than right angles with the flange was taken into account. The results of these computations are presented in

Table 4.8.

The computed values of adequate and actual moments of inertia show that using the full flange width, only purlin type C is adequately stiffened. The others were as much as 56 percent less than adequate. Computations showed that increasing the lip-stiffener angle would increase the required moment of inertia. For purlin type E however, increasing the lip angle to 90 degrees would not help. A longer lip-stiffener is required to meet the minimum stiffener requirements.

Using the flat flange width as a basis for computing the minimum stiffener requirement showed that all the purlin types except E are adequate. It has been shown in Section 4.4.2 that since the corner radius to thickness ratios are generally larger than 4, computations based on sharp corners are reasonable. Hence, the total widths were preferred in the computations. The Specification states that in order that a flat compression element may be considered a stiffened compression element, the stiffeners must have the minimum moment of inertia as given above. This being the case, one can treat all the purlin types tested, except C, as being unstiffened. The Specification does not provide for obtaining the effective width of an unstiffened element. This will be considered in Section 4.4.4.

4.4.4 Computations Based on Desmond's Flange and Stiffener Adequacy Requirements[5]

Desmond's study was briefly discussed in Section 4.2.3 and his procedure for the determination of flange and stiffener adequacy and formulas for effective widths are presented in

Appendix B. Using this procedure then, effective widths of the compression flanges, and effective widths of adequate lip stiffeners or reduced length of partial stiffeners as the case may be, were computed. Both the total widths and flat widths of the compression flanges and lip-stiffeners were used as the bases for the computations. The computations were done using F_y (the tensile coupon test yield stress) as ultimate stresses. The computed widths are presented in Table 4.9. These computed widths were used for the compression flange area in computing the section properties required in the Douty approach for determining ultimate stresses in laterally unbraced compression flanges. The ultimate loads were then obtained as in the previous computations, and compared with the test ultimate loads. The ratios of the computed and ultimate loads were obtained for the four cases as given in Tables 4.6 and 4.7 (Columns c, d,e and f).

Desmond also gave provisions for the case when the compression element is unstiffened (Refer Appendix B). To obtain a lower bound for the computed strength the width of the compression flange was also taken as the total of the actual length of the flange and the lip-stiffener length. Equation B.18 of Appendix B was then used to obtain the flange effective widths for the two cases using F_y and F_{bw} as ultimate stresses. These widths are given in Table 4.7. It is interesting to note that the computed effective widths vary from 28.3 to 46.7 percent of the actual widths considered which are rather small.

The ultimate loads were obtained as before and compared with the test loads. These load ratios are presented in columns (g) and (h) of Tables 4.6 and 4.7. With these computations, the series of computed ultimate loads for the five tested purlin types are completed.

4.5 Discussion of Analysis

The analyses undertaken in the preceding sections were done to establish a reliable failure criteria for cold-formed steel Z-purlins. Although the analyses were done based on experimental data that were obtained under uplift load conditions, any prediction of ultimate loads should be generally applicable due to the point symmetric nature of the Z section. Any flexural action of the purlins would introduce torsional weakening, hence reduce ultimate loads computed simply on the basis of only flexural beam action.

The ultimate stresses in the diaphragm-braced purlins at failure were below their yield stresses. The failures were due to local buckling of the plate elements at the compression flange-web junction or at the lip-stiffener of the compression flange, rather than by yielding. In the beam tests, the strains measured indicated that yielding occurred for purlin types B, C and D, although local buckling in the compression flange-web junction did occur in most cases.

Referring to Table 4.6, the mean, standard deviation and standard deviation/mean of the test load/computed load ratios were computed for each analysis type for the vacuum tests.

From column (a) of this table, purlin types A and B (depth 9.45 and 9.46 inches respectively) showed excellent correlation between observed and computed ultimate loads, allowing for slight conservatism, when full flange widths were used. The load ratios are low however, for purlin types C and D and lowest for purlin type E. Overall, a mean of 0.88 was obtained which is not a satisfactory correlation. Column (b) of the same table shows a slight improvement in the mean value, but still unsatisfactory. The use of a lower ultimate stress, F_{bw} (the maximum web stress - see Table 4.4), which underestimates the strength, does not help when full flange width was used.

An improved correlation between observed and computed loads was obtained when effective flange widths and effective widths of the lip-stiffeners, or reduced lengths of partial stiffeners as the case may be, were used in the computations. Analysis type (d) shows an overall mean of 1.01. This analysis used the maximum web stress, F_{bw}, as the ultimate stress. Ignoring the load ratio for purlin type E gives a mean of 1.05 for analysis type (c) which is satisfactory. Excluding results for purlin type E could probably be justified by the fact that its observed ultimate load compared with the computed load seems consistently small for the first six analysis types and by other considerations discussed variously in the preceding sections of this chapter.

Analysis types (e) and (f) used effective widths computed on the basis of flat flange and stiffener widths, and using the yield stress, F_y and F_{bw} respectively for ultimate stresses.

Slight improvements over analysis types (a) and (b) are indicated. Analysis types (g) and (h) used the effective widths of unstiffened compression flanges (which they were shown to be in Section 4.4.3). Both analyses are evidently very conservative to be of design use. The concept of partial stiffeners proposed by Desmond[5] would be more realistic for inadequately stiffened flanges.

Looking at the analysis for the beam test ultimate loads presented in Table 4.7, one can say that analysis type (f) shows good correlation between observed and computed ultimate loads. This analysis used effective widths computed from flat flange and stiffener widths and F_{bw} as the ultimate stress. However, again ignoring the load ratio for purlin type E, analysis type (c) gives a mean of 1.03 for the load ratios, which is good.

Inherent in all the analysis types for both vacuum and beam tests is the use of a unique rotational restraint factor, F, for each purlin type. Besides using an experimental procedure to determine F, a simple design method need yet to be established.

4.6 Summary

The analyses showed that the Douty approach as given in the current AISI Design Manual[1] (Part III, Section 3) on the design of laterally unbraced compression flanges is inadequate for the determination of ultimate strength of cold-formed steel Z-purlins. The use of effective widths for compression

flanges and effective widths of adequate stiffeners or reduced length of partial stiffeners as the case may be, as proposed by Desmond[5] gave a good correlation between observed and computed ultimate loads. Using the maximum web stress, F_{bw}, of unstiffened compression flange as proposed by Yu[13] provided slightly more conservative results. The value of the rotational restraint factor, F, to be used in the analyses is of significant importance.

CHAPTER 5

CONCLUSION

5.1 Summary of Results

The research described herein studied the ultimate strength of braced cold-formed steel Z-purlins subjected to uplift loads.

An experimental investigation was undertaken to obtain quantitative information. Five types of cold-formed steel Z-purlin were used in large-scale tests of two kinds: vacuum and beam tests. These purlin types have different flange width to thickness ratios. The tests were undertaken to determine the ultimate load capacity of the purlins. Experimental values of the rotational factors, F, were determined at least once for each purlin and test type. The information obtained from the tests conducted and the analyses done on them were reported in Chapter 3 and 4 respectively. Chapter 2 detailed a Cornell University study undertaken by Douty.[6]

The experimental results were analysed using the AISI (or Douty's) approach given in its Design Manual[1] (Part III, Section 3) and Desmond's[5] design method for edge-stiffened thin-walled compression elements. The AISI approach was found to be generally unsatisfactory in predicting the ultimate strength of the Z-purlins used. The analyses showed that the compression flanges and their lip-stiffeners cannot be treated as fully effective in most cases, especially for purlin types that have high flange width to thickness ratios. The AISI

approach as it stands lead to unconservative results. When used in conjunction with Desmond's design method however, which uses the concept of effective plate widths, the AISI approach was found to be able to predict ultimate strengths reasonably well. A more conservative result could be obtained by using Yu's maximum web stress, based on an unstiffened compression flange, as the ultimate stress in the design procedure given in the AISI Specification.

5.2 Recommendations

On the basis of the experimental results obtained and the analyses done through this research project, it is possible to recommend modifications to the current AISI Design Manual,[1] Part III, Section 3, which deals with the design of laterally unbraced compression flanges insofar as it is used to predict ultimate strengths of cold-formed steel Z-purlins.

The AISI Design Manual Part III, Section 3 can be utilized to determine the ultimate strength of Z-purlins, with the proviso that the compression flange and lip-stiffener be checked for their effectiveness by Desmond's design method as presented in Appendix B. The effective width of the compression flange and the effective width of the lip-stiffener or the reduced length of the partial stiffener, as the case may be, should be used. For a reasonably conservative prediction of ultimate strength, the maximum web stress as proposed by Yu[13] could be used as the ultimate stress instead of the yield stress.

Further, the rotational restraint factor, F, needs to be known, or at least a reasonably close approximation of it. Currently, the suggested method is by a simple test such as the method proposed by Haussler.[9] A convenient design procedure to obtain F is being studied at Cornell University.

5.3 Suggestions for Future Work

This study is limited to the determination of ultimate strength of cold-formed Z-purlins. The use of channel-section purlins is also common in metal building construction for similar applications as the Z-purlins. Hence, besides further confirmatory tests on the applicability of Desmond's design method in determining effective widths for use in the AISI Design Manual, Part III, Section 3, the ultimate strength of channel-section purlins under uplift loads need to be looked into.

Another important area to be looked into is a design procedure to determine the rotational restraint factor, F. An empirical relationship between web depth to thickness ratio, yield stress, and F seems reasonable, should further quantitative information be available from extensive testing to justify it.

APPENDIX A

LOCATION OF SHEAR CENTER FOR EQUIVALENT COLUMN

For the purpose of the computations detailed in Chapter 4, it is necessary to obtain the distance y_o, the vertical distance from the centroid of the equivalent column to the shear center. It is not necessary to know the exact location of the shear center. Referring to Figure A.1, let the shear center (S.C.) be as indicated, distance y_v from the flange centerline.

Applying a force P_v as indicated on the shear center parallel to the flange, no twisting of the equivalent column could occur. Considering this condition, an attempt is made to obtain a good approximation of the shear center location. The variation of the shear flow along the lip-stiffener is taken to be linear as shown. This would be true for a regular channel section, but since the stiffener length for this case is normally short compared to the flange width, this would be a reasonable approximation.

Using the usual notations, the maximum shear flow in the stiffener is:

$$\frac{VQ}{I} = \frac{V(st)(\ell + \frac{s}{2}\cos\alpha)}{I_{yy}}$$

where I_{yy} = moment of inertia of the lip stiffener about axis y-y

$$\text{Total shear force} = \frac{Vs^2t(\ell + \frac{s}{2}\cos\alpha)}{2I_{yy}}$$

Moment of shear force about 0, M_o:

$$M_o = \frac{Vs^2t(\ell + \frac{s}{2}\cos\alpha)(\ell + m)\sin\alpha}{2I_{yy}}$$

Moment of applied force P_v about 0, M_{P_v}:

$$M_{P_v} = P_v y_v$$

For no twisting:

$$M_o = M_{P_v}$$

Since $P_v = V$ and with $b = \ell + m$

$$y_v = \frac{s^2t(\ell + \frac{s}{2}\cos\alpha)b\sin\alpha}{2I_{yy}}$$

The location of the shear center above the centroid is then:

$$y_o = y_{NA} + y_v$$

APPENDIX B

DESIGN METHOD FOR EDGE STIFFENED ELEMENT

Introduction

The following design method for an edge stiffened element is taken from Reference 5. This design method is part of a complete design method proposed for stiffened elements which include intermediately stiffened elements. The stiffener requirements and design procedures for predicting effective widths are presented.

Notation

The following symbolism and definitions pertain to the typical edge stiffened elements shown in Figure B.1 and will be used in the subsequent design recommendations.

$$(w/t)_{\alpha} = 221/\sqrt{\sigma_y} \qquad \text{B.1}$$

$$(w/t)_{\beta} = 0.64\sqrt{(k_w)_{u.s.}\, E/\sigma_y} \qquad \text{B.2}$$

in which $(k_w)_{u.s.}$ is determined by rotational analysis per Figure 2.2.2 of Reference 16. If rotational restraint at supported edge is neglected, then

$$(k_w)_{u.s.} = 0.425$$

and

$$(w/t)_{\beta} = 71.7/\sqrt{\sigma_y} \qquad \text{B.3}$$

I_s = effective moment of inertia of edge stiffener about

its own centroidal axis parallel to the stiffened element, in.^{4}

If the stiffener is a straight lip then

$$I_s = D_{eff}^3 \, t/12 \qquad \text{B.4}$$

where

$$D_{eff} = d_{eff} + r \qquad \text{B.5}$$

in which r is the inside radius at the corner of the stiffener and flange, and from Equation 4.1.3

$$(d/t)_{eff} = .95 \sqrt{\frac{.425\ E}{\sigma_y}} \left(1. - \frac{.209}{d/t} \sqrt{\frac{.425\ E}{\sigma_y}}\right) \qquad \text{B.6}$$

when k_d is taken as 0.425.

Also, if the straight lip stiffener is at an angle to the flange, d_{eff} is determined from the above equation, but I_s is calculated by

$$I_s = \frac{D_{eff}^3 \, t}{12} \cos^2\theta \qquad \text{B.7}$$

where θ is defined in Figure 6.1b.

$(I_s)_{adequate}$ = Required minimum centroidal moment of inertia of stiffener necessary to adequately support the flange. Stiffener moment of inertia is taken about its own centroidal axis parallel to the stiffened element, in^4.

and

w = flat width of edge stiffened flange, in.

d = flat width of straight lip edge stiffener, in.

k_d = buckling coefficient for straight lip stiffener

k_w = buckling coefficient for edge stiffened flange

σ_y = yield stress, ksi

E = Young's modulus, ksi

Edge Stiffener Requirements

The required minimum stiffener rigidities, $(I_s)_{adequate}$, necessary to adequately support the edge stiffened flange are as follows:

--For $(w/t) < (w/t)_\beta$; fully effective as an unstiffened element

$$(I_s)_{adequate} = 0$$

--For $(w/t)_\beta \leq (w/t) < (w/t)_\alpha$; fully effective range when adequately stiffened

$$(I_s/t^4)_{adequate} = 120 \frac{[(w/t)/(w/t)_\alpha - (w/t)_\beta/(w/t)_\alpha]^3}{[1.0 - (w/t)_\beta/(w/t)_\alpha]^3} \qquad \text{B.8}$$

If rotational restraint is neglected at supported ege such that $(w/t)_\alpha$ and $(w/t)_\beta$ are defined per Equations 5.4.3a and 5.4.4a in Section 6.1.1, then

$$(I_s/t^4)_{adequate} = 120 \frac{[(w/t) - (71.7/\sqrt{\sigma_y})]^3}{[(221/\sqrt{\sigma_y}) - (71.7/\sqrt{\sigma_y})]^3}$$

$$= 36.1 \times 10^{-6} [(w/t)\sqrt{\sigma_y} - 71.7]^3$$

--For $(w/t) \geq (w/t)_\alpha$; post-buckling range

From Figure 5.3.3, Stiffener Requirement V is given by

$$(I_s/t^4)_{adequate} = 115\ (w/t)/(w/t)_\alpha + 5 \qquad B.10$$

Substituting Equation 5.4.3a,

$$(I_s/t^4)_{adequate} = 0.52\ (w/t)\sqrt{\sigma_y} + 5 \qquad B.11$$

etermination of Effective Widths and Areas

-For $I_s \geq (I_s)_{adequate}$; Adequately Stiffened Element

Effective Width of Flange is given by

$$(w/t)_{eff} = 0.95\sqrt{\frac{E(k_w)_{a.s.}}{\sigma_y}}\left(1. - \frac{.209}{w/t}\sqrt{\frac{E(k_w)_{a.s.}}{\sigma_y}}\right) \qquad B.12$$

If $D_s/w \leq 0.25$ or if stiffener other than a straight lip (such as L-shaped stiffener in Figure 6.1c)

$$(k_w)_{a.s.} = 4$$

If $D_s/w > 0.25$ then $\qquad B.13$

$$(k_w)_{a.s.} = -5\ D_s/w + 5.25$$

where D_s is the unstiffened flat width of the stiffener plus the corner radius.

Effective Area of Adequate Edge Stiffener

If straight lip stiffener

$$(A_s)_{eff} = d_{eff}\ t$$

where

$$(d/t)_{eff} = .95\sqrt{\frac{k_d\ E}{\sigma_y}}\left(1. - \frac{.209}{d/t}\sqrt{\frac{k_d\ E}{\sigma_y}}\right) \qquad B.14$$

in which

$$k_d = 0.425$$

If other than straight lip and if for none of the stiffener's component elements $w/t > (w/t)_{lim}$ then

$(A_s)_{eff}$ = unreduced cross-sectional area of stiffener

--For $0 < I_s < (I_s)_{adequate}$; Partially Stiffened Element

Effective Width of Flange is given by

$$(w/t)_{eff} = 0.95 \sqrt{\frac{E(k_w)_{p.s.}}{\sigma_y}} \left(1. - \frac{.209}{w/t} \sqrt{\frac{E(k_w)_{p.s.}}{\sigma_y}}\right) \qquad B.15$$

where

$$(k_w)_{p.s.} = \left[\frac{I_s}{(I_s)_{adequate}}\right]^{\frac{1}{n}} [(k_w)_{a.s.} - (k_w)_{u.s.}] + (k_w)_{u.s.} \qquad B.16$$

in which $(k_w)_{a.s.}$ is defined above for the adequate stiffener and $(k_w)_{u.s.}$ and is defined in the plate buckling coefficient if the plate element were stiffened and if

$w/t < (w/t)_\alpha$ $\quad n = 2$

$w/t \geq (w/t)_\alpha$ $\quad n = 3$

Reduced Area of the Partial Stiffener is given by

$$(A_s)_{p.s.} = (A_s)_{eff} \, I_s/(I_s)_{adequate} \qquad B.17$$

where $(A_s)_{eff}$ is defined above for the adequate edge stiffener.

--For $I_s = 0$; <u>Unstiffened Element</u>

Effective Width of Unstiffened Flange is given by

$$(w/t)_{eff} = 0.95\sqrt{\frac{E(k_w)_{u.s.}}{\sigma_y}}\left(1. - \frac{.209}{w/t}\sqrt{\frac{E(k_w)_{u.s.}}{\sigma_y}}\right) \quad \text{B.18}$$

where

$$(k_w)_{u.s.} = 0.425$$

unless determined by rational analysis per Figure 2.2.2 of Reference 16.

REFERENCES

1. American Iron and Steel Institute, Cold-Formed Steel Design Manual, Washington, D.C., 1977.

2. Apparao, T.V.S.R. and Errera, S.J., "Design Recommendations for Diaphragm-Braced Beams, Columns and Wall-Studs," Report No. 332, Department of Structural Engineering, Cornell University, Ithaca, N.Y., 1968.

3. Bleich, F., Buckling Strength of Metal Structures, McGraw-Hill, New York, 1952.

4. Celebi, N., "Diaphragm Braced Channel and Z-Section Beams," Report No. 344, Department of Structural Engineering, Cornell University, Ithaca, N.Y., 1972.

5. Desmond, T.P., "The Behavior and Strength of Thin-Walled Compression Elements with Longitudinal Stiffeners," Report No. 369, Department of Structural Engineering, Cornell University, Ithaca, N.Y., 1978.

6. Douty, R.T., "A Design Approach to the Strength of Laterally Unbraced Compression Flanges," Bulletin No. 37, Cornell University Engineering Experiment Station, Ithaca, N.Y., 1962.

7. Ellifritt, D., Private Communication.

8. Haussler, R.W., "Strength of Elastically Stabilized Beams," Journal of Structural Division, ASCE Proceedings, Vol. 90, No. ST3, June 1964.

9. Haussler, R.W., Private Communication.

10. Kalyanaraman, V., "Performance of Unstiffened Compression Elements," Research Report No. 362, Department of Structu- Engineering, Cornell University, Ithaca, N.Y., 1976.

11. Peköz, T., "Continuous Purlin Tests," Department of Structural Engineering, Cornell University, Ithaca, N.Y., 1974.

12. Winter, G., "Lateral Bracing of Columns and Beams," Transactions ASCE, Vol. 125, Part I, Paper No. 3044, 1960.

13. Yu, Wei-Wen, Private Communication.

14. Yu, Wei-Wen, Cold-Formed Steel Structures, McGraw-Hill, New York, 1973.

TABLES

TABLE 3.1

MATERIAL PROPERTIES (Tensile)

Purlin Type	Yield Stress (ksi)	Ultimate Stress (ksi)	Percent Elongation
A	57.3	79.9	26.0
B	57.6	81.2	27.5
C	61.5	85.0	23.5
D	65.9	91.2	23.2
E	70.5	94.8	17.8

TABLE 3.2

AVERAGE PURLIN DIMENSIONS[1]

PURLIN TYPE	H (in)	b_t (in)	w_t (in)	s_t (in)	d_t (in)	ϕ_t (degrees)	R_t/t	r_t/t	t (in)
A	9.45	2.56	2.03	0.76	0.60	42	5.17	8.13	0.063
B	9.46	2.65	2.02	1.12	0.90	40	3.12	6.24	0.109
C	7.92	2.49	2.01	0.86	0.64	40	5.00	6.54	0.060
D	7.93	2.56	1.86	1.10	0.81	35.5	3.87	7.00	0.115
E	7.92	2.96	2.33	0.74	0.48	35	4.42	8.70	0.069

PURLIN TYPE	b_b (in)	w_b (in)	s_b (in)	d_b (in)	ϕ_b (degrees)	R_b/t	r_b/t
A	2.65	2.10	0.84	0.64	44.5	5.40	8.60
B	2.72	2.08	1.25	0.90	42	3.76	7.06
C	2.42	2.01	0.86	0.68	36	3.67	8.67
D	2.57	1.88	1.22	0.85	42	3.52	7.48
E	2.92	2.38	0.74	0.47	36	5.14	9.86

[1] Dimensions as in Figure 3.5

TABLE 3.3

SUMMARY OF TEST RESULTS

TEST (1)	PURLIN TYPE	NOM. DEPTH (IN)	NOM. THICK (IN)	FAIL LOAD(2) (LBS/FT)	LOCATION OF LOCAL BUCKLE		COMMENTS(4)
					AT A HOLE(3)	DIST. OF BUCKLE TO MIDSPAN(IN)	
V1	A	9-1/2	.063	145	Y	4.8	(9)
V5	A	9-1/2	.063	114	N	m.s.	
B1	A	9-1/2	.063	119	Y	15	
B2	A	9-1/2	.063	96	-	-	(10)
B3	A	9-1/2	.063	119	N	m.s.	
V2	B	9-1/2	.110	229	Y	1.6	(5)
V7	B	9-1/2	.110	224	Y	6	
B5	B	9-1/2	.110	280	N	m.s.	
V4	C	8	.063	82	Y	6	(6)
B6	C	8	.063	95	Y	6	
V3	D	8	.110	177	N	m.s.	
B4	D	8	.110	254	N	m.s.	(7)
V6	E	8	.07	88	N	m.s.	(8)
B7	E	8	.07	105	N	m.s.	(8)

(1) V designates vacuum - B designates beam test

(2) In the beam test, failure load is given as the total load on the span divided by the span length.

TABLE 3.3 (continued)

(3) Y-Yes; N-No.

(4) Unless otherwise noted, local buckle occurred only in one purlin and in the web and the flange.

(5) Yielding accompanied by large deflections.

(6) Indicated buckling was in the web and the flange of one purlin. The other purlin buckled locally in the flange stiffener.

(7) Indicated buckling was in the flange stiffener. The other purlin was restrained by the test machine due to large lateral deflections.

(8) Flange stiffener buckling.

(9) Ends of purlins were fixed.

(10) One purlin was tested previously and was badly distorted.

TABLE 4.1

TEST ULTIMATE STRESSES[3]

Purlin Type	Yield Stress (σ_y)	Vacuum Test Stress	Vacuum Test $\%\sigma_y$	Beam Test Stress	Beam Test $\%\sigma_y$
A	57.3	39.2	68.4	53.8	93.9
B	57.6	y[1,2]		y	
C	61.5	45.5	74.0	y	
D	65.9	57.5	87.3	y	
E	70.5	31.9	45.3	45.4	64.4

(1) (y)ield

(2) Duplicate test (V7) gave ultimate stress of 45.6 ksi (79.2 $\%\sigma_y$)

(3) All stresses are in ksi.

TABLE 4.2

ROTATIONAL RESTRAINT FACTORS (F)[2]

PURLIN TYPE	Vacuum Test Max. Rot. (rad.)	Vacuum Test F	Beam Test Max. Rot. (rad.)	Beam Test F
A	.250	.084	.284	.173
B	.275	.141	.223	.392
C	.203	.073	.225	.185
D	.238	.150	.137	.413
E	.060[1]	.115	.144	.246

[1] F not based on this value (see Fig. 4.21).

[2] F is in k-in/in/rad.

TABLE 4.3

ROTATIONAL DEFORMATION OF PURLIN WEB

Purlin Type	H/t	$(\theta_p/\theta)_V$ [1]	$(\theta_p/\theta)_B$ [2]
A	150.0	.32	.53
B	86.8	.11	.29
C	132.0	.31	.58
D	69.0	.10	.27
E	114.8	.39	.66

(1) Ratio of rotational deformation of purlin web (θ_p) to total rotation (θ) in diaphragm-braced F tests.

(2) Ratio of rotational deformation of purlin web (θ_p) to total rotation (θ) in channel-braced F tests.

TABLE 4.4

YIELD AND ULTIMATE STRESSES

PURLIN TYPE	F_y (KSI)	$F_{bw,s}$ (KSI) (1)	$F_{bw,u}$ (KSI) (2)
A	57.3	47.41	38.97
B	57.6	56.91	53.13
C	61.5	52.96	44.96
D	65.9	67.31	64.10
E	70.5	62.41	54.10

(1) Computed using the F_{bw} equation for beams with stiffened compression flanges (Reference 13). $F_{bw} = [1.21 - .000337(h/t)\sqrt{F_y}]F_y$.

(2) Computed using the F_{bw} equation for beams with unstiffened compression flanges (Reference 13). $F_{bw} = [1.257 - .000508(h/t)\sqrt{F_y}]F_y$.

TABLE 4.5

SUMMARY OF ANALYSIS TYPES(1)

ANALYSIS TYPE	ULTIMATE STRESS(2)	FLANGE TYPE(3)	BASIS OF EFFECTIVE WIDTH(4)
a	F_y	F	NA
b	F_{bw}	F	NA
c	F_y	S	TW
d	F_{bw}	S	TW
e	F_y	S	FW
f	F_{bw}	S	FW
g	F_y	U	TW
h	F_{bw}	U	TW

(1) This table deals with the parameters used in the AISI Design Manual Part III Section 3 "type" analyses.

All moments of inertias and section moduli were found on the basis of sharp corners.

(2) The stress indicated was substituted for F_y required in the column formulas to be used with the procedure. F_{bw} were the web ultimate stresses as listed in Table 4.4 for unstiffened compression flanges since this equation gives lower stresses and hence underestimates the strength.

(3) F - Full flange width (unreduced).
S - The effective width was determined with the equations given in Appendix B for plate elements with edge stiffeners.
U - The effective width was determined with the equations given in Appendix B for unstiffened flanges (with k = 0.7). In this case the width of the flange was taken as the total width of the flange plus the width of the lip.

(4) NA - Not applicable, full flange width was used.
TW - w/t was based on the full flange width. In all cases, the r/t was greater than 4 for the lip-flange corner, thus possibly justifying the approach.
FW - w/t was based on the flange flat width.

When flange effective width was used, the lip effective width determined according to Appendix B was also used.

Even when F_{bw} was used for failure criteria, the effective width was based on F_y and not F_{bw}, thus eliminating a very tedious iterative procedure. This procedure leads to underestimating the capacity.

TABLE 4.6

COMPARISON OF OBSERVED
AND COMPUTED ULTIMATE LOADS
IN VACUUM TESTS

$q_{test}/q_{computed}$

PURLIN TYPE	F	ANALYSIS TYPE[1] (a)	(b)	(c)	(d)	(e)	(f)	(g)	(h)
A	.084	1.03	1.05	1.18	1.22	1.13	1.15	3.98	3.98
B	.141	1.06	1.06	1.11	1.11	1.06	1.06	2.41	2.41
C	.073	.88	.89	1.00	1.05	.93	.97	3.53	3.53
D	.150	.87	.87	.91	.91	.87	.87	1.88	1.88
E	.115	.58	.60	.68	.74	.62	.67	2.52	2.52
Mean		.88	.89	.98	1.01	.92	.94	2.86	2.86
St. Dev.		.19	.19	.20	.19	.20	.19	.86	.86
St. Dev. / Mean		.22	.21	.20	.18	.21	.20	.30	.30
Ultimate Stress		F_y	F_{bw}	F_y	F_{bw}	F_y	F_{bw}	F_y	F_{bw}
Flange Type		F	F	S	S	S	S	U	U
Basis of eff. w		NA	NA	TW	TW	FW	FW	TW	TW

[1] See Table 4.5 for further information.

TABLE 4.7

COMPARISON OF OBSERVED
AND COMPUTED ULTIMATE LOADS
BEAM TESTS

$(load)_{test}/(load)_{comp.}$

PURLIN TYPE	F	(a)	(b)	(c)	(d)	(e)	(f)	(g)	(h)
A	.173	.91	1.06	1.06	1.26	1.00	1.18	3.47	3.47
B	.392	1.00	1.04	1.06	1.09	1.00	1.04	2.15	2.15
C	.185	.81	.95	.98	1.18	.90	1.07	3.09	3.09
D	.413	.97	.98	1.03	1.04	.97	.98	1.96	1.96
E	.246	.62	.71	.77	.91	.69	.81	2.47	2.47
Mean		.86	.95	.98	1.10	.91	1.02	2.63	2.63
St. Dev.		.15	.14	.12	.13	.13	.14	.64	.64
$\frac{\text{St. Dev.}}{\text{Mean}}$		.18	.15	.12	.12	.14	.13	.24	.24
Ultimate Stress		F_y	F_{bw}	F_y	F_{bw}	F_y	F_{bw}	F_y	F_{bw}
Flange Type		F	F	S	S	S	S	U	U
Basis of eff. w		NA	NA	TW	TW	FW	FW	TW	TW

(1) See Table 4.5 for further information.

TABLE 4.8

MINIMUM STIFFENER REQUIREMENT ACCORDING TO AISI

	I[1]		II[2]		
PURLIN TYPE	FLANGE WIDTH (in)	I_{min}[3] (in^4)	FLANGE WIDTH (in)	I_{min}[3] (in^4)	STIFFENER I[4] (in^4)
A	2.56	.00115	2.03	.00090	.00103
B	2.65	.00590	2.02	.00428	.00527
C	2.49	.00097	2.01	.00077	.00131
D	2.56	.00667	1.86	.00454	.00494
E	2.96	.00175	2.33	.00137	.00077

---

[1] Total flange width used.

[2] Flat flange width used.

[3] Minimum stiffener moment of inertia required.

[4] Moment of inertia of stiffener.

TABLE 4.9

EFFECTIVE WIDTHS OF COMPRESSION FLANGES AND LIP-STIFFENERS

(Desmond Method)

	I		II		III
PURLIN TYPE	W(in(	S[1](in)	W(in)	S[1](in)	(in)
A	1.75	0.17	1.64	0.14	1.051
B	2.56	0.67	2.02[2]	0.90[2]	1.736
C	1.58	0.16	1.51	0.13	0.973
D	2.44	0.56	1.86[2]	0.81[2]	1.709
E	1.68	0.08	1.50	0.03	1.047

I Based on total width.

II Based on flat width.

III Based on total length of flange + stiffener and considered as unstiffened.

---

[1] Reduced length of partial stiffener unless otherwise noted.

[2] Fully effective.

W = flange width. S = stiffener length.

FIGURES

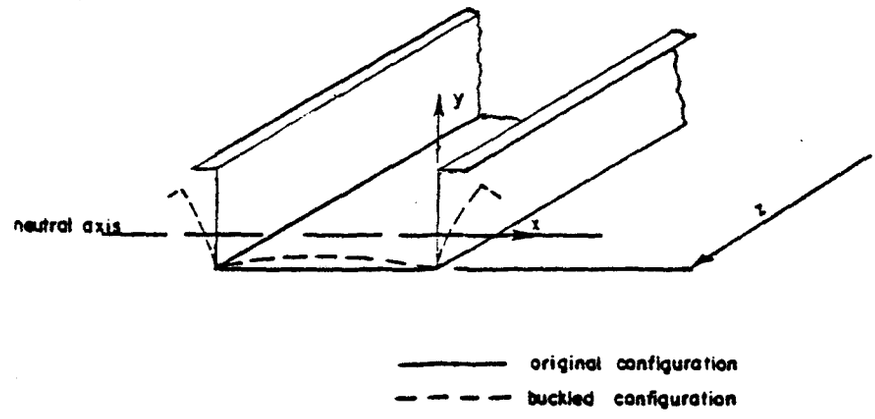

FIG. 2.1 MODE OF BUCKLING[6,14]

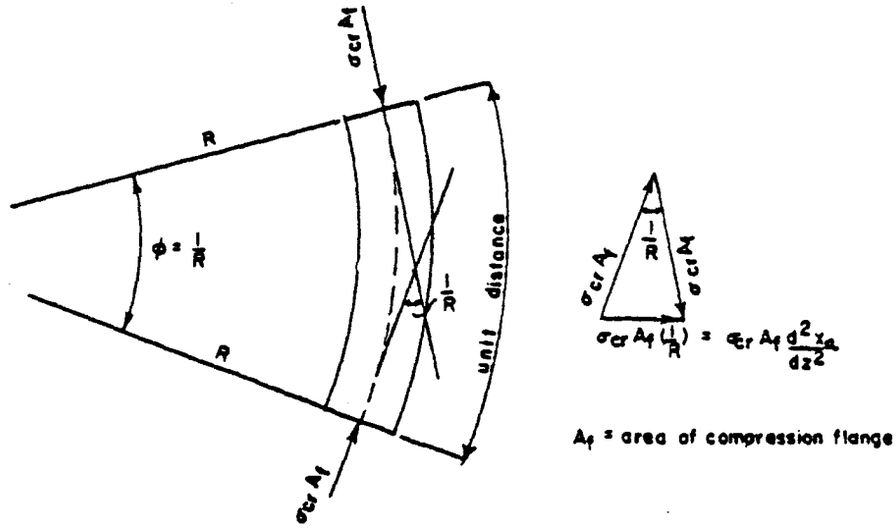

FIG. 2.2 FORCE NORMAL TO BUCKLED FLANGE[6]

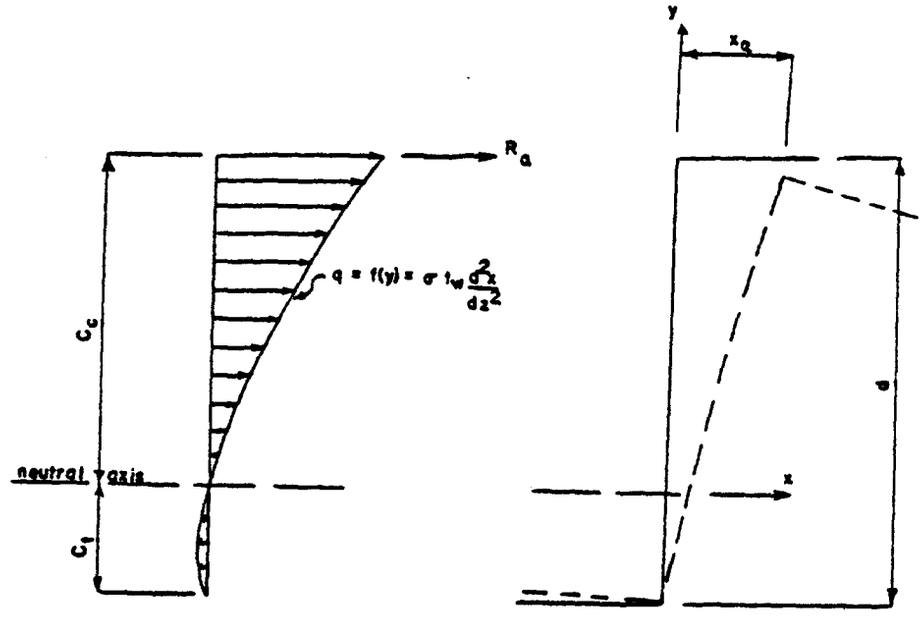

FIG. 2.3 FORCE NORMAL TO BUCKLED WEB[6,14]

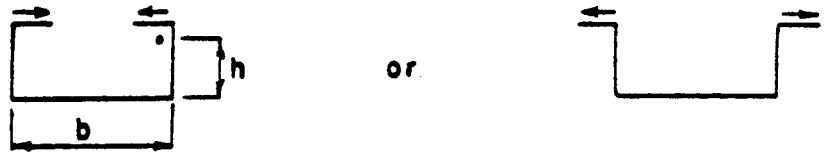

Case I Beam with symmetric flanges

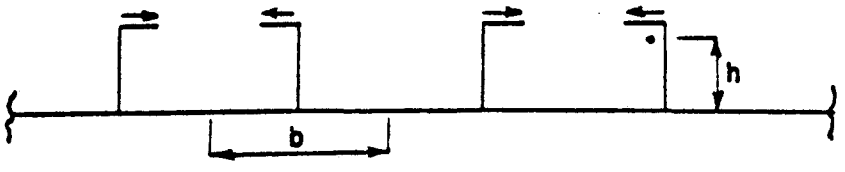

Case II Sheet with stiffeners—symmetric flanges

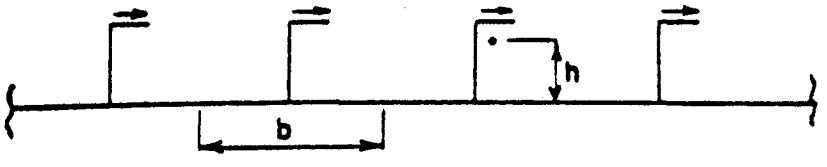

Case III Sheet with stiffeners—antisymmetric flanges

Note 1. Arrows indicate probable direction of collapse due to shear
2. "b" is portion of tension flange supporting web
3. "h" is distance from tension flange to centroid of equivalent column

FIG. 2.4 THREE POSSIBLE TYPES OF SUPPORTING ELASTIC FRAME FOR EQUIVALENT COLUMN[6]

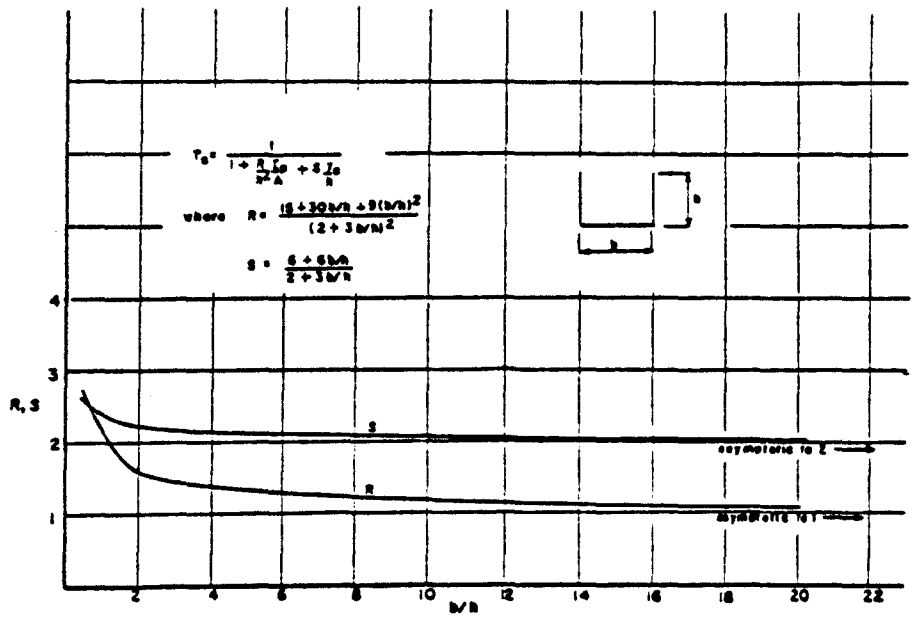

FIG. 2.5 THE EFFECT OF THE RATIO b/h ON R AND S FOR CASE 1[6]

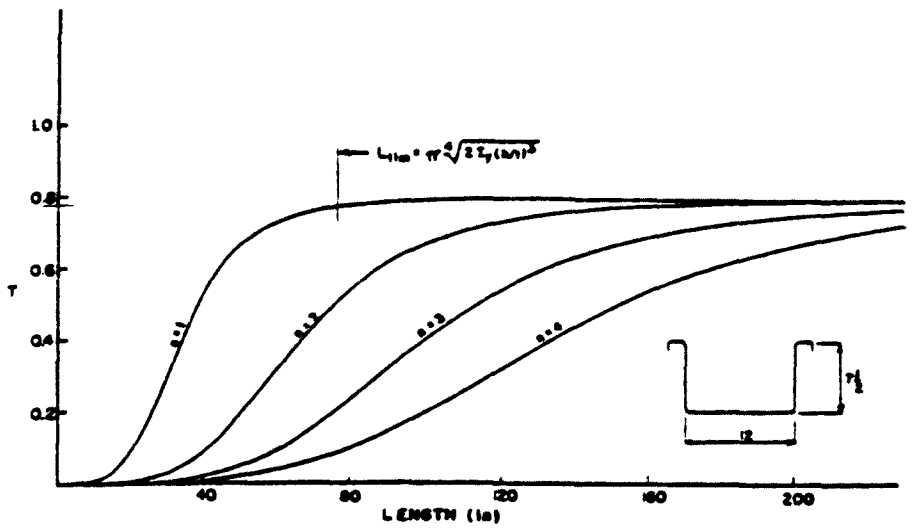

FIG. 2.6 T vs. LENGTH CURVES[6]

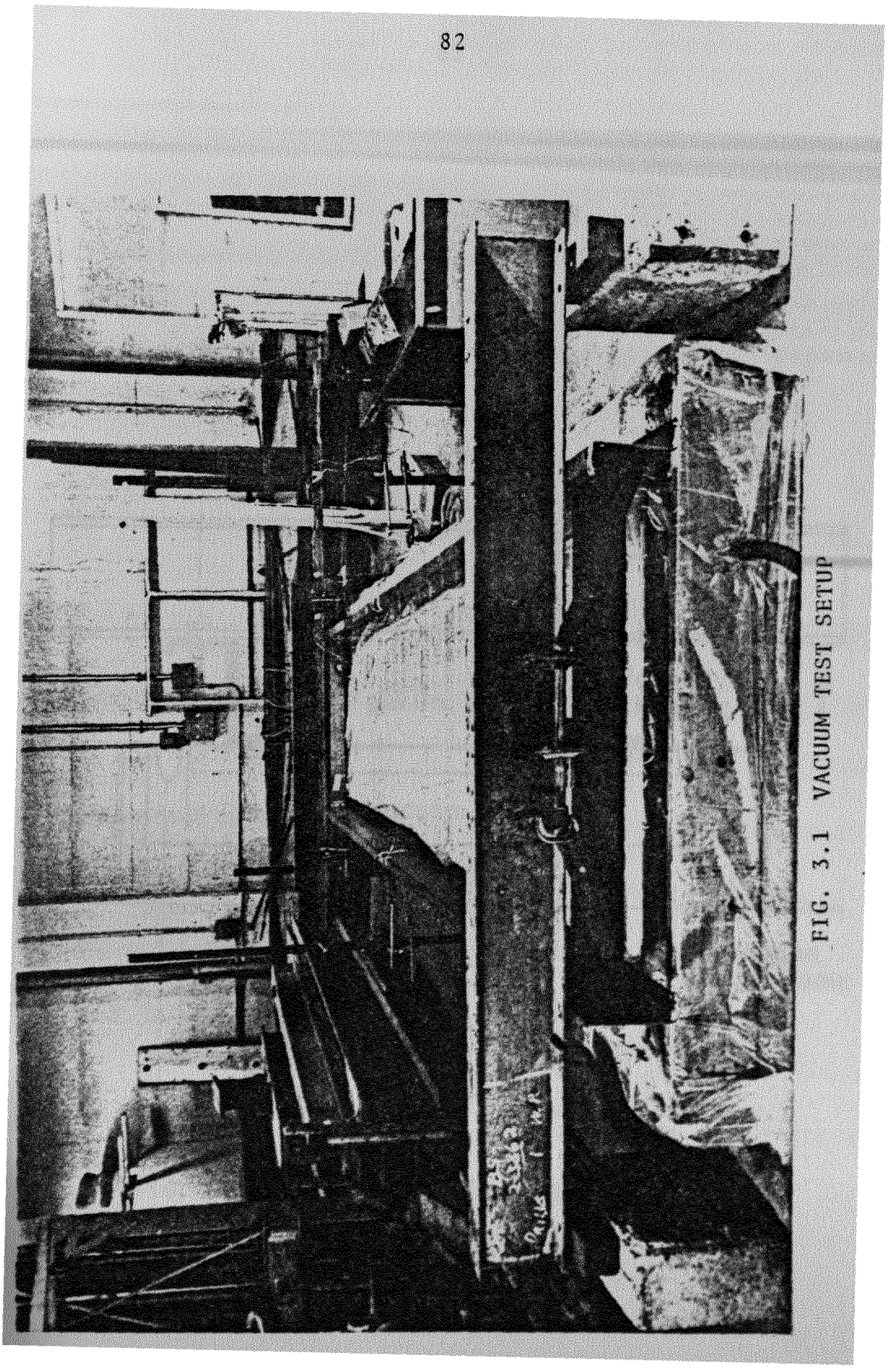

FIG. 3.1 VACUUM TEST SETUP

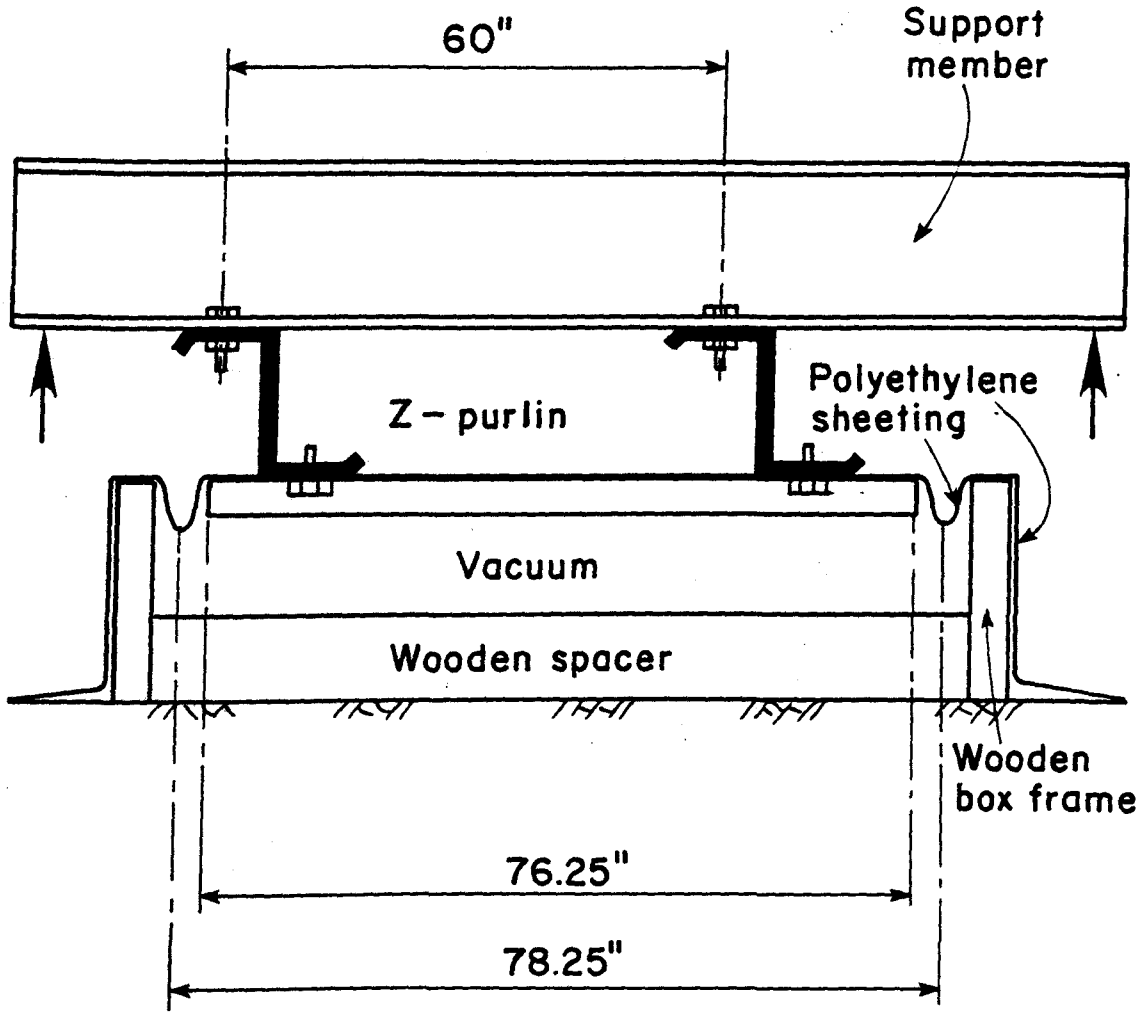

FIG. 3.2 SECTION OF VACUUM TEST SETUP

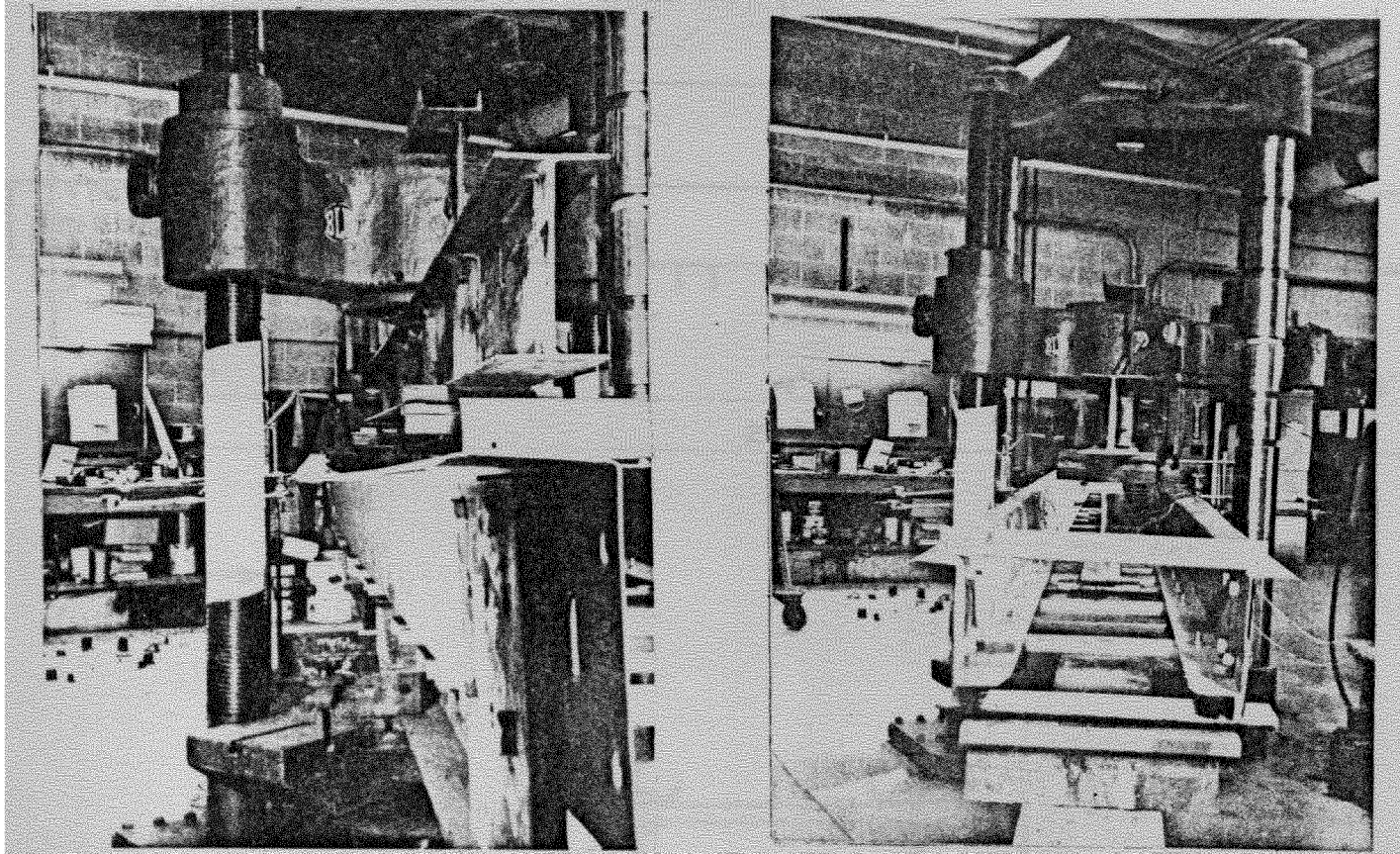

FIG. 3.3 VIEWS SHOWING BEAM TEST SETUP

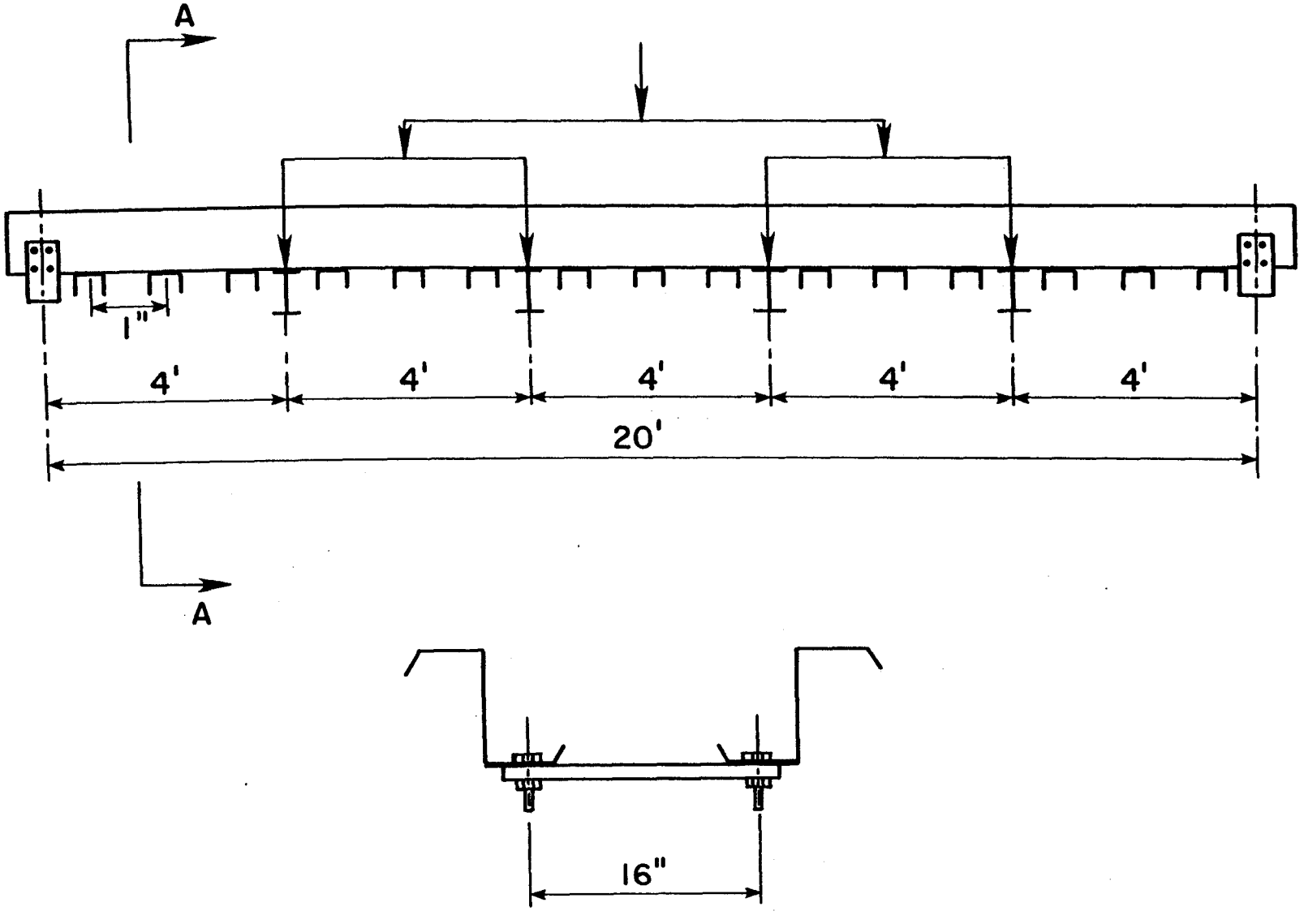

FIG. 3.4 DETAILS OF BEAM TEST SETUP

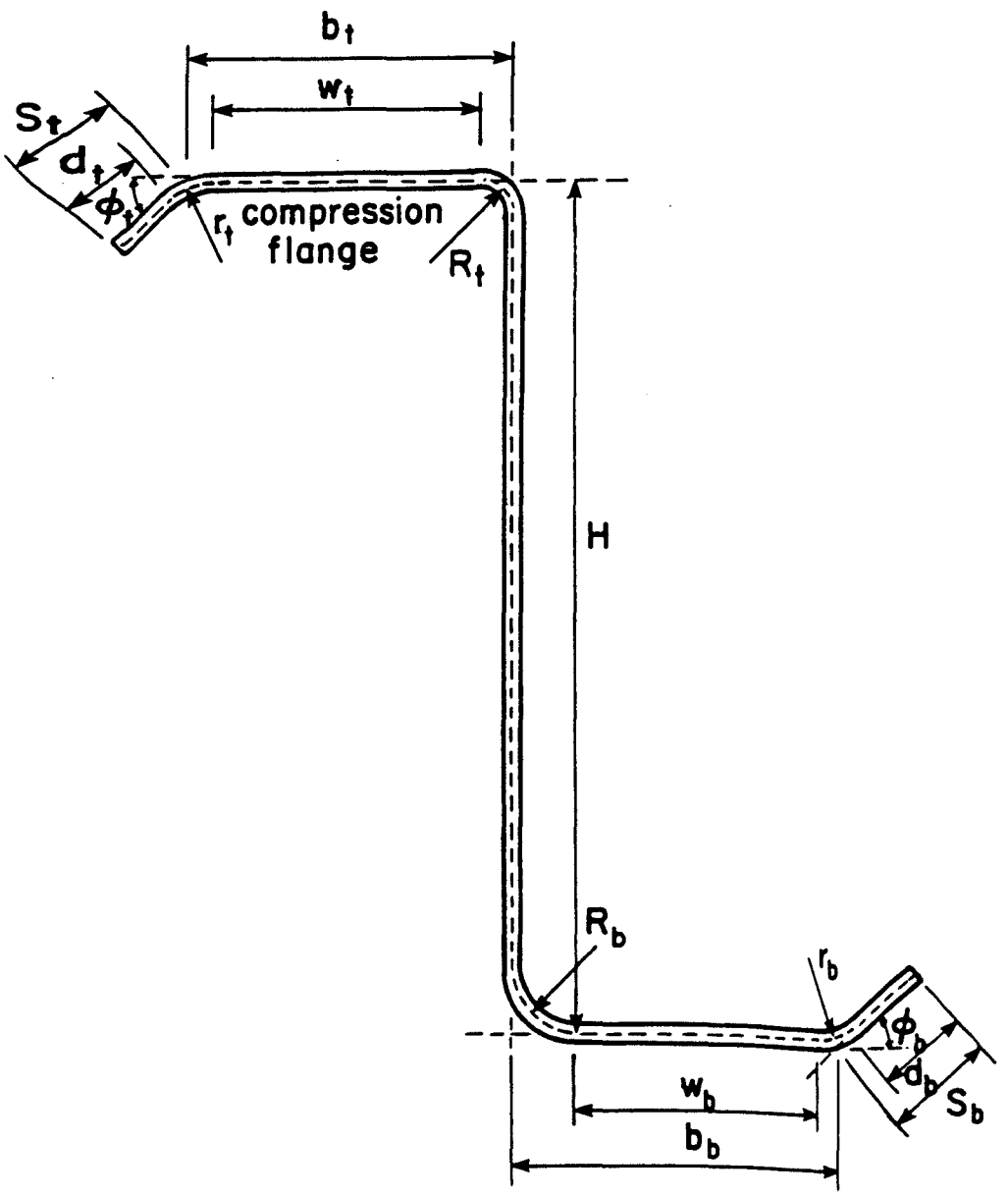

FIG. 3.5 Z-SECTION DIMENSION

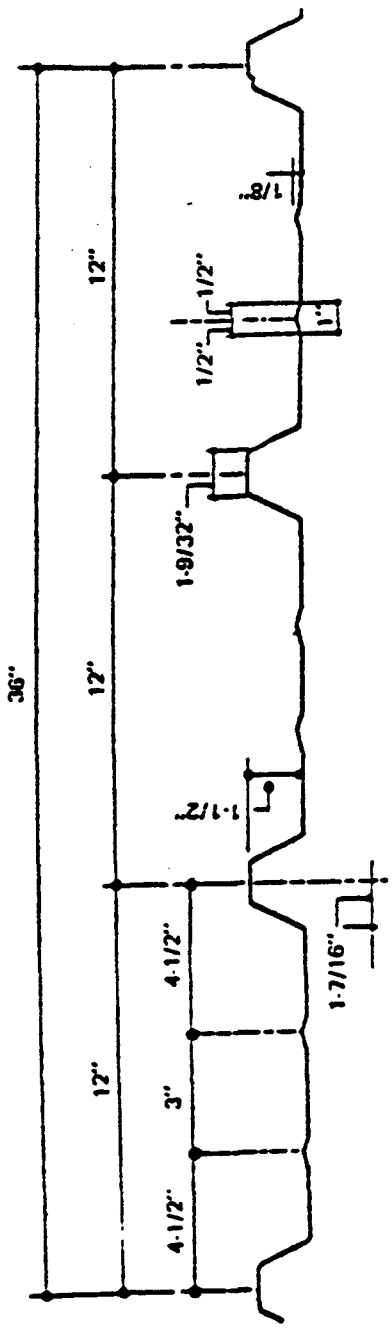

FIG. 3.6 PANEL CROSS-SECTION (Gage 24)

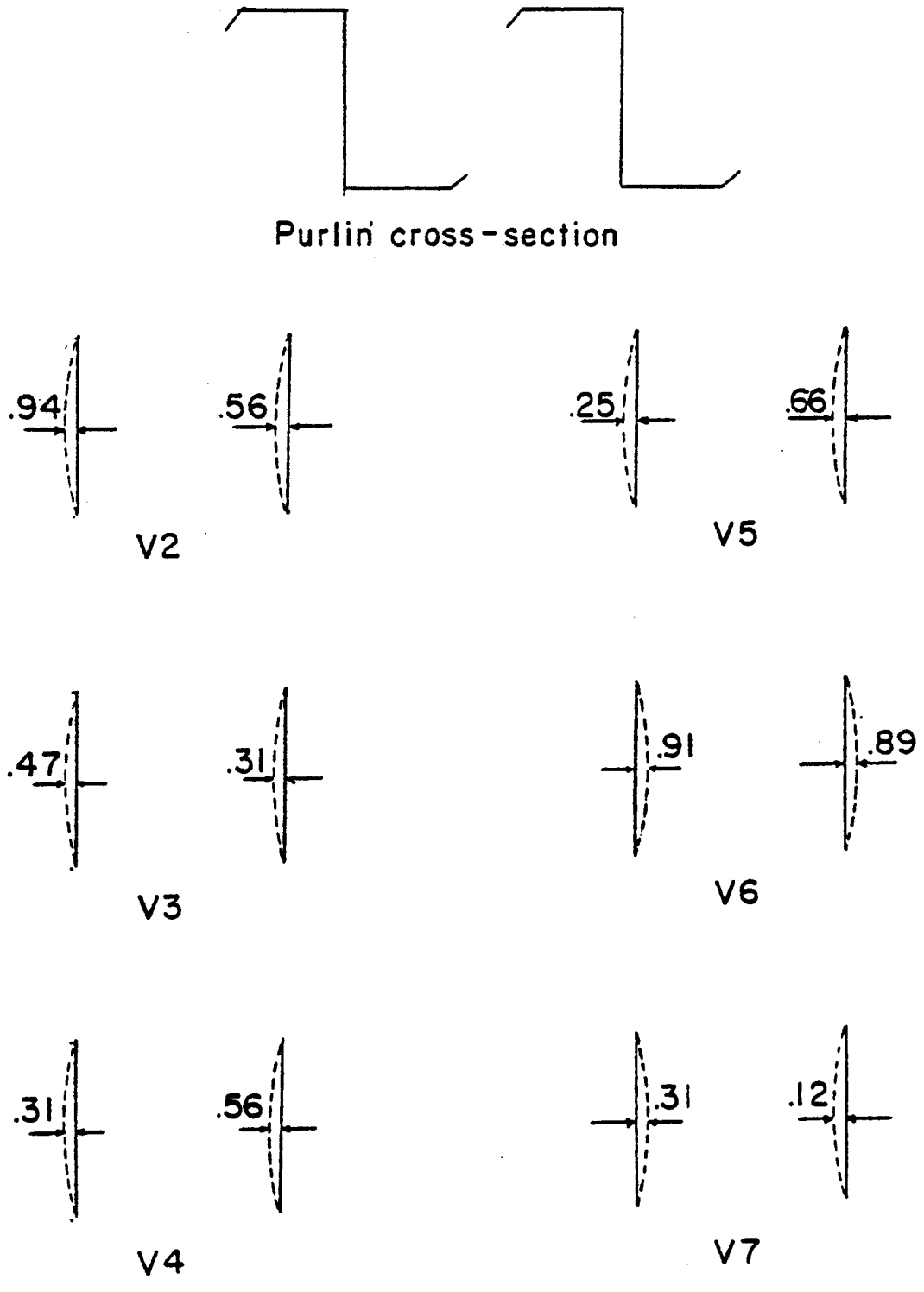

FIG. 3.7 INITIAL SWEEPS OF COMPRESSION FLANGES AT MIDSPAN IN VACUUM TESTS (INCHES).

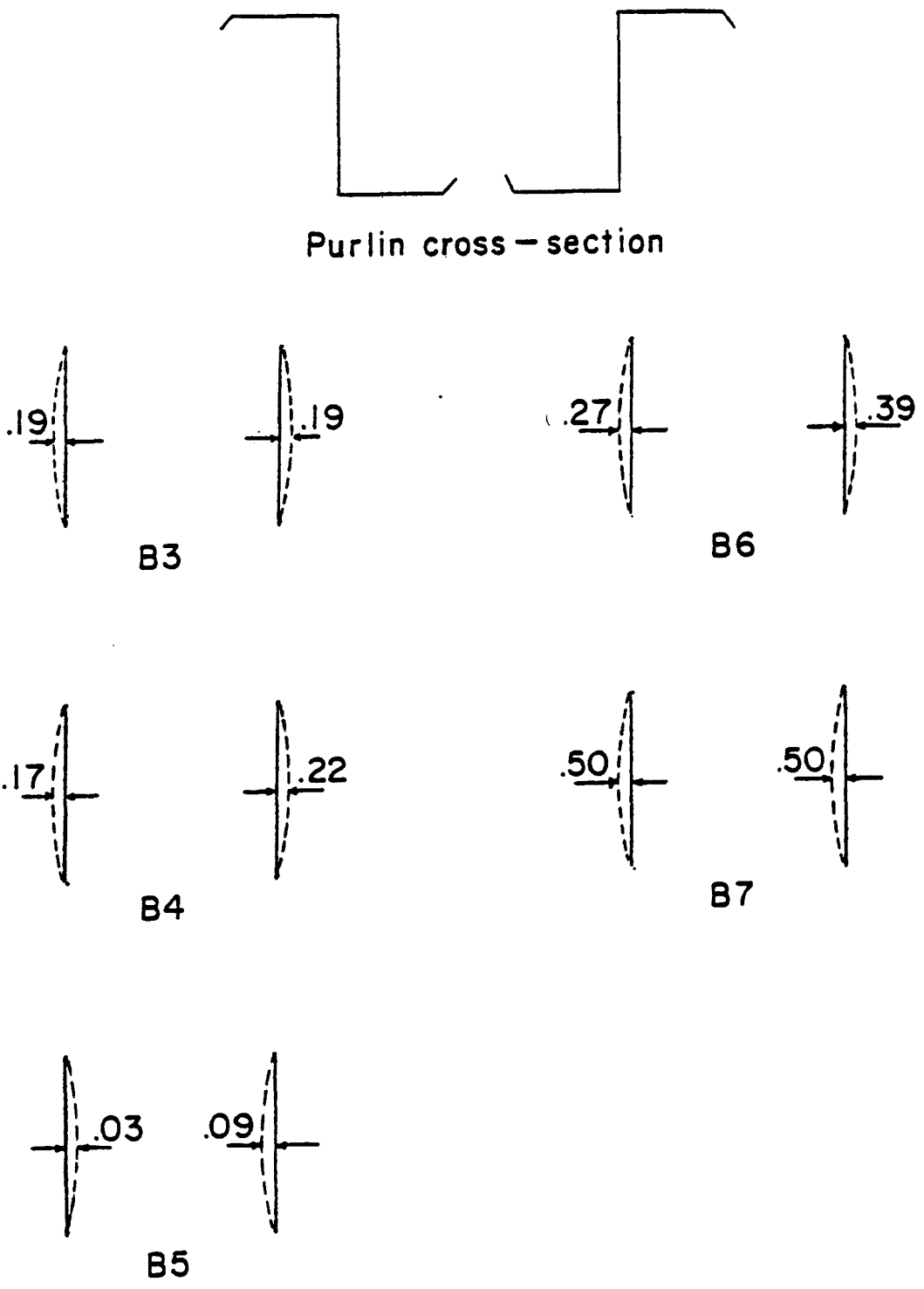

FIG. 3.8 INITIAL SWEEPS OF COMPRESSION FLANGES IN BEAM TESTS (INCHES).

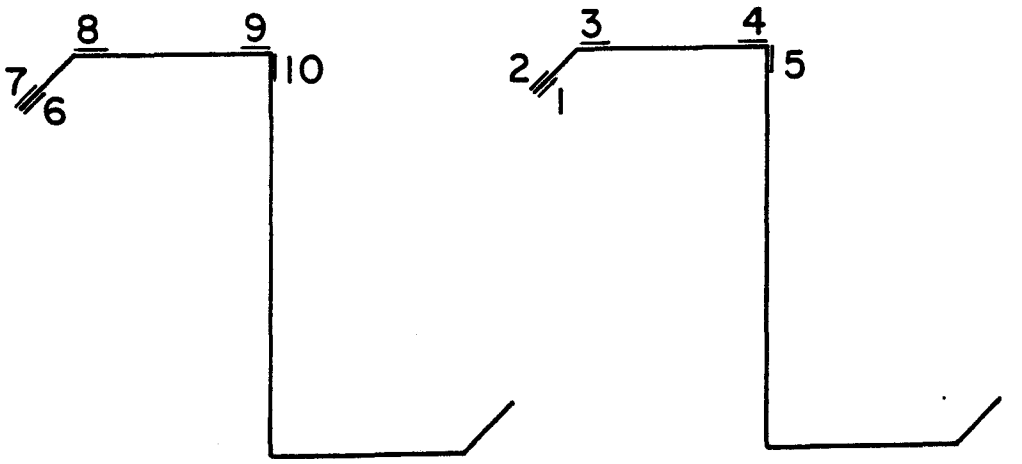

Vacuum tests

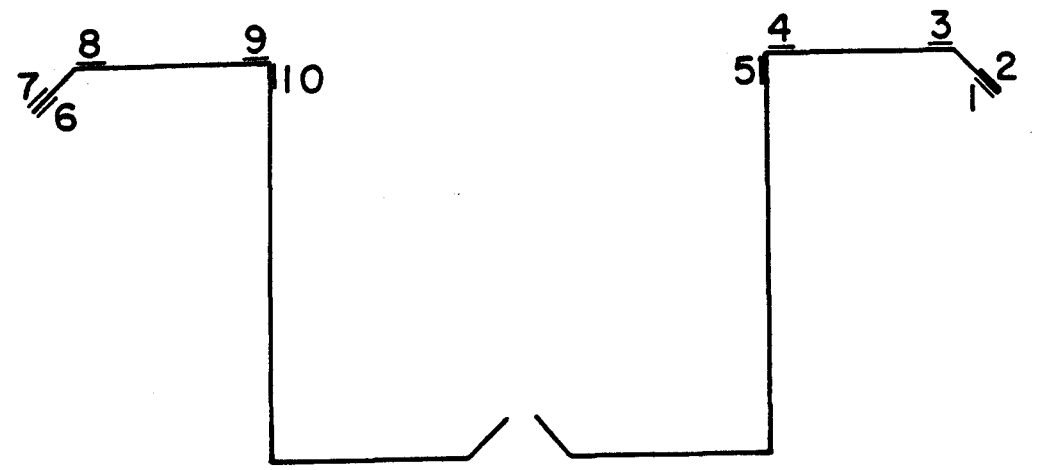

Beam tests

FIG. 3.9 LOCATION OF STRAIN GAGES

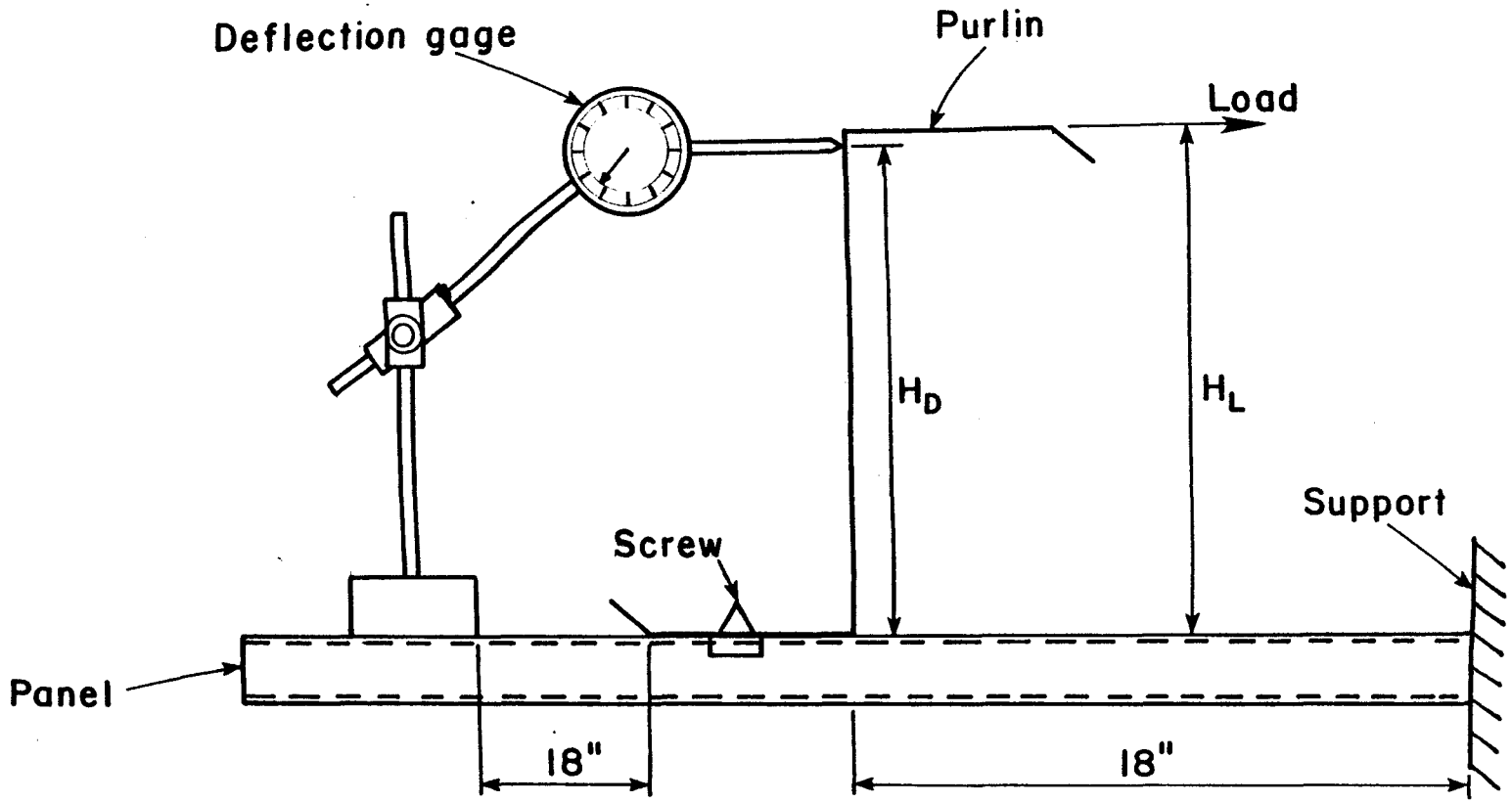

FIG. 3.10 F TEST: DIAPHRAGM-BRACED PURLIN

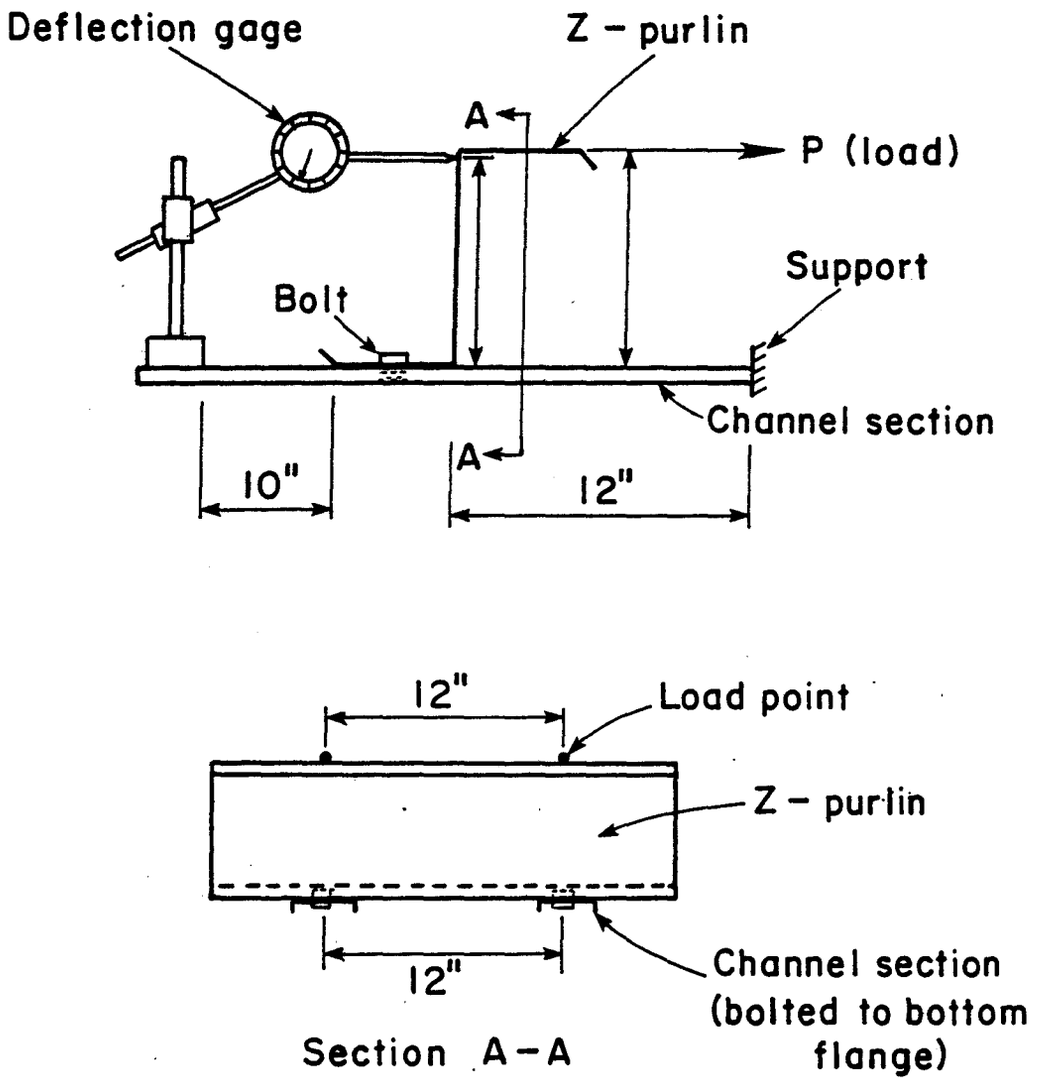

FIG. 3.11 F TEST: CHANNEL-BRACED PURLIN

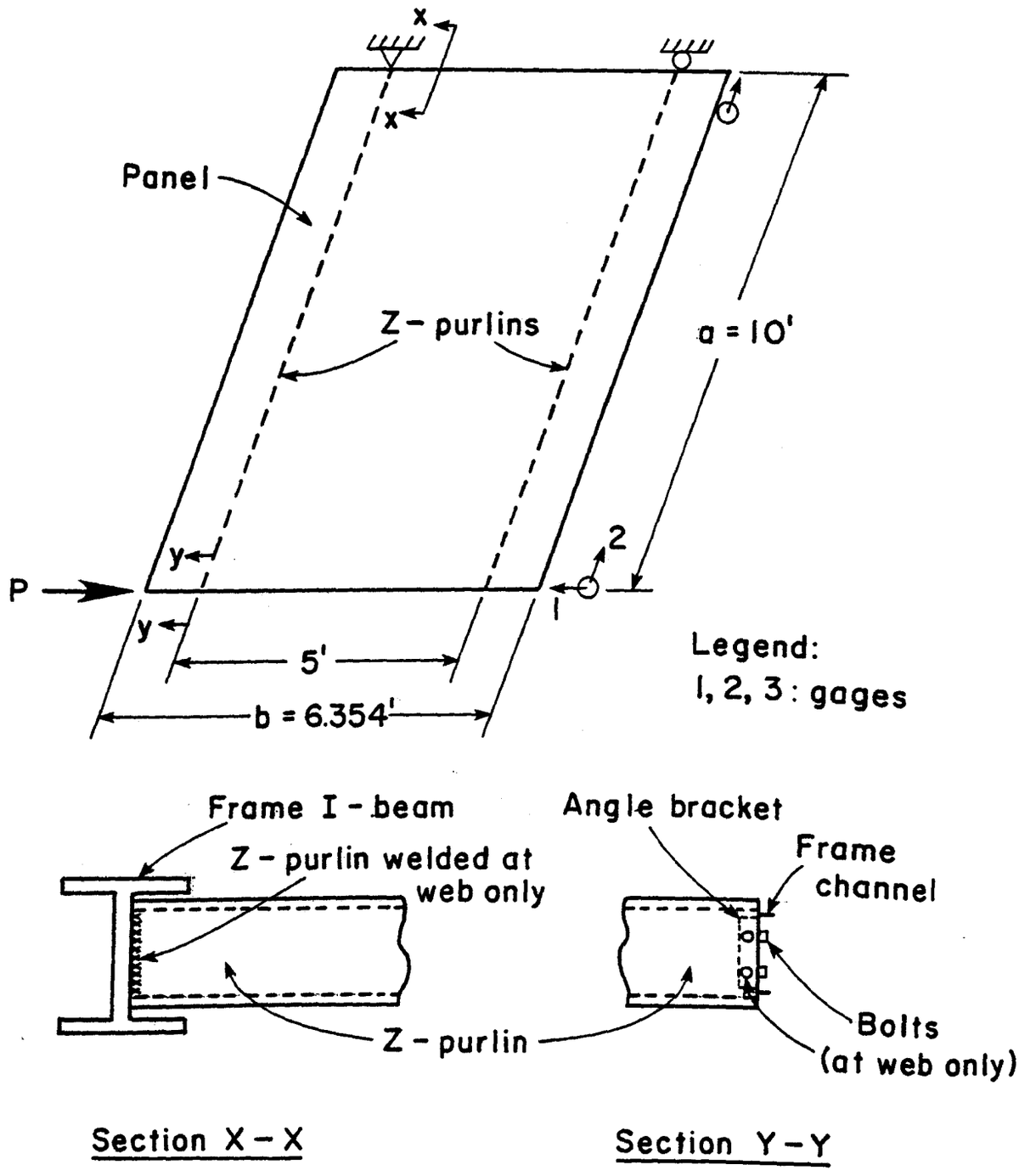

FIG. 3.12 SHEAR RIGIDITY TEST SETUP

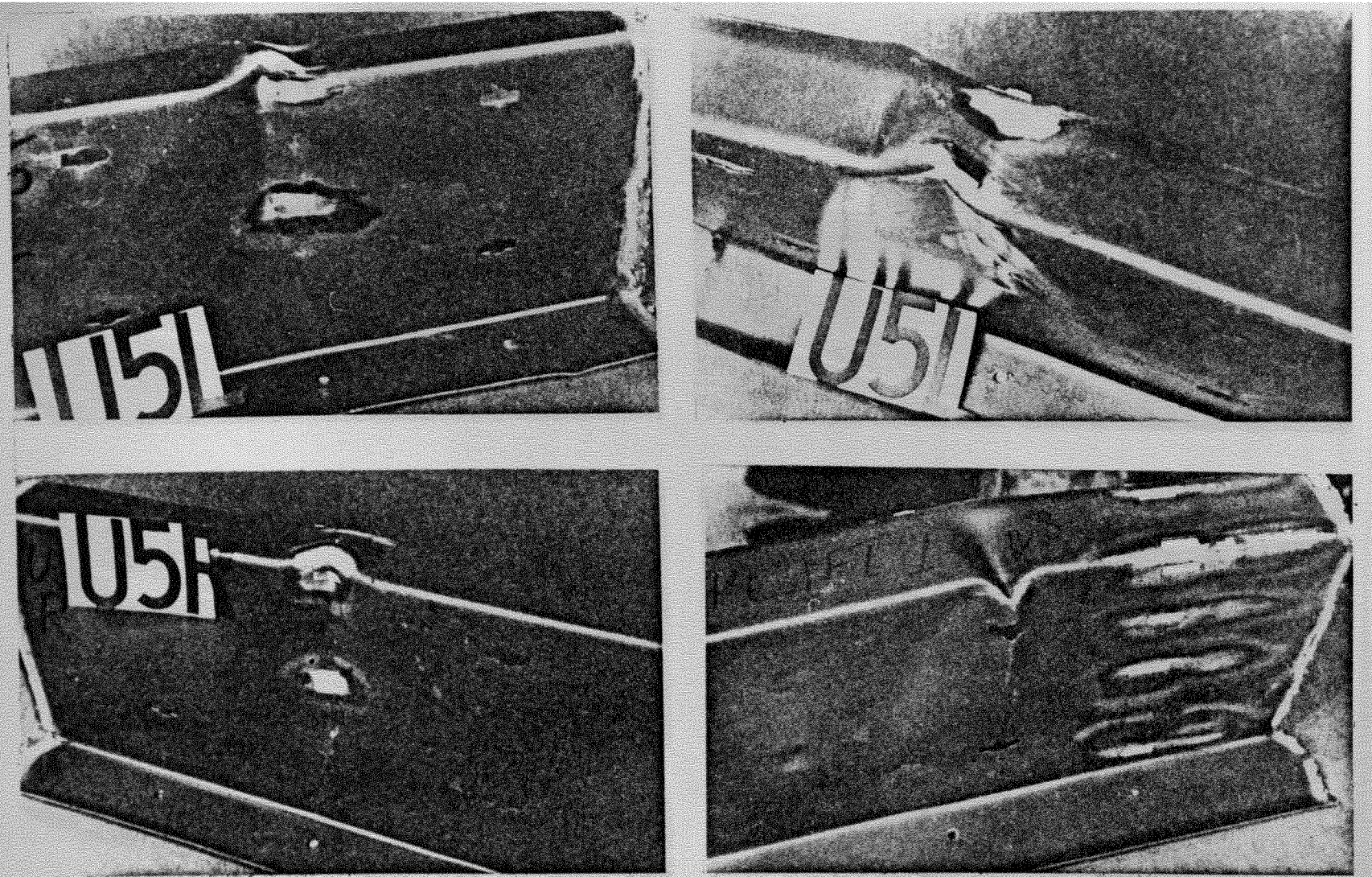

FIG. 3.13 LOCAL BUCKLES IN TEST V1 AND V5
(PURLIN TYPE A)

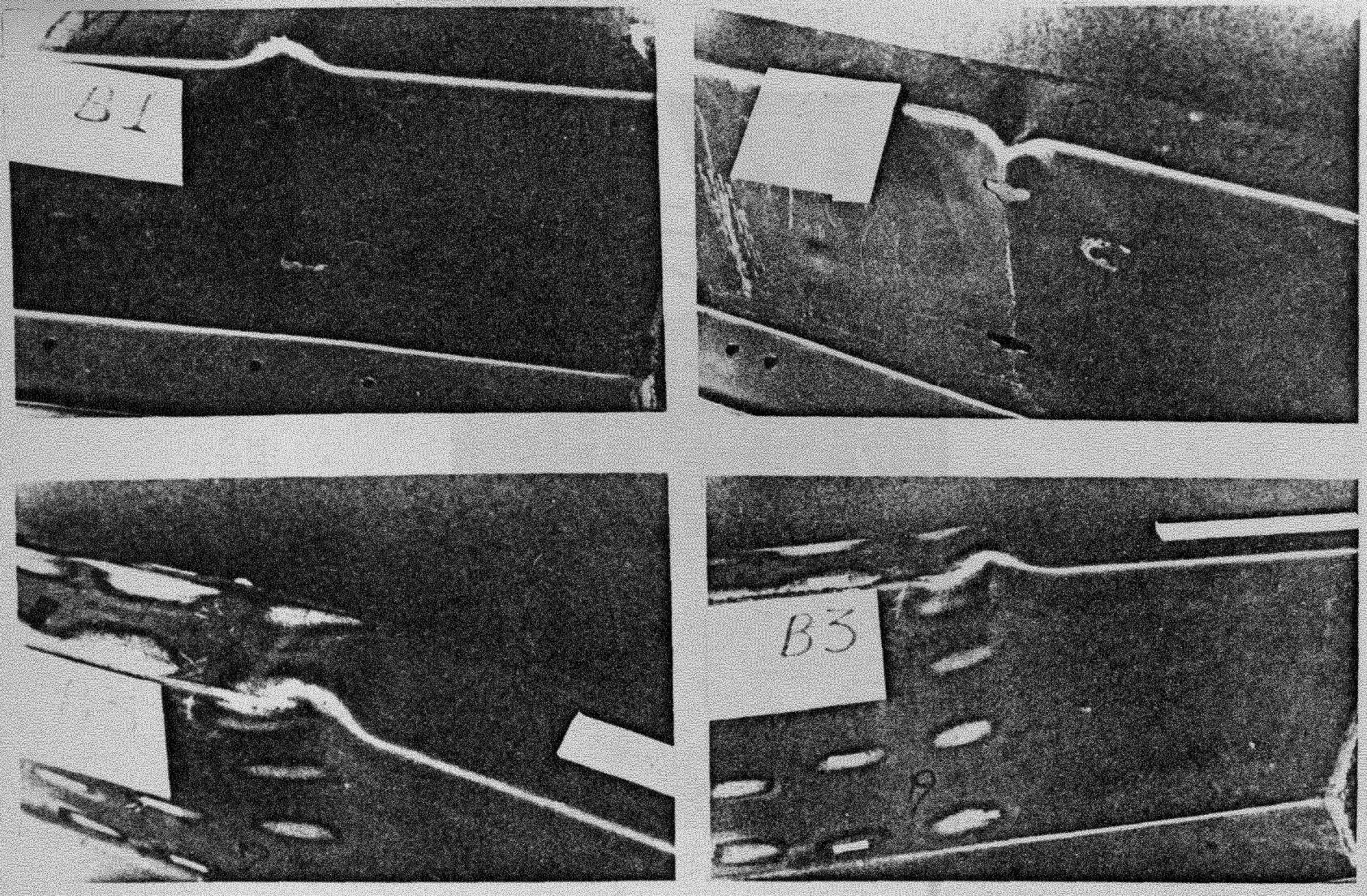

FIG. 3.14 LOCAL BUCKLES IN TEST B1, B2 AND B3 (PURLIN TYPE A)

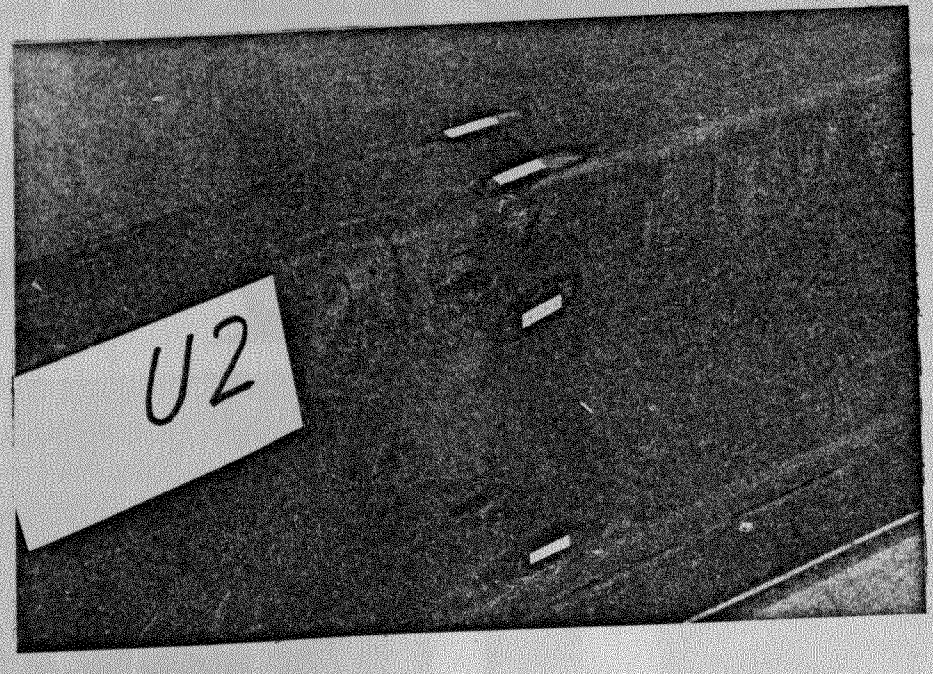

FIG. 3.15 LOCAL BUCKLE IN TEST V2
(PURLIN TYPE B)

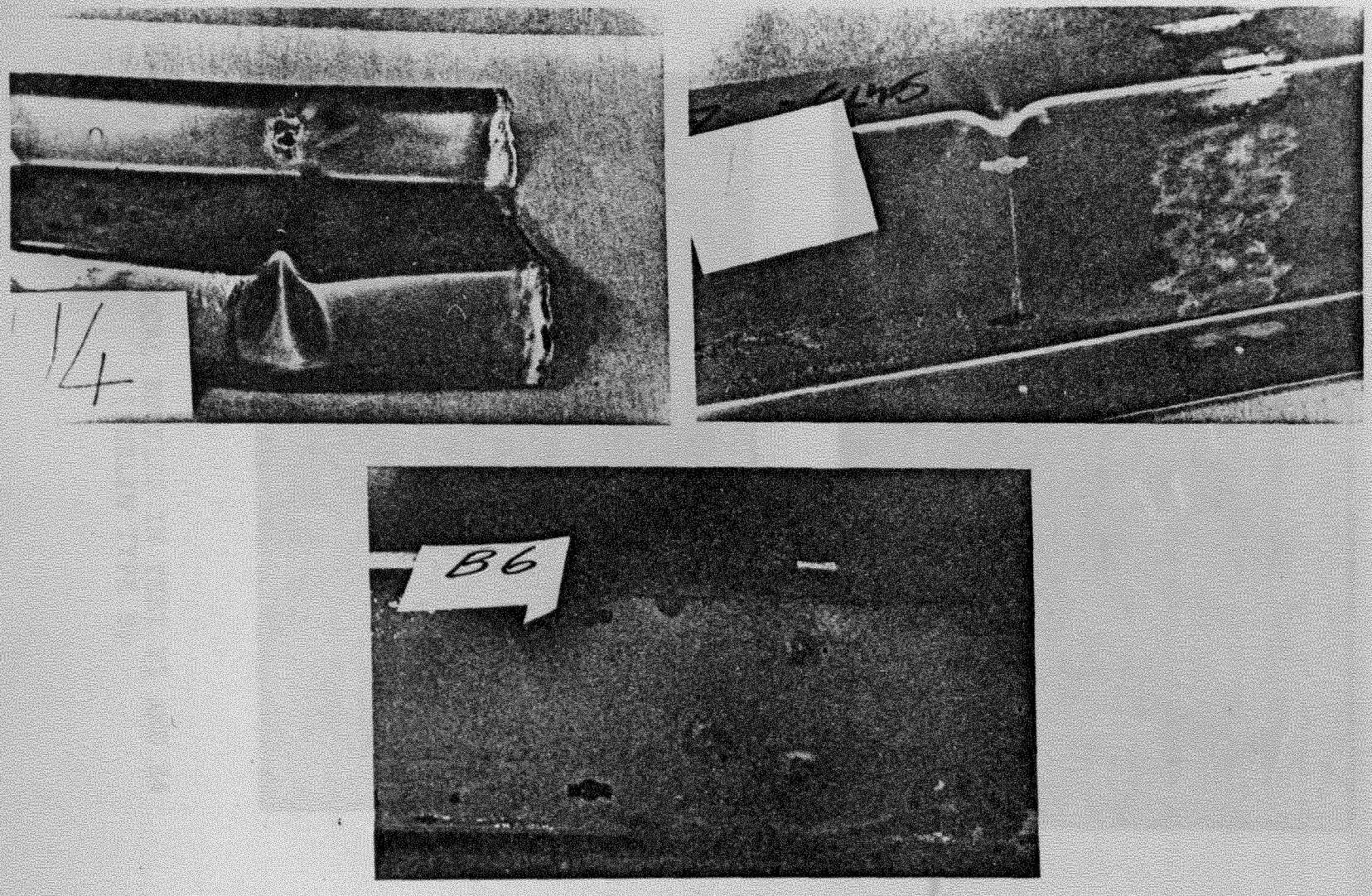

FIG. 3.16 LOCAL BUCKLES IN TEST V4 and B6
(PURLIN TYPE C)

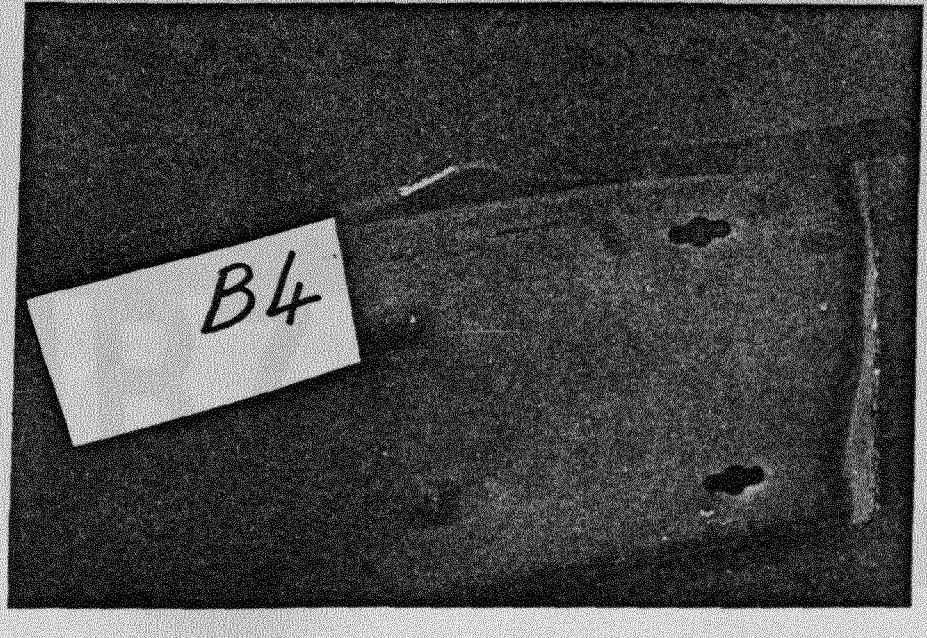

FIG. 3.17 LOCAL BUCKLES IN TEST V3 AND B4 (PURLIN TYPE D)

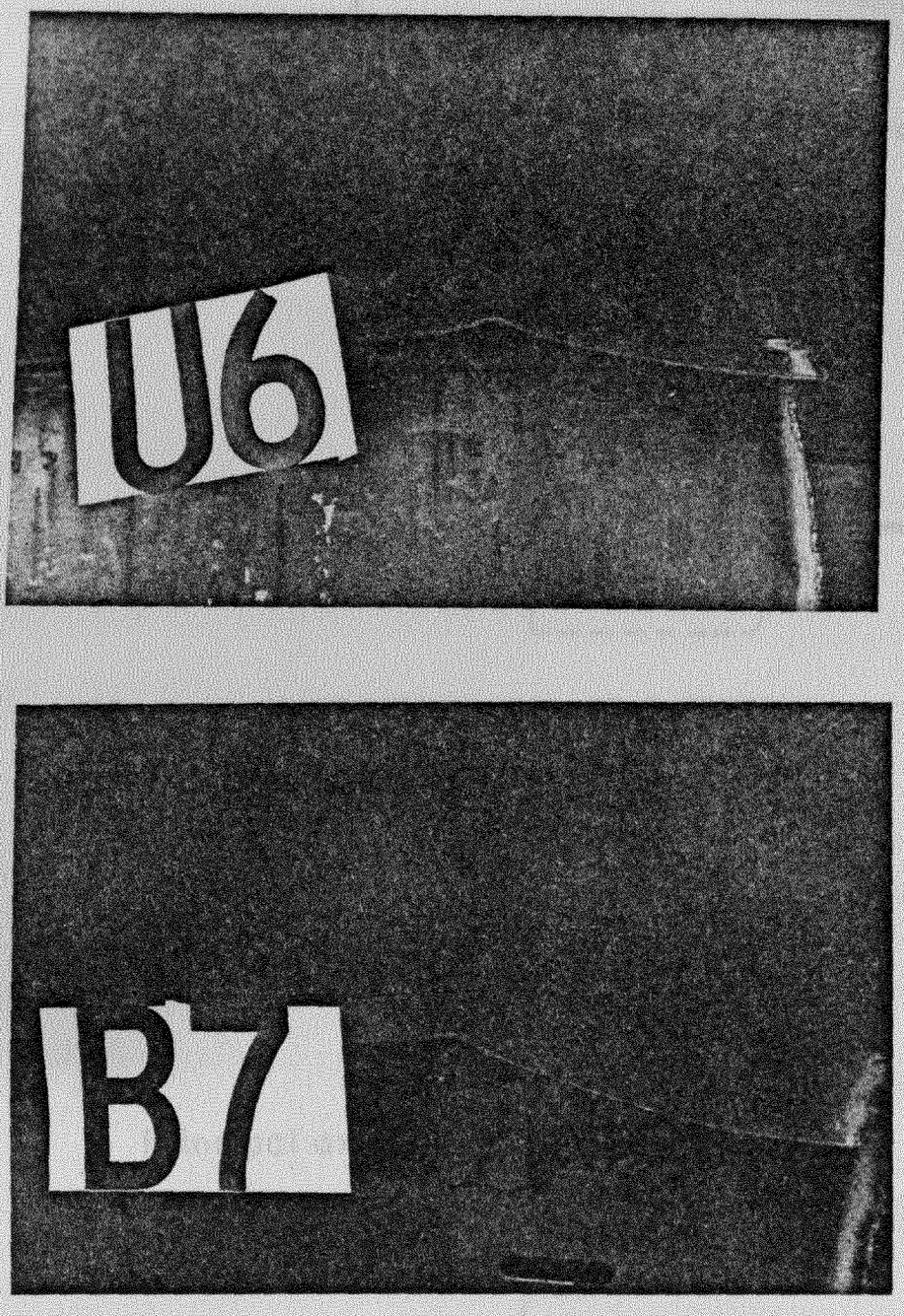

FIG. 3.18 LOCAL BUCKLES IN TEST V6 AND B7
(PURLIN TYPE E)

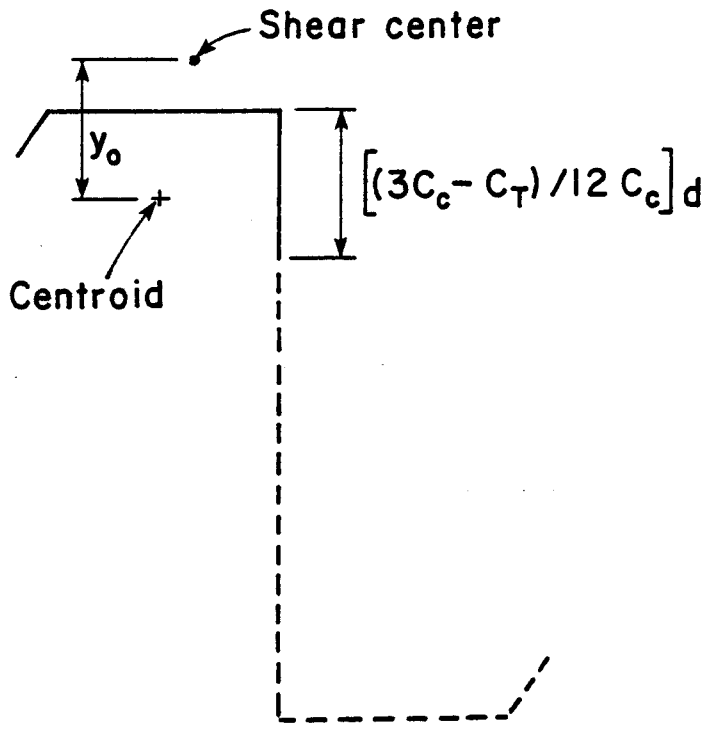

FIG. 4.1 COMPRESSION AREA OF Z-SECTION

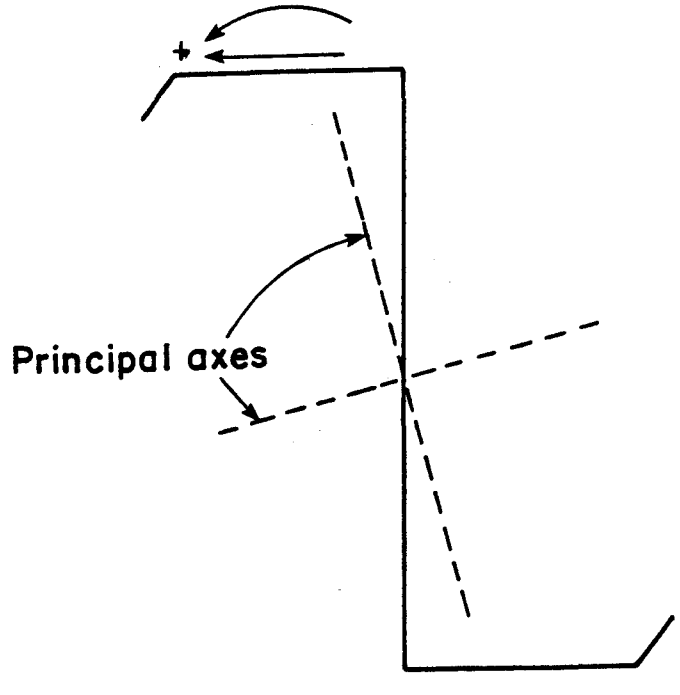

FIG. 4.2 DISPLACEMENT SIGN CONVENTION

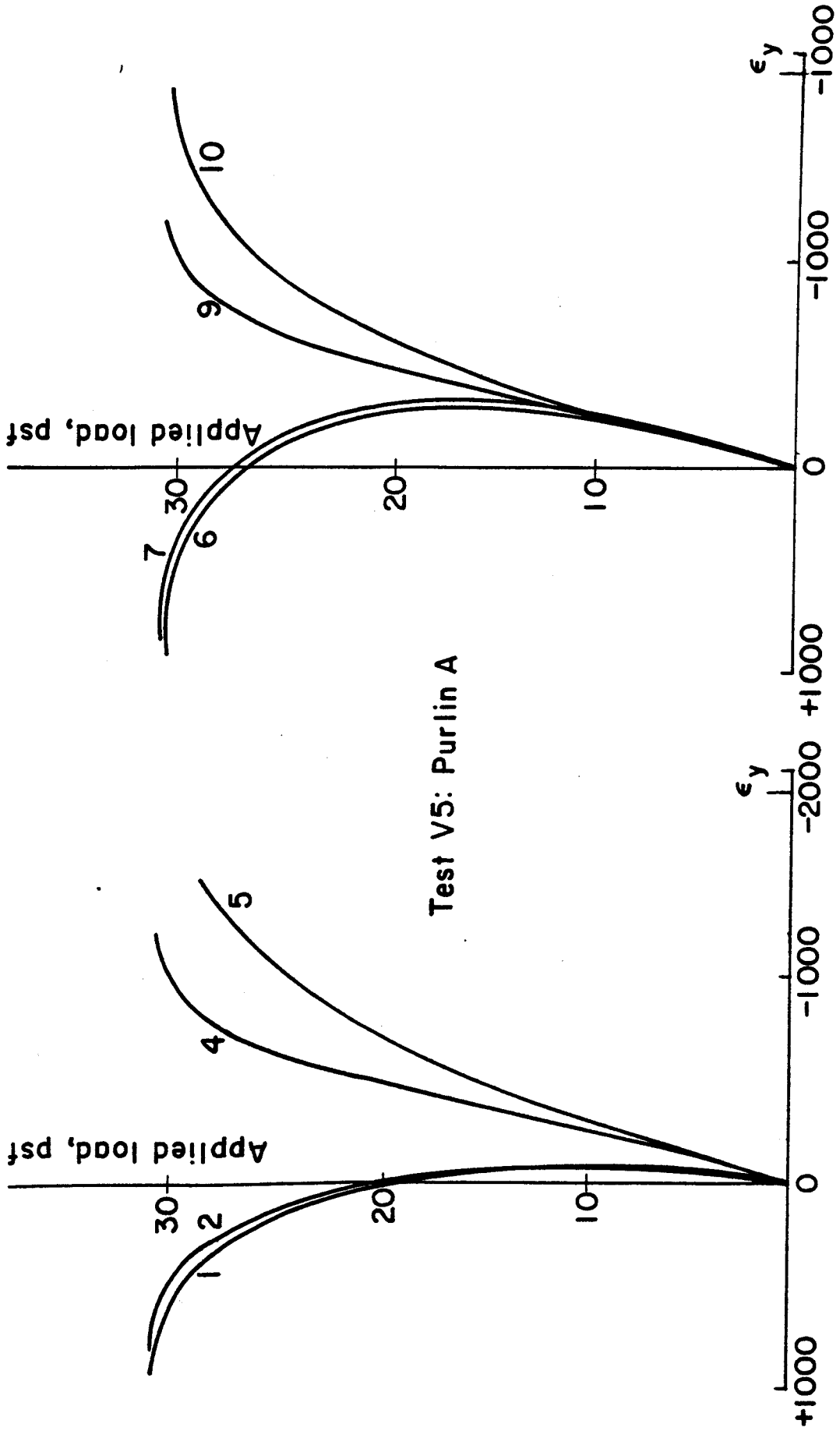

FIG. 4.3 LOAD vs. STRAIN

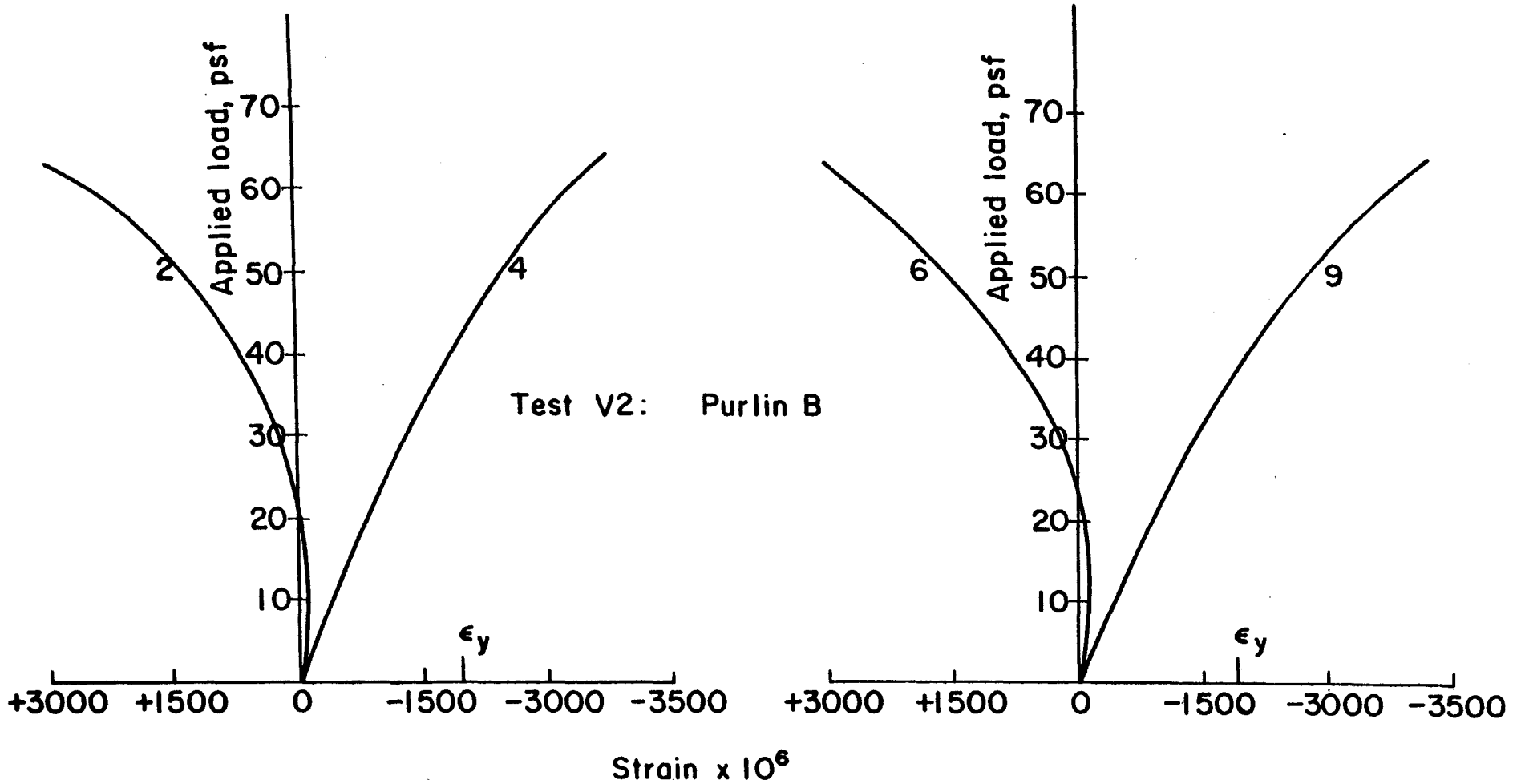

FIG. 4.4 LOAD vs. STRAIN

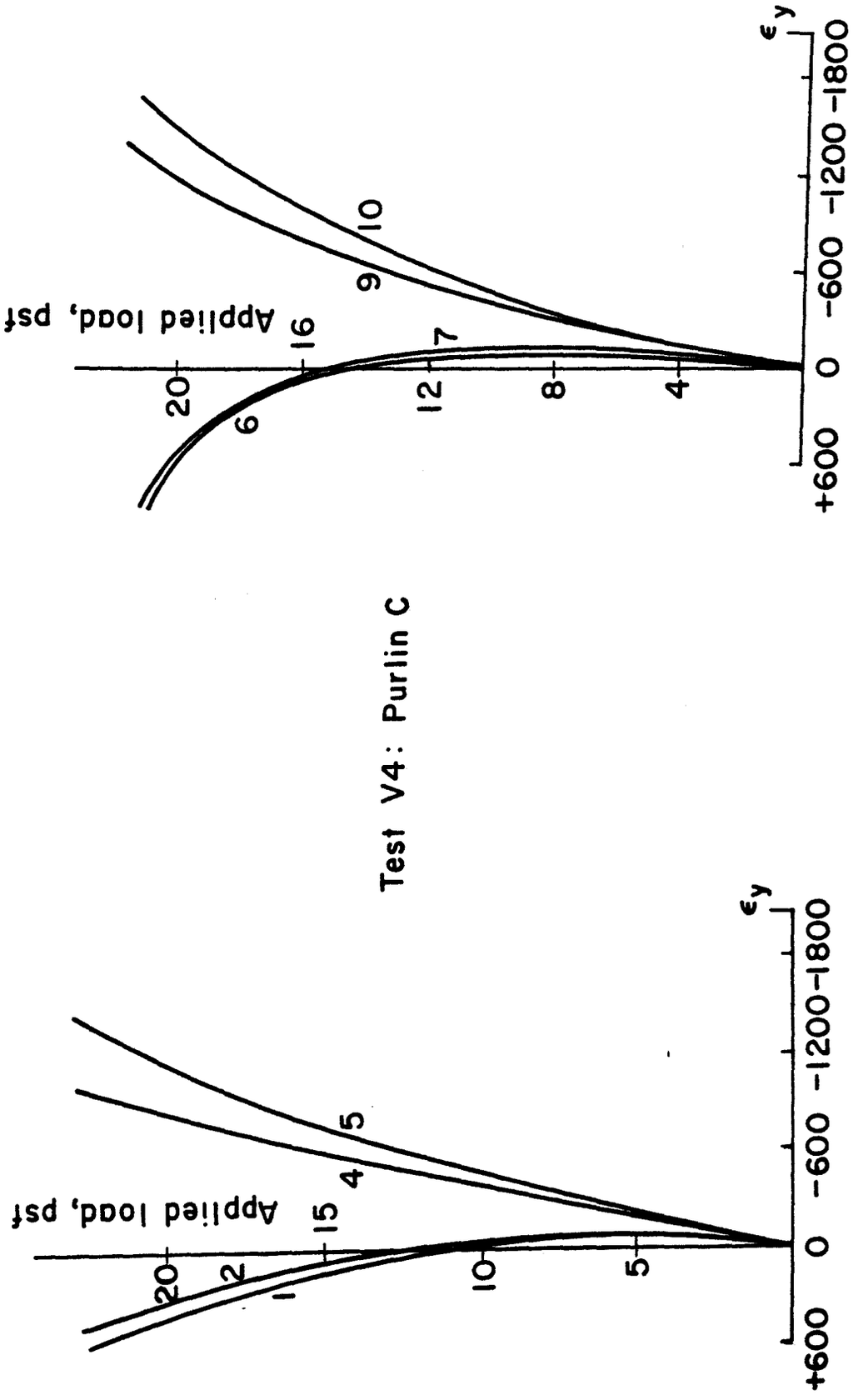

FIG. 4.5 LOAD vs. STRAIN

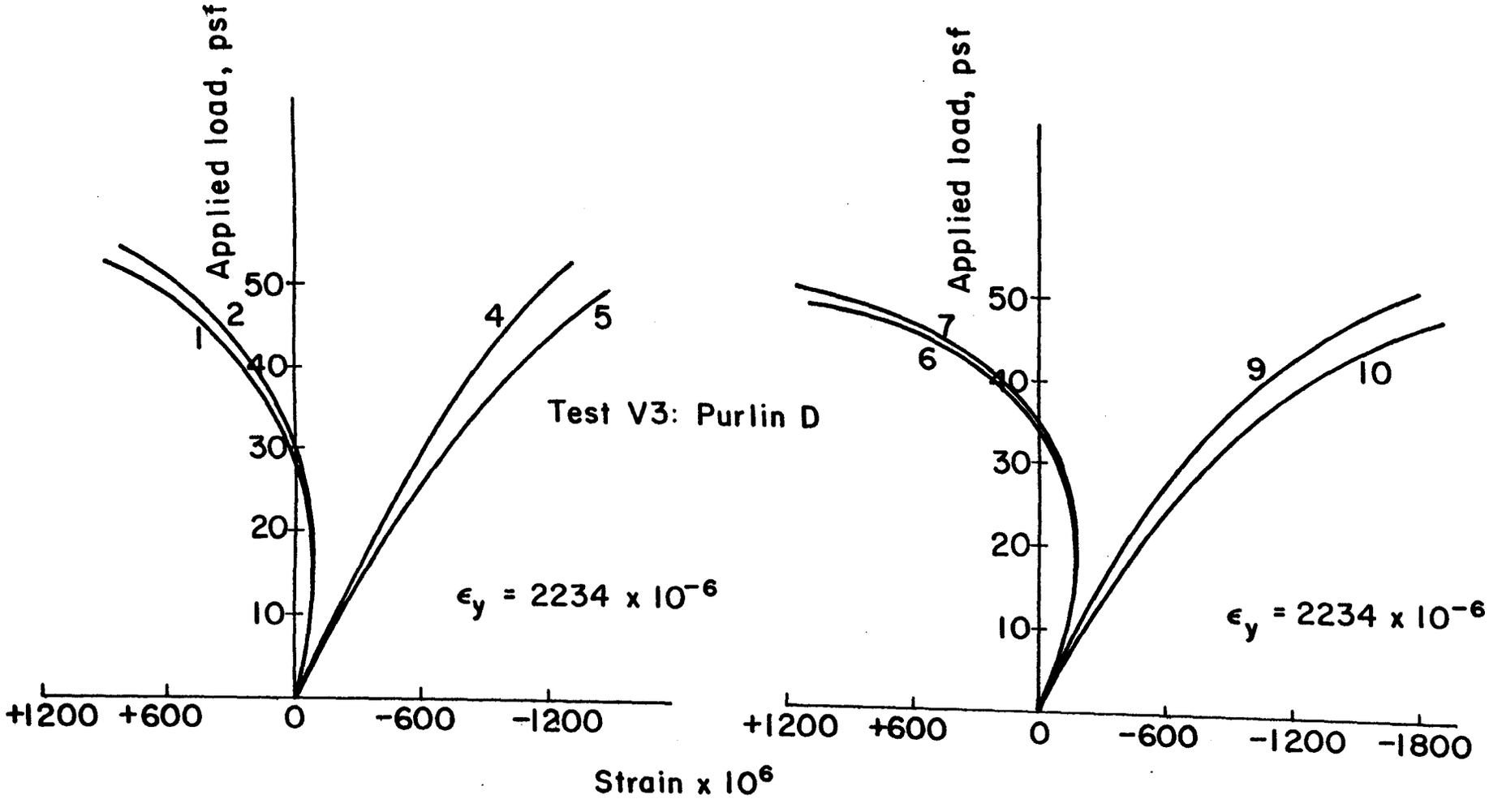

FIG. 4.6 LOAD vs. STRAIN

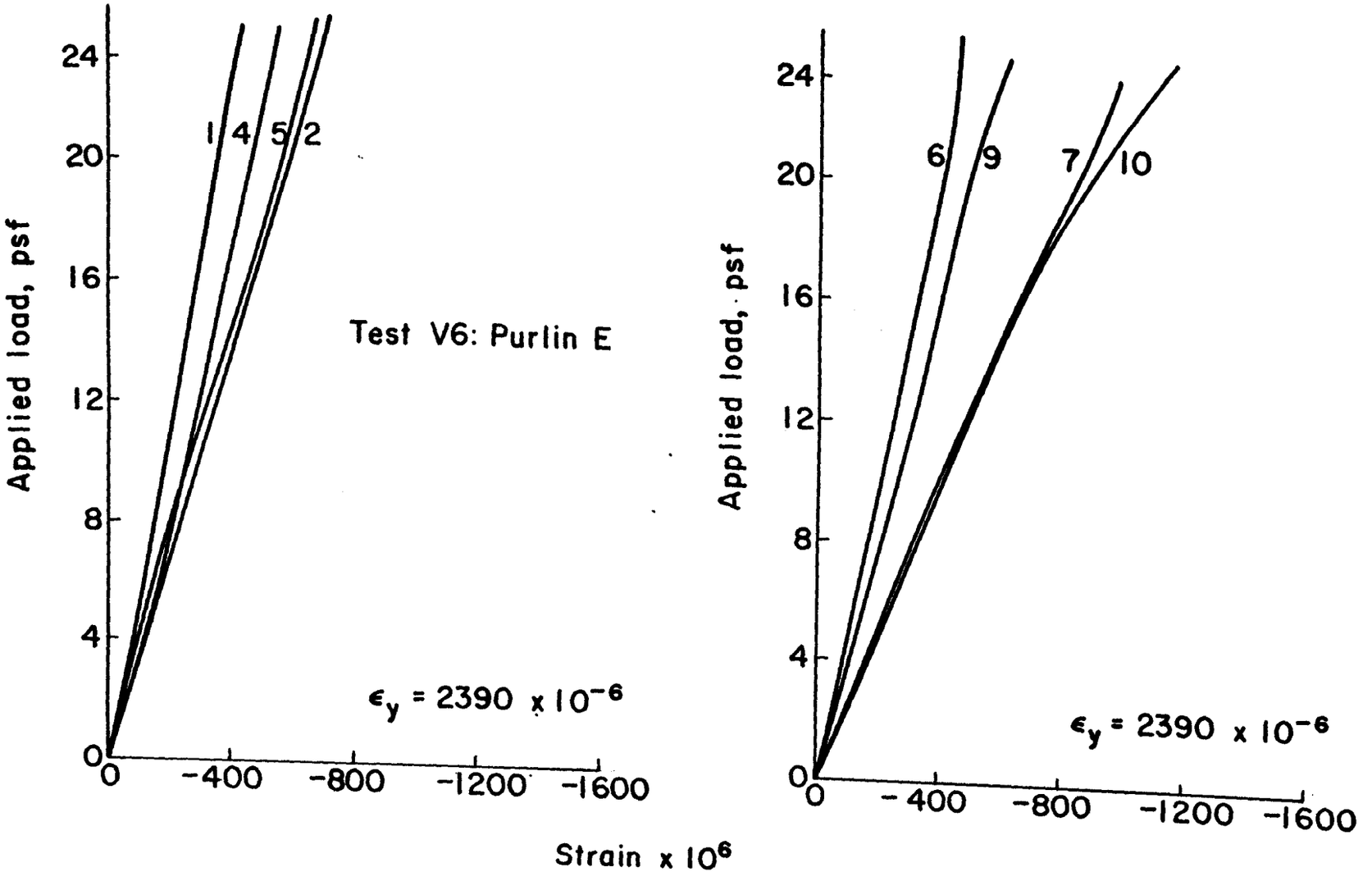

FIG. 4.7 LOAD vs. STRAIN

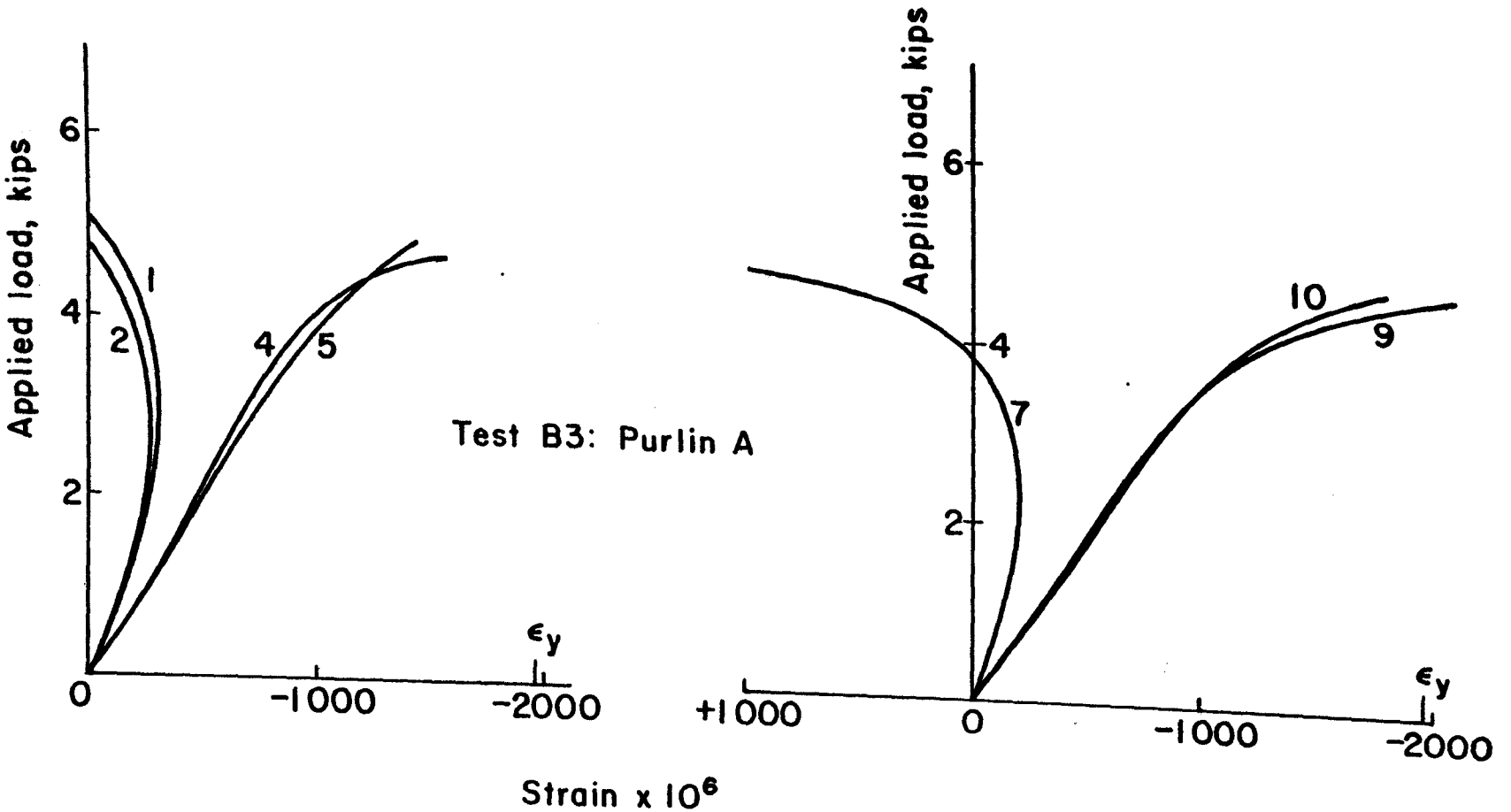

FIG. 4.8 LOAD vs. STRAIN

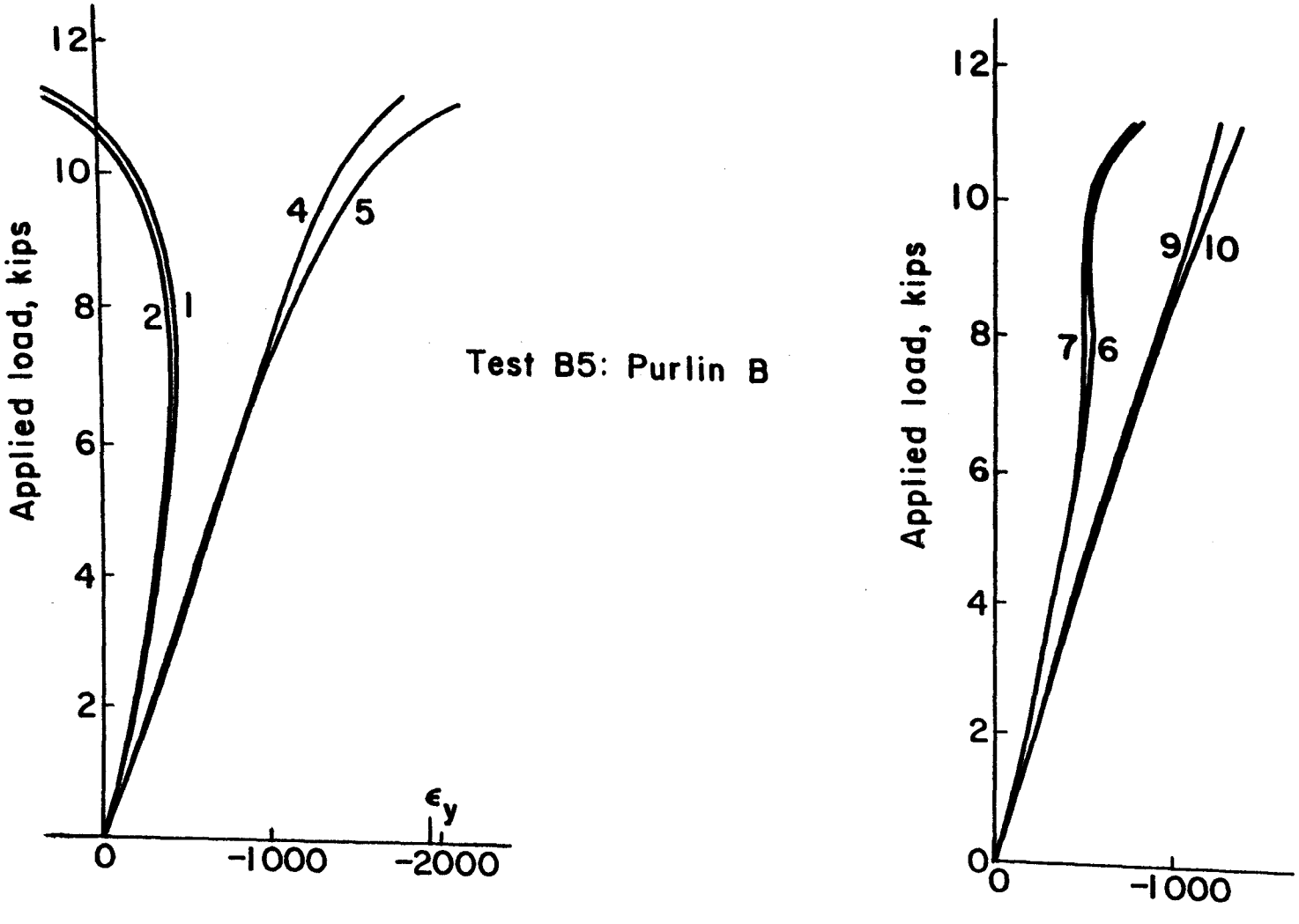

FIG. 4.9 LOAD vs. STRAIN

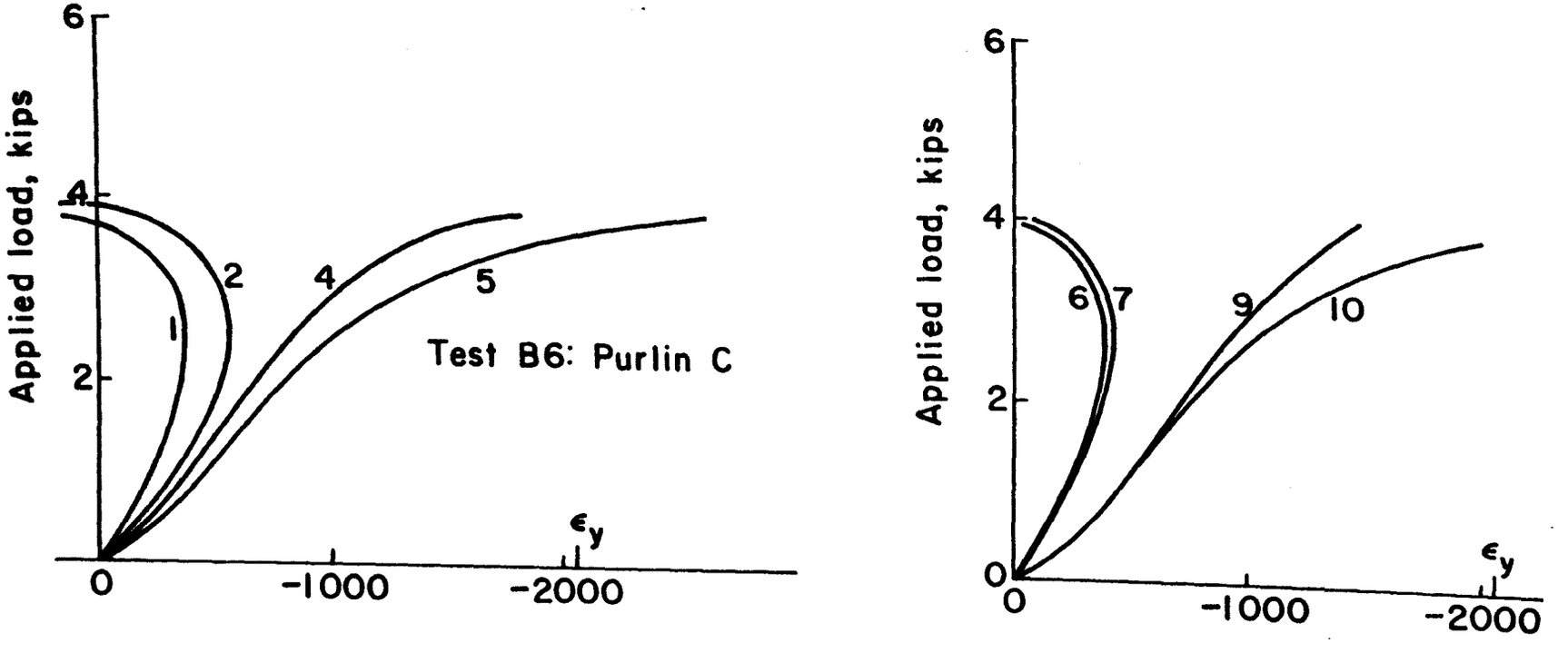

FIG. 4.10 LOAD vs. STRAIN

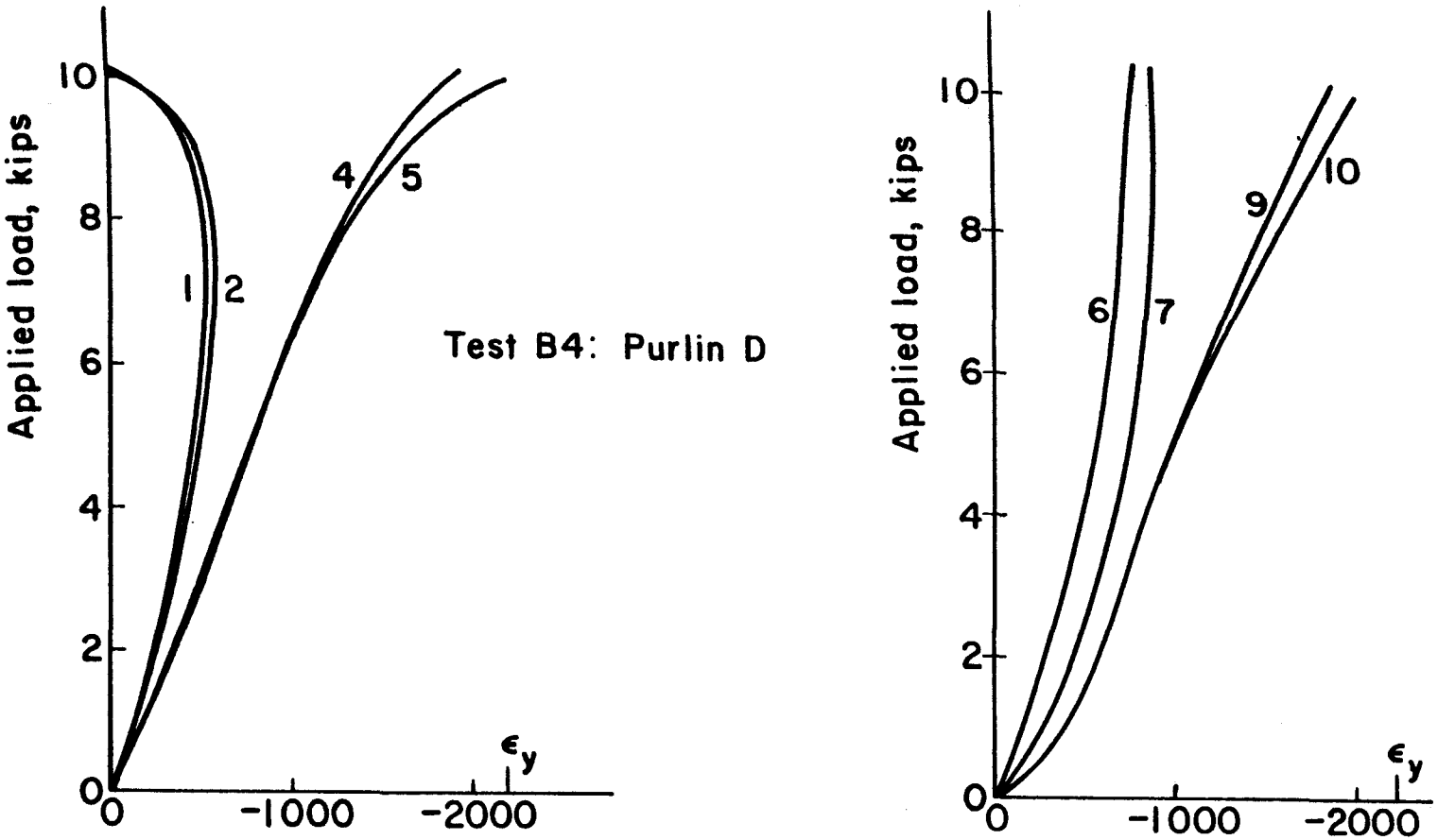

FIG. 4.11 LOAD vs. STRAIN

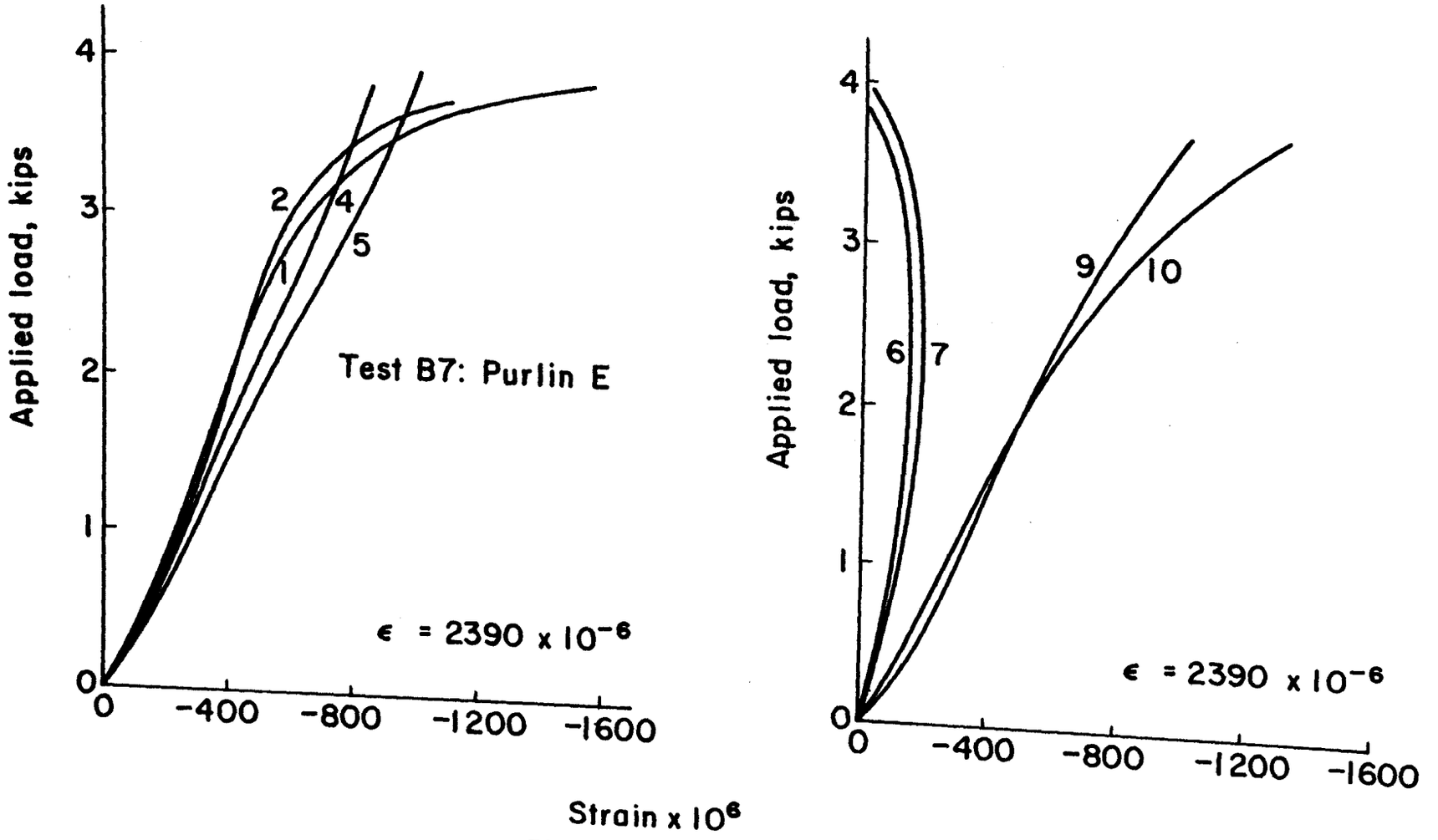

FIG. 4.12 LOAD vs. STRAIN

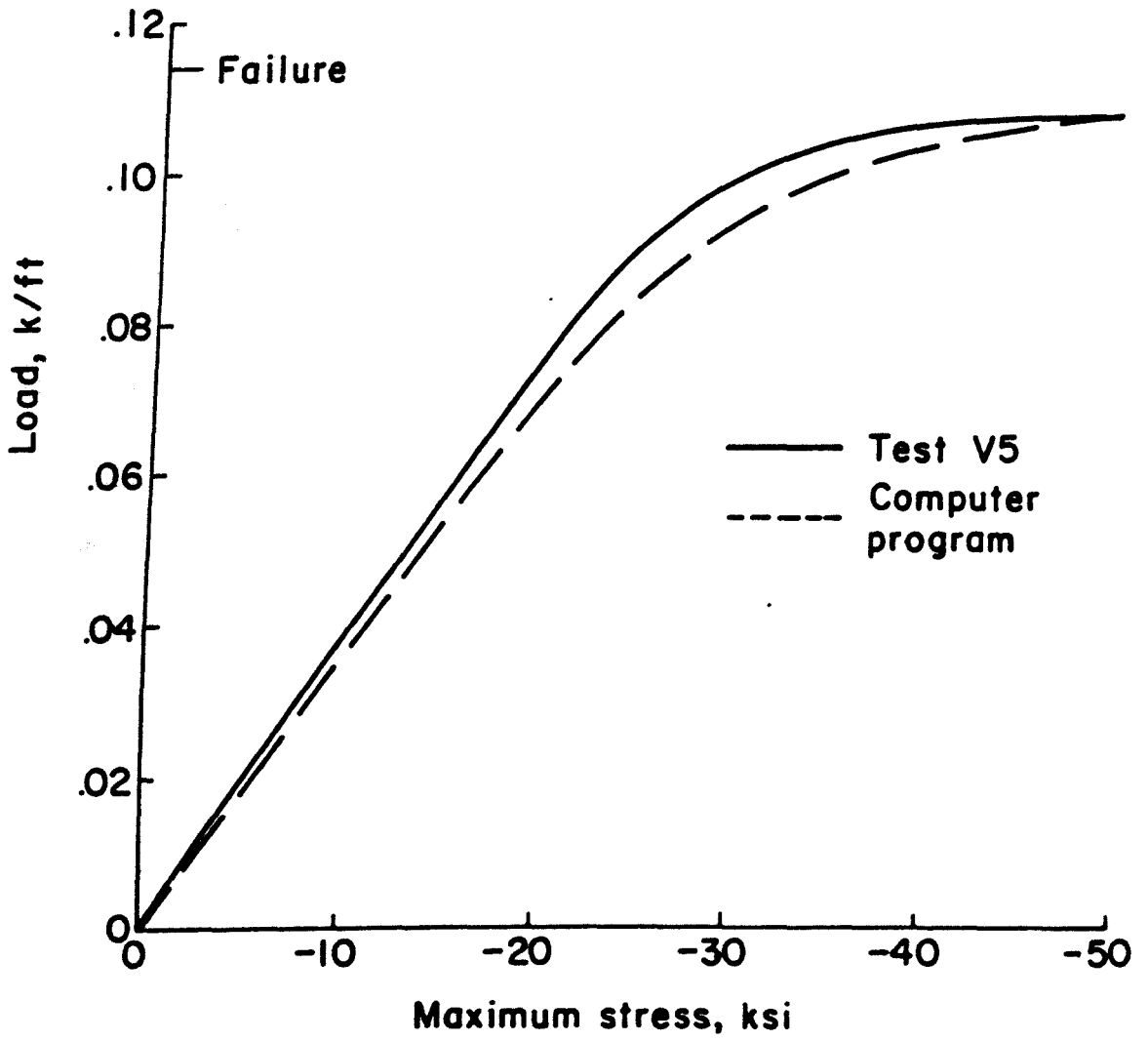

FIG. 4.13 COMPARISON OF STRESSES
(PURLIN TYPE A)

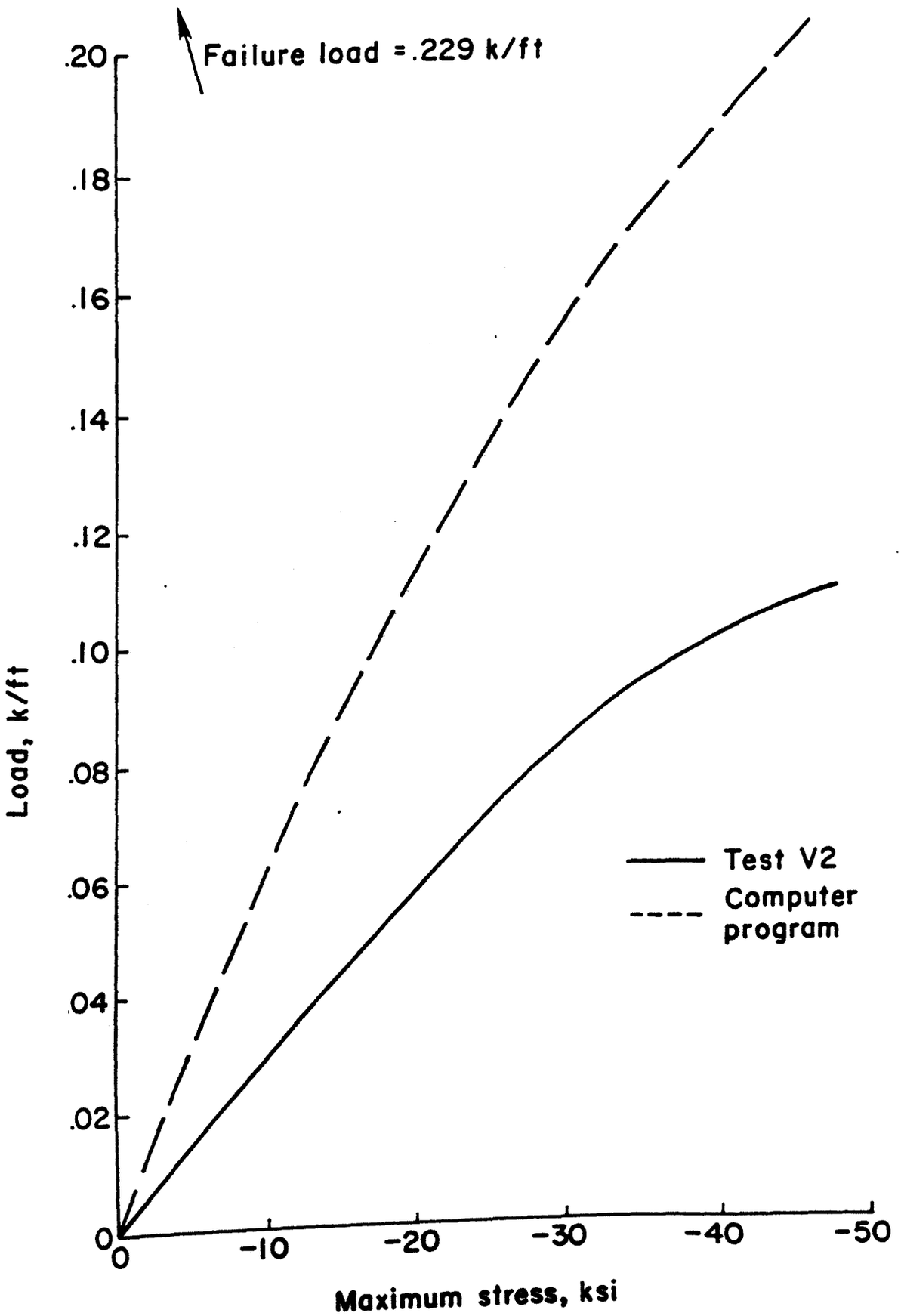

FIG. 4.14 COMPARISON OF STRESSES (PURLIN TYPE B)

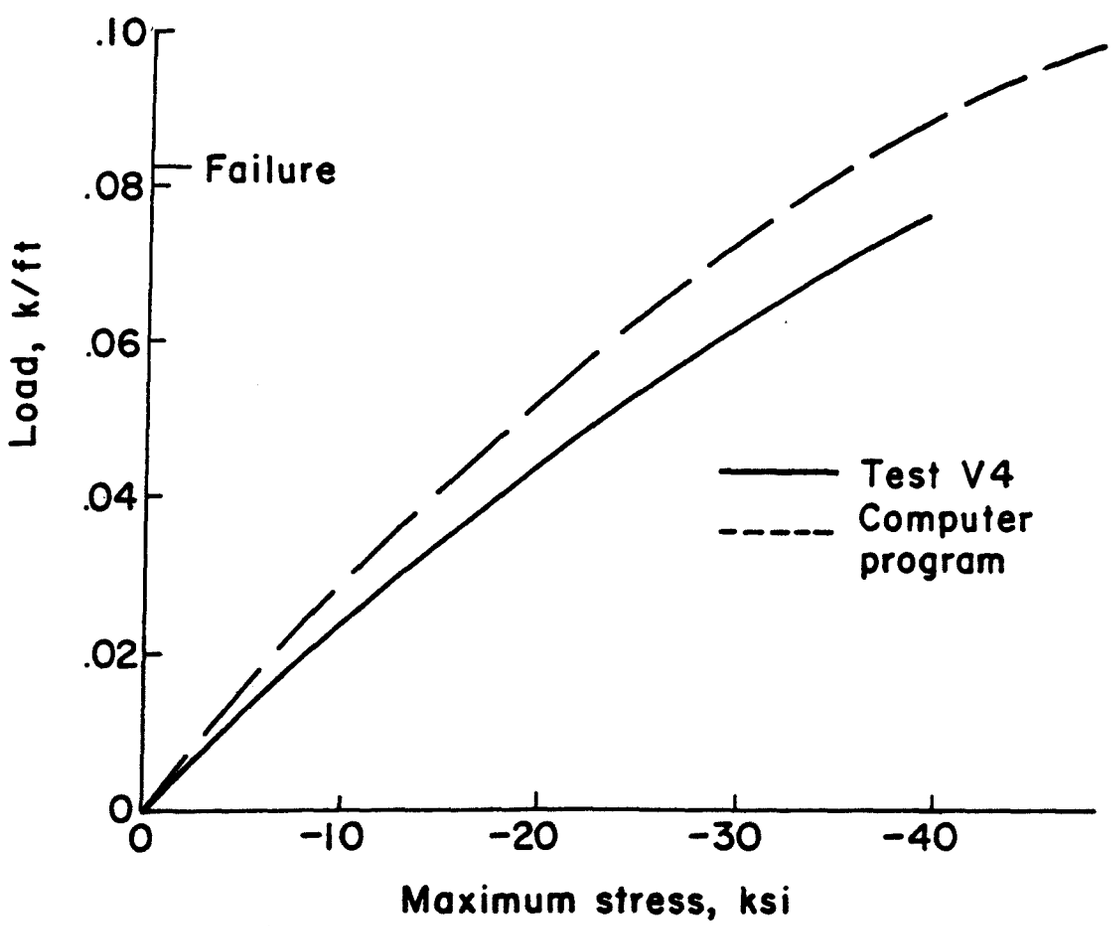

FIG. 4.15 COMPARISON OF STRESSES (PURLIN TYPE C)

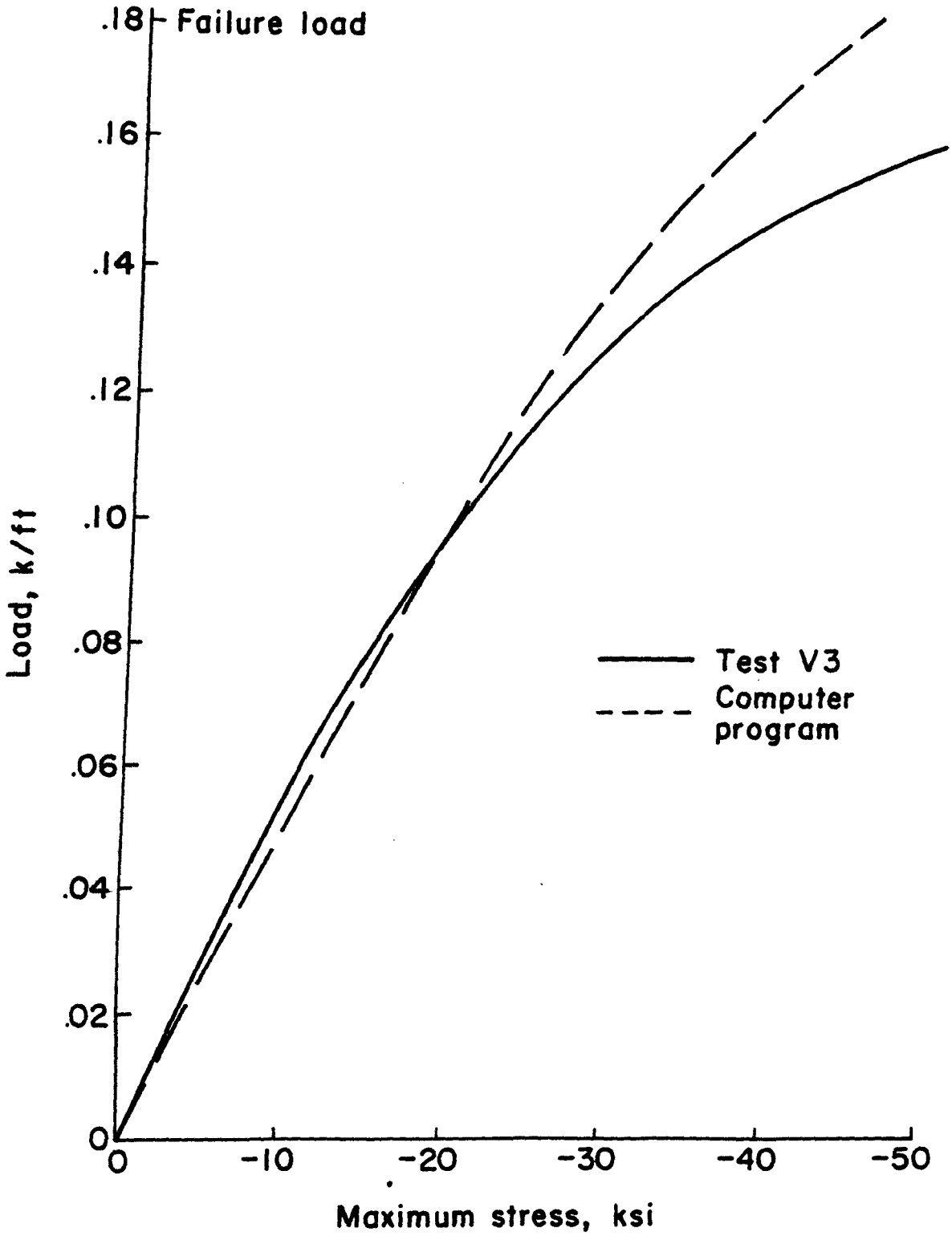

FIG. 4.16 COMPARISON OF STRESSES (PURLIN TYPE D)

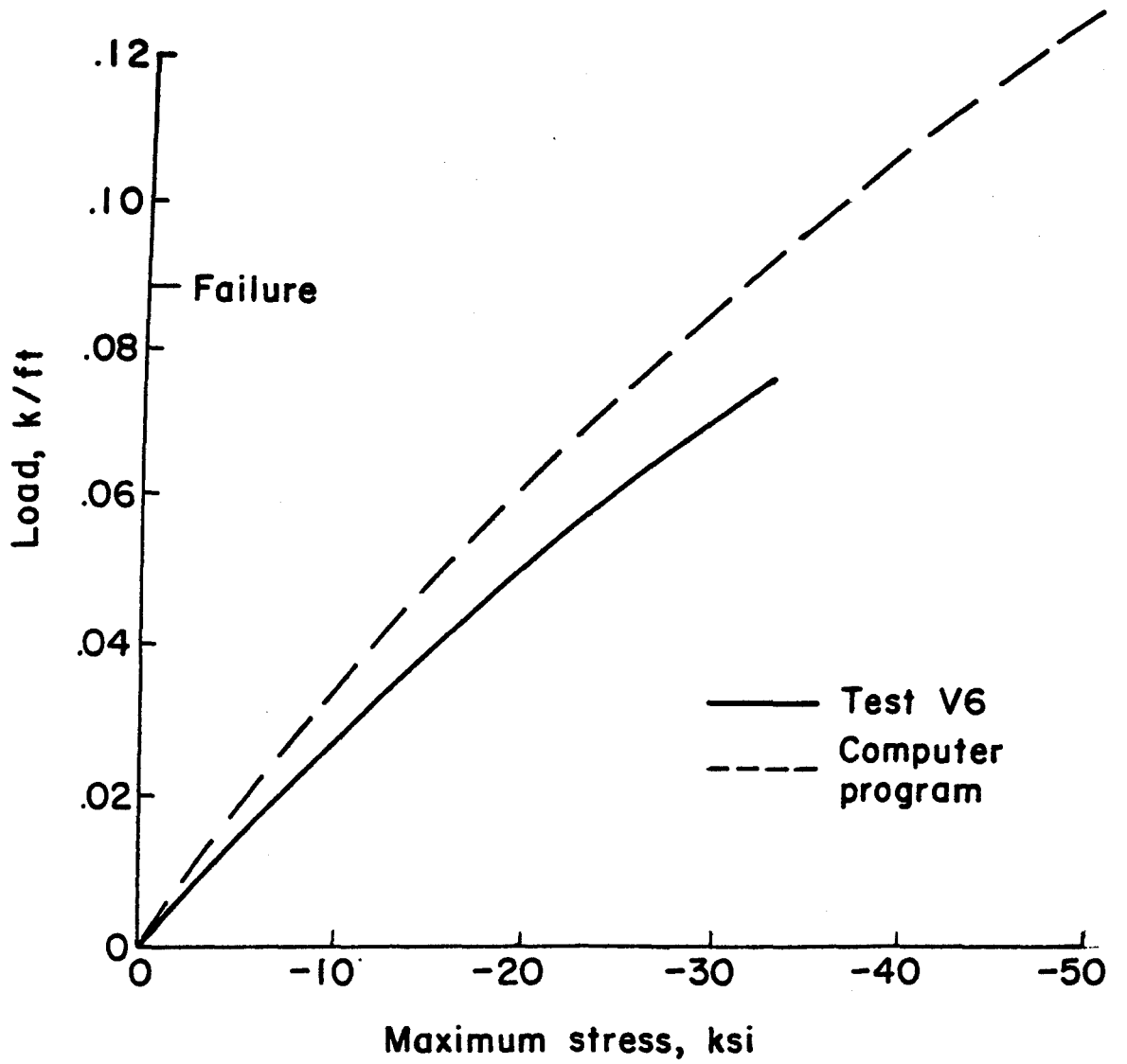

FIG. 4.17 COMPARISON OF STRESSES (PURLIN TYPE E)

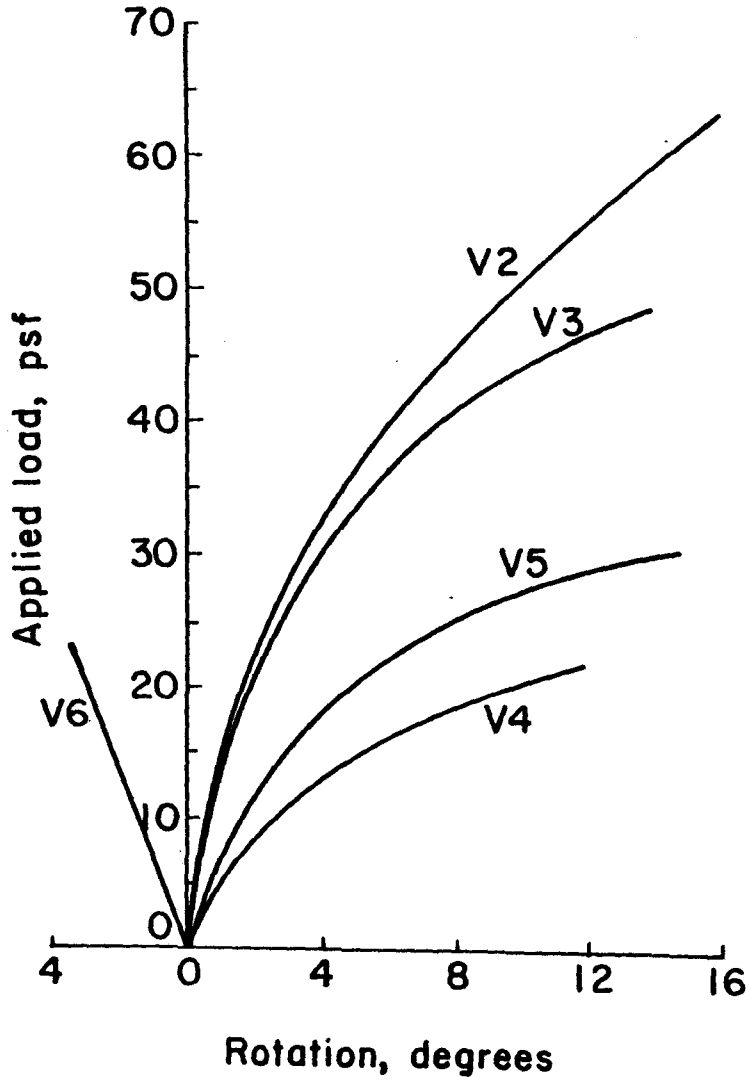

FIG. 4.18 VACUUM TESTS: LOAD-ROTATION CURVES

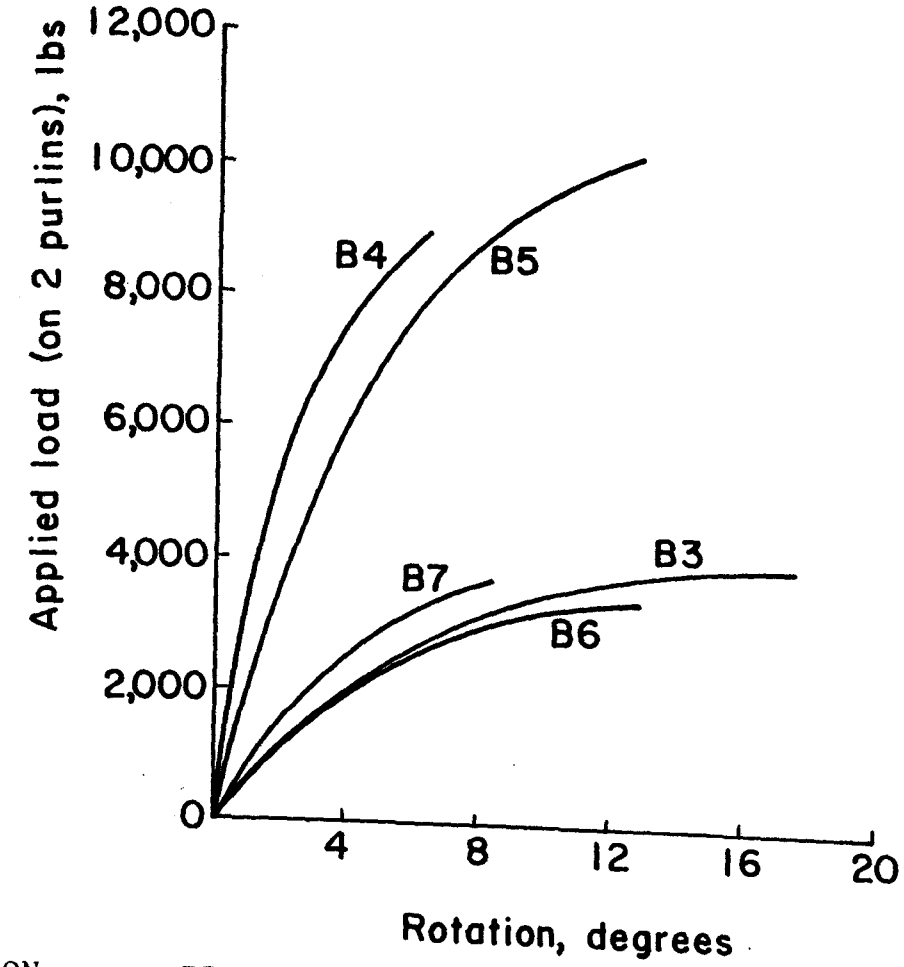

FIG. 4.19 BEAM TESTS: LOAD-ROTATION CURVES

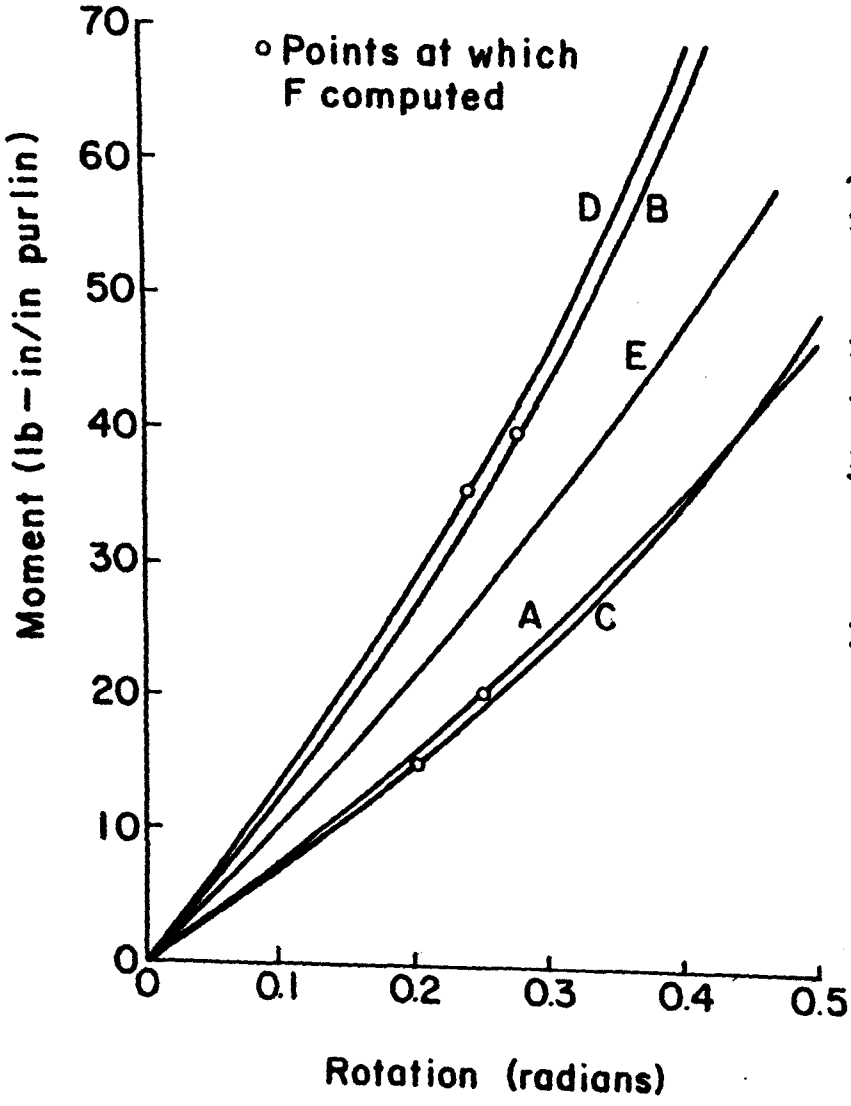

FIG. 4.20 F TESTS (DIAPHRAGM-BRACED PURLINS (MOMENT-ROTATION CURVES

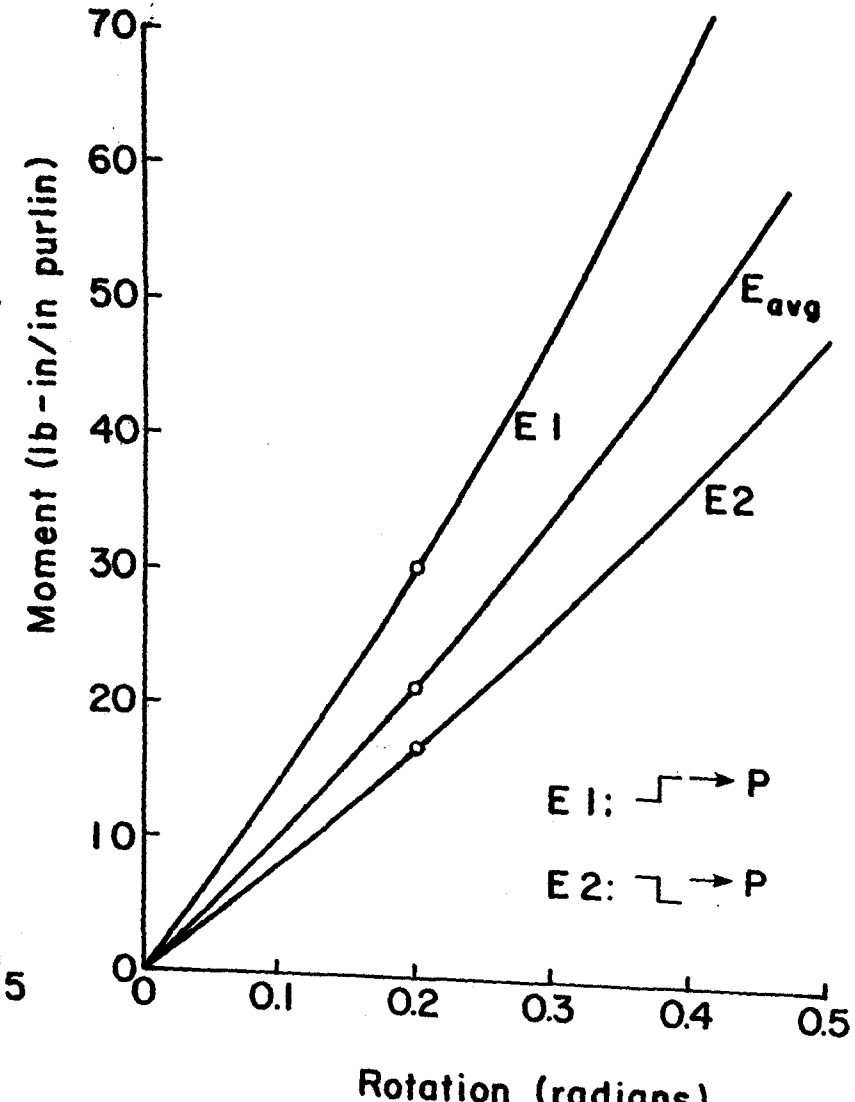

FIG. 4.21 F TESTS: PURLIN TYPE E (DIAPHRAGM-BRACED PURLINS) MOMENT-ROTATION CURVES

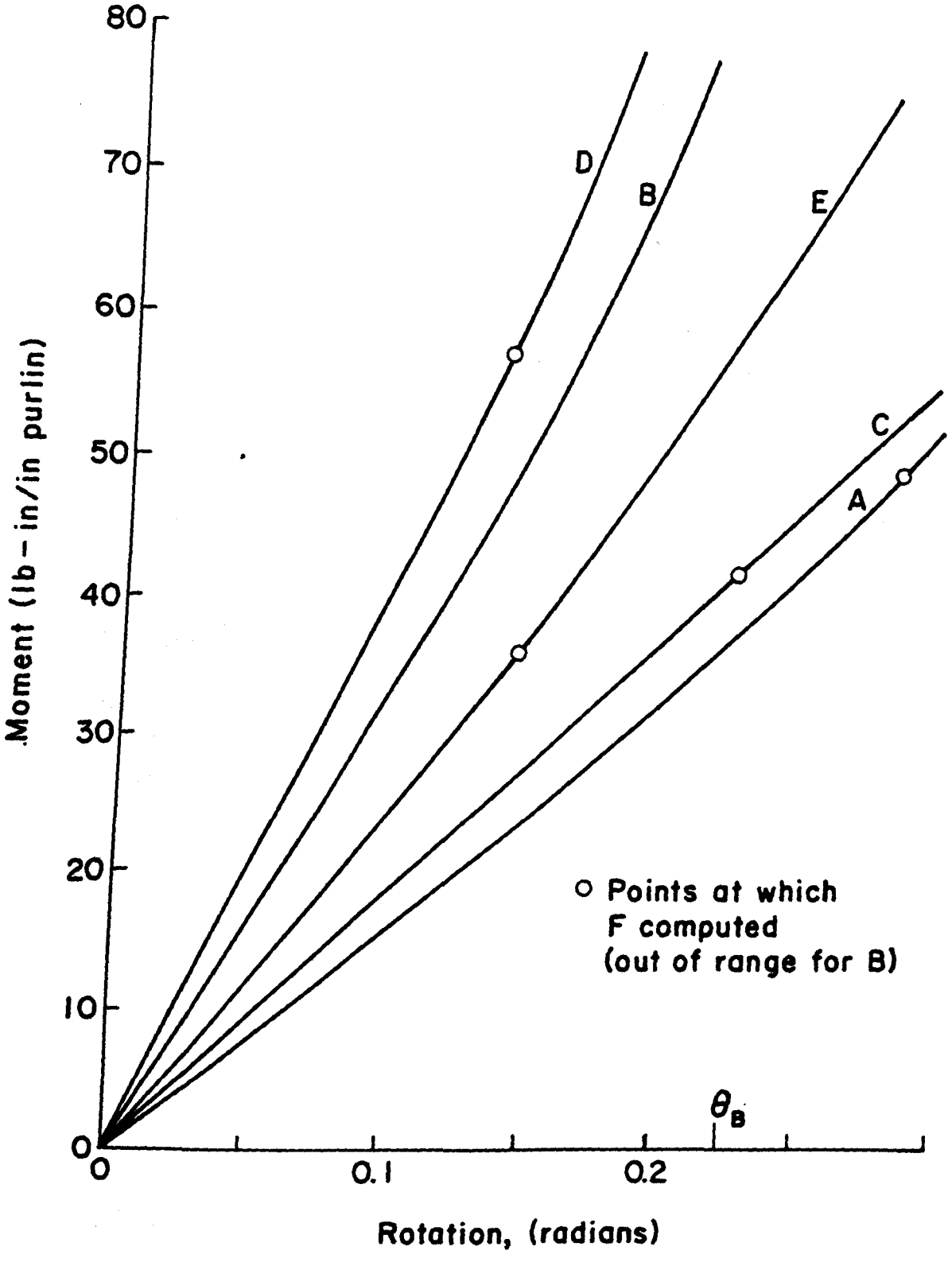

FIG. 4.22 F TESTS (CHANNEL-BRACED PURLINS)
MOMENT-ROTATION CURVES

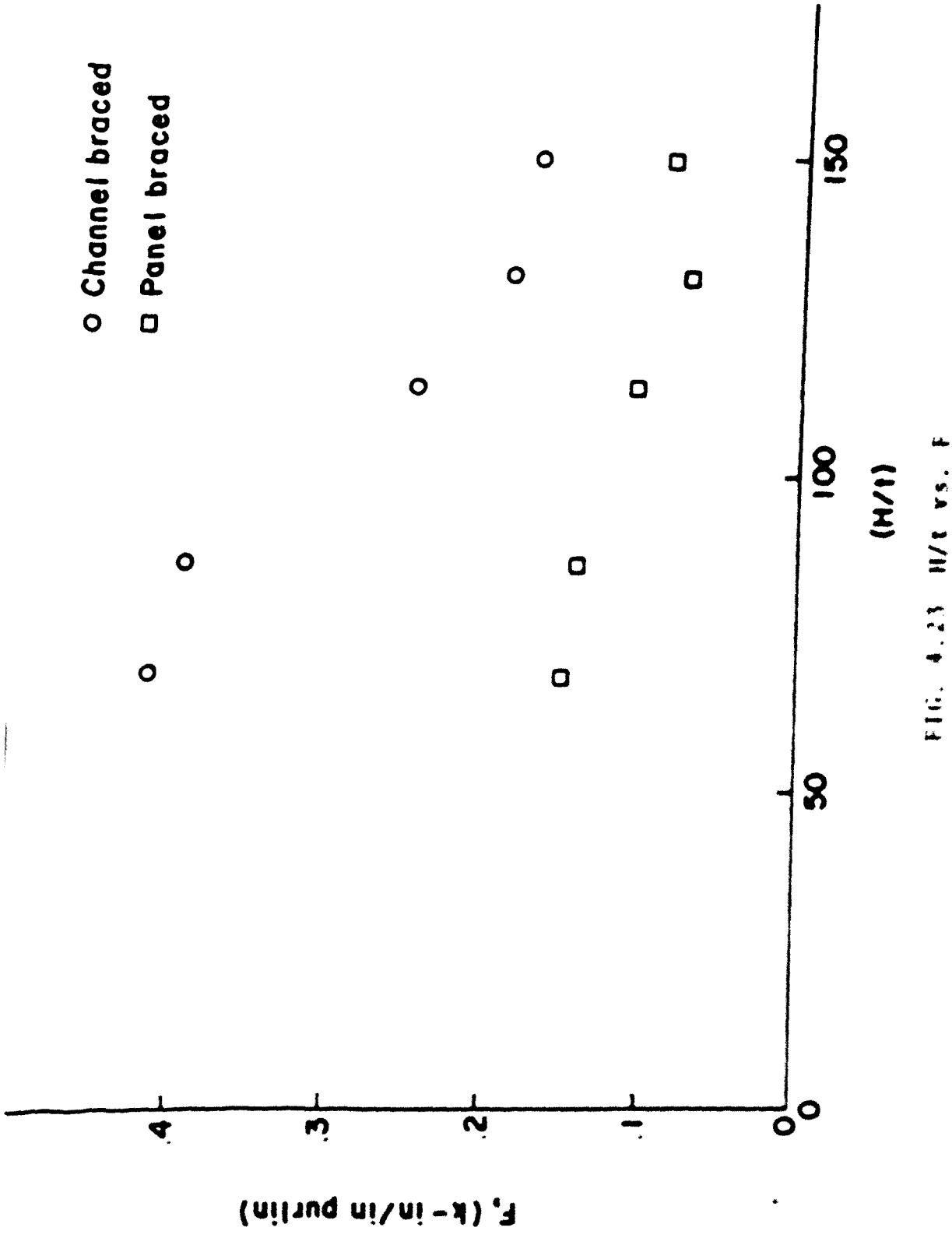

FIG. 4.23 H/t vs. F

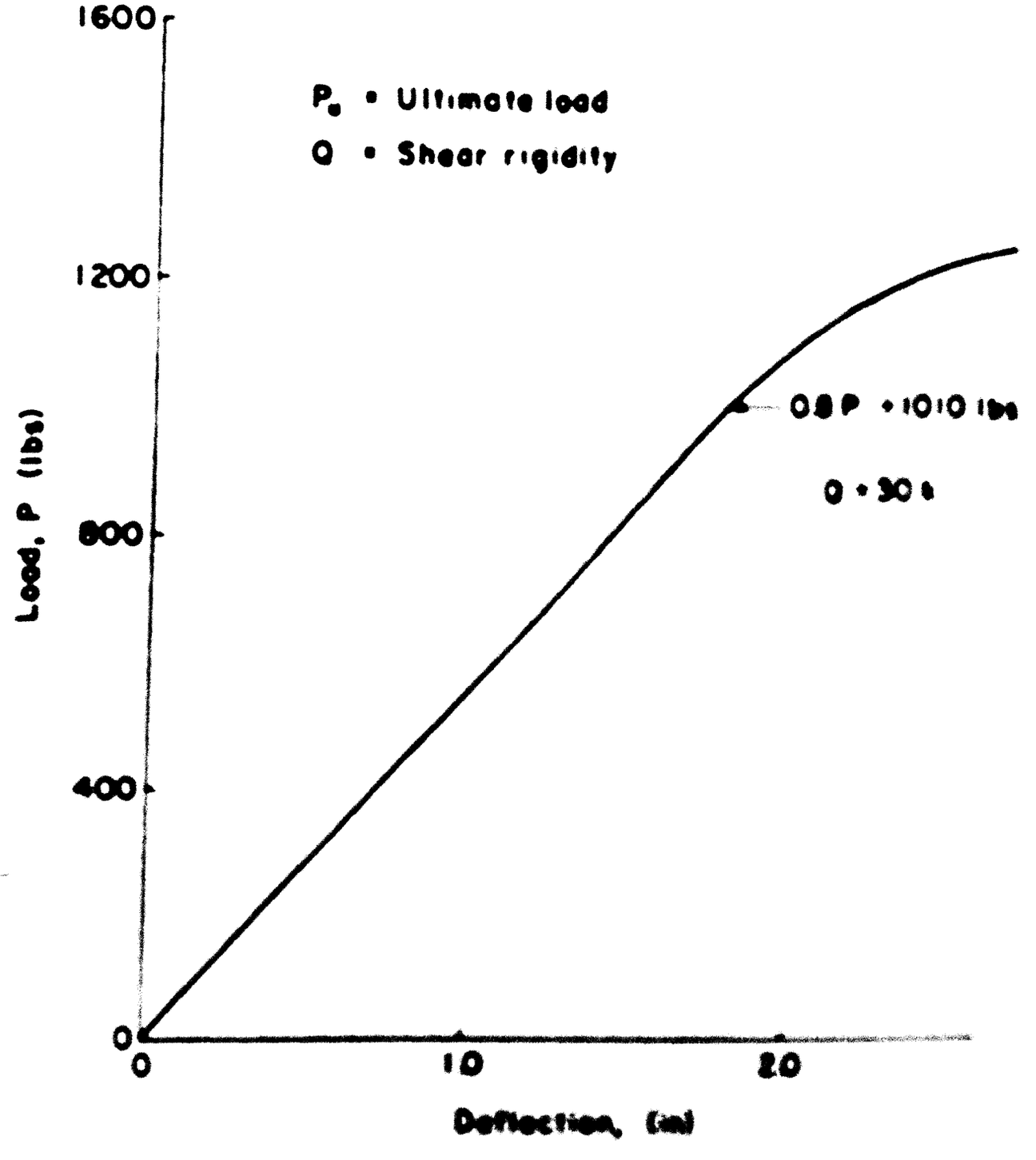

FIG. 8.28 SHEAR RIGIDITY TEST
LOAD-DEFLECTION CURVE

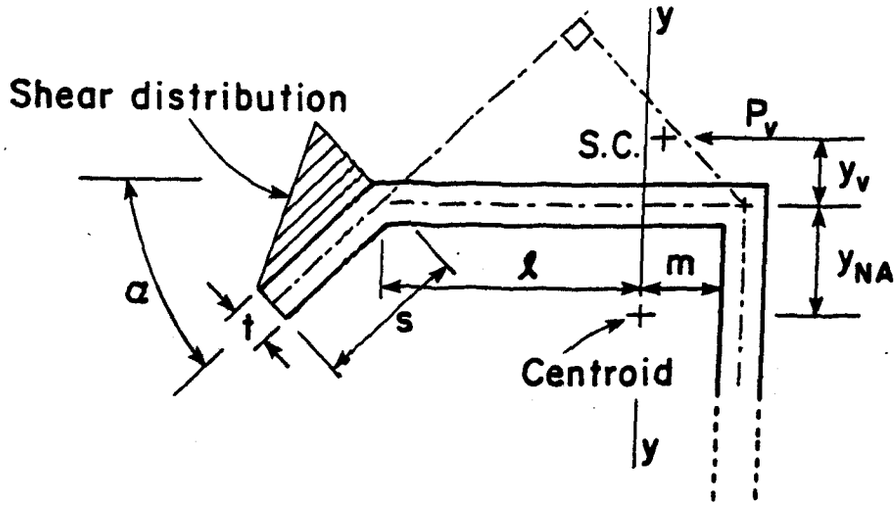

FIG. A.1 LOCATION OF SHEAR CENTER FOR EQUIVALENT COLUMN

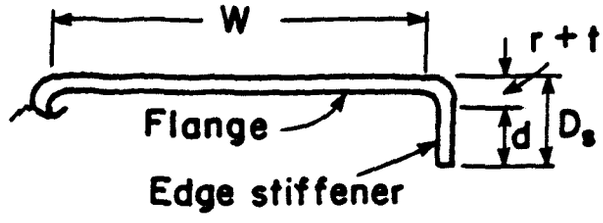

a) Straight lip stiffener

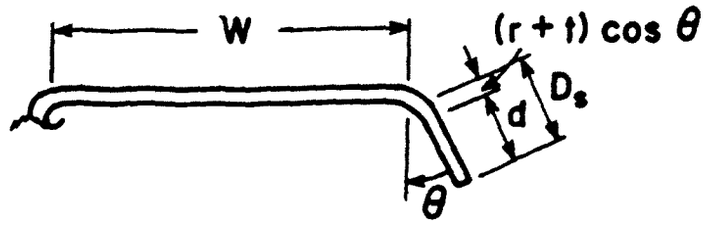

b) Angled straight lip stiffener

FIG. B.1 TYPICAL EDGE STIFFENED ELEMENTS

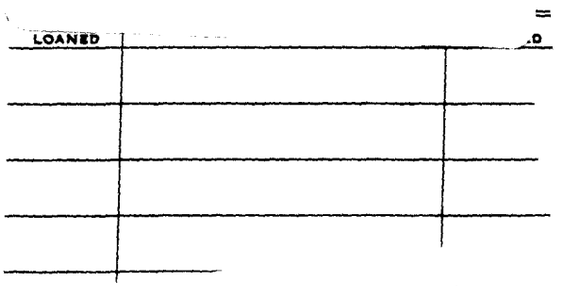

CCFSS LIBRARY Pekoz, Teoman M.A.A. Razak
22 1 * 4925 ULTIMATE STRENGTH OF COLD-FORMED
February STEEL Z-PURLINS
1980